

THE TRIANGULAR APPROXIMATION FOR HIGHLY ANISOTROPIC
GROUP-TO-GROUP TRANSFER CROSS SECTIONS

by

WAYNE JOHN MIKOLS

B.S. Kansas State University, 1974

A MASTER'S THESIS

submitted in partial fulfillment of the
requirements for the degree

MASTER OF SCIENCE

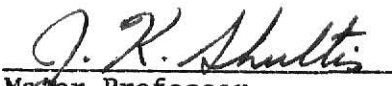
Department of Nuclear Engineering

Kansas State University

Manhattan, Kansas

1976

Approved by:


Major Professor

LD
2668
T4
1976
M56
C.2
document

Table of Contents

175

	Page
List of Figures	ii
List of Tables	v
1.0 Introduction	1
2.0 Theoretical Considerations	4
2.1 Equations for Neutron Transport	4
2.1.1 Monoenergetic Model	4
2.1.2 Multigroup Model	6
2.2 Anisotropic Group-to-Group Scattering Cross Sections	8
2.2.1 Legendre Expansion Techniques	10
2.2.2 Exact Kernel Techniques	11
2.3 Cross Section Approximation	18
2.3.1 Approximation of $\sigma_{g' \rightarrow g}(\mu)$ for General Multigroup Energy Structures	19
2.3.2 Approximation of $\sigma_{g' \rightarrow g}(\mu)$ for Energy Structures Having Equal lethargy Widths	25
2.3.3 Comparison of Exact and Triangularly Approximated Elastic Transfer Cross Sections	30
3.0 Anisotropic Transport Methods and Calculations	40
3.1 Transport Techniques for Evaluating the Utility of Approximated Cross Sections	41
3.2 Discrete Ordinate Quadrature Set Selection	44
3.2.1 Incident Direction Considerations	46
3.2.2 Angular Scattering Quadrature Coverage	53
3.3 Transport Calculations Using Triangularly Approximated Cross Sections	69
3.3.1 Comparison of Emergent Angular Densities	69
3.3.2 Comparison of Calculated and Experimental Results	81
4.0 Conclusions	93
5.0 Acknowledgements	97
6.0 References	98
7.0 Appendices	100
Appendix A: Computer Programs	100

List of Figures

Figure		Page
1	Coordinates for Slab Geometry	5
2	Hydrogen Multigroup Scattering Cross Section for a Group 20 to 20 Transfer	12
3	Hydrogen Multigroup Scattering Cross Section for a Group 20 to 24 Transfer	13
4	Integral Evaluation of $\sigma_{g' \rightarrow g}(\mu)$ in the (E,E') Plane	16
5	Integral Regions in the (E,E') Plane for Evaluation of $\sigma_{g' \rightarrow g}(\mu)$	20
6	Oxygen Multigroup Scattering Cross Sections Between Energy Groups of Different Lethargy	24
7	Oxygen Multigroup Scattering Cross Section for a Group 20 to 22 Transfer	27
8	Oxygen Multigroup Scattering Cross Section for a Group 22 to 24 Transfer	28
9	Evaluation of Approximating Triangle Height	29
10	Hydrogen Multigroup Scattering Cross Section for a Group 20 to 23 Transfer	32
11	Comparison of Exact and Triangularly Approximated Oxygen Elastic Transfer Cross Sections	34
12	ENDF Oxygen Elastic Scattering Point Data between DLC/2 Energy Groups 16 and 17	36
13	Water Multigroup Scattering Cross Section for a Group 16 to 18 Transfer	39
14	Transmitted Angular Density for Isotropic Scattering when $c=0.6$	47
15	Transmitted Angular Density for Isotropic Scattering when $c=1.0$	48
16	Transmitted Angular Density from Group 1 to 1 for an 8 inch Water Slab	49
17	Transmitted Angular Density from Group 20 to 20 for an 8 inch Water Slab	50

List of Figures (Cont.)

Figure		Page
18	Transmitted Angular Density from Group 20 to 20 through a Hydrogen Slab	51
19	Neutron Scattering in 3-Dimensions	59
20	Azimuthally Symmetric Neutron Scattering Shell	60
21	Neutron Scattering Shell Positioning About the x-Axis	61
22	β_{\max} and β_{\min} versus the Incident Neutron Direction θ_1	65
23	Non-Zero Scattering Domain for $\sigma_{g' \rightarrow g}(\mu_1 \rightarrow \mu_j)$ as a Function of Initial Neutron Direction μ_1	66
24	Example of Non-Zero Scattering Domain for $\sigma_{g' \rightarrow g}(0.82 \rightarrow \mu_j)$	67
25	Comparison of Lobatto-12 and -14 Quadrature Sets for Use with Hydrogen Scattering	68
26	Transmitted Angular Density for a Group 20 to 20 Transfer through 4 inches of Water	71
27	Transmitted Angular Density for a Group 20 to 22 Transfer through 4 inches of Water	72
28	Transmitted Angular Density for a Group 20 to 24 Transfer through 4 inches of Water	73
29	Transmitted Angular Density for a Group 20 to 20 Transfer through 8 inches of Water	74
30	Transmitted Angular Density for a Group 20 to 22 Transfer through 8 inches of Water	75
31	Transmitted Angular Density for a Group 20 to 24 Transfer through 8 inches of Water	76
32	Reflected Angular Density for a Group 20 to 20 Transfer from 8 inches of Water	77
33	Reflected Angular Density for a Group 20 to 22 Transfer from 8 inches of Water	78
34	Reflected Angular Density for a Group 20 to 24 Transfer from 8 inches of Water	79

List of Figures (Cont.)

Figure		Page
35	Transmitted Angular Density through 4 inches of Water Using a Gauss-30 Quadrature	80
36	Experimental Penetration Data through 8 Inches of Water	83
37	Comparison between Pencil Beam Experimental Configuration and Transport Model Configuration . . .	85
38	Approximate Equivalence between Pencil Beam Illumination and Uniform Slant Source Illumination	86
39	Comparison of Experimental and Calculated Slab Transmission Spectra	90
40	Comparison of Transport Calculations Based Upon Exact and Approximated Cross Sections (11.2°)	91
41	Comparison of Transmitted Fluxes through Water for a 29.8° Exit Angle	92

List of Tables

Table		Page
1	Hydrogen Multigroup Scattering Cross Section for a Group 20 to 23 Transfer	31
2	Hydrogen and Oxygen Total Cross Sections	37
3	Transport Computer Code Execution Times	43
4	Comparison of Transport Calculations Using Lobbato-12 and -14 Quadrature Sets	54
5	Total Group 20 to 20 Scattering Cross Sections Calculated by Lobatto-12 and -14 Quadrature Sets . .	57
6	Incident Neutron Spectrum for 8 inch Water Penetration Problem	82

1.0 Introduction

The analysis of neutron transport through matter has been a subject of considerable investigation in recent years. With the advent of advanced reactors, reliable fast-neutron penetration information is critical to the further development of optimal reactor core and radiation shield designs. Consequently, much attention has been focused upon simple geometries in order to better understand the interactions and transport processes involved.

Many institutions, including the Nuclear Engineering Department at Kansas State University, have been actively engaged in a continuing program to analyze the energy and angular dependent flux which penetrates slabs of various test materials. From such studies it is hoped to establish experimental benchmark data for simple well defined geometries. This data could then be used to improve and verify computational methods employed in standard neutron transport calculations. The present study represents an investigation of some approximate numerical techniques which can be applied to the analysis of problems involving highly anisotropic neutron scattering. Anisotropic scattering occurs in many important particle transport problems. The one studied in the present work is that of multigroup neutron transport through water slabs.

Until recently, much of the work done with anisotropic particle transport has relied upon Legendre polynomial expansions of the elastic scattering cross sections. Although these expansions yield a relatively accurate description of transfer probabilities for media comprised of atoms with large mass number, light materials offer a special problem. Multigroup angular transfer cross sections for elastic scattering from light elements tend to be highly anisotropic in the scattering angle. Legendre expansions of extremely high order are required to accurately model angular transfer. Timmons [1] indicates

that in some cases, Legendre orders in excess of 160 terms are needed to eliminate significant oscillations in reconstructed angular scattering distributions. Recent work by Carter and Forest [2] as well as Attia and Harms [32] suggest approximate techniques which can be used to evaluate transfer cross sections without resorting to Legendre expansions. They examine these methods as they apply to neutron transport through hydrogen and water slabs. Unlike other elements, hydrogen scatters isotropically in the center of mass coordinate systems. Hence, hydrogen angular transfer cross sections lend themselves to a somewhat simplified treatment.

Odom [3] employed an *exact kernel* technique to obtain very accurate anisotropic elastic scattering cross section information for not only the special hydrogen case, but for materials of arbitrary mass number. He compares transport results using these refined anisotropic elastic scattering cross sections to similar ANISN calculations [4] which employ ninth order Legendre cross section expansions. Such ninth order truncation of the Legendre cross section expansion severely impairs its ability to represent highly anisotropic scattering cross sections. These cross sections often appear as sharply peaked distributions. Odom concludes that the *exact kernel* technique provides for a far more realistic representation of highly anisotropic angular particle transport. His results as well as theoretical and empirical considerations presented in Section 2 of this work suggest that multigroup angular cross sections for equal lethargy energy structures might successfully be modeled by triangularly shaped distributions. Use of a triangular representation considerably simplifies evaluation of angular cross section information. The only actual cross section information required for such an evaluation is the total group-to-group transfer cross sections for all group transfers being considered. This is in sharp contrast to Legendre expansion techniques

which usually require a minimum of nine angular moments for evaluation of each group-to-group transfer cross section considered.

A discrete ordinates transport code [3] has been used to draw comparisons between Odom's refined cross section data and triangularly approximated values. Triangular approximation of hydrogen and oxygen data has been studied extensively. Angular distributions calculated using triangular and refined elastic scattering water cross section data are compared for few-group scattering problems as well as a 20 group scattering problem. Particular emphasis is given to selection of numerical quadrature sets for use in the discrete analysis. Methods for selection of the minimum order numerical quadrature needed for a given set of anisotropic cross sections is introduced in this work. The method removes much of the guess work involved in selection of numerical quadratures for transport calculations.

2.0 Theoretical Considerations

2.1 Equations for Neutron Transport

Extensive treatment of the linearized Boltzmann particle transport equation can be found in numerous references [5,6,7]. Brief introductory comments concerning this equation are presented here so as to aid in the later discussion of multigroup elastic scattering transfer cross sections. For the sake of clarity, the monoenergetic form of the transport equation is discussed first. Subsequent sections make the extension to the more general multigroup form of this equation. Since this work is concerned primarily with the transport of neutrons through homogeneous slabs, only the one-dimensional, time-independent form of the equation is considered. However, extension of the results to other geometries presents no special problem [6].

2.1.1 Monoenergetic Model

The general one dimensional steady-state form of the Boltzmann transport equation can be written as

$$\mu \frac{\partial}{\partial x} \psi(x, \mu, \phi) + \sigma_T \psi(x, \mu, \phi) = \int_{\underline{\Omega}'} d\underline{\Omega}' \sigma_s(\underline{\Omega}' \cdot \underline{\Omega}) \psi(x, \mu', \phi') + Q(x, \mu, \phi) , \quad (2.1)$$

where:

μ = cosine of the polar angle between a particle's velocity vector and the positive x axis,

x = the distance traveled into the slab,

ϕ = the azimuthal angle between the z axis and the projection of the particle's velocity vector onto the slab face.

$\underline{\Omega}$ = a unit vector in the direction of particle travel,

σ_T = the total macroscopic cross section of the slab,

**THIS BOOK
CONTAINS
NUMEROUS PAGES
WITH DIAGRAMS
THAT ARE CROOKED
COMPARED TO THE
REST OF THE
INFORMATION ON
THE PAGE.**

**THIS IS AS
RECEIVED FROM
CUSTOMER.**

ϕ = Azimuthal Angle

μ = Cosine of Polar Angle

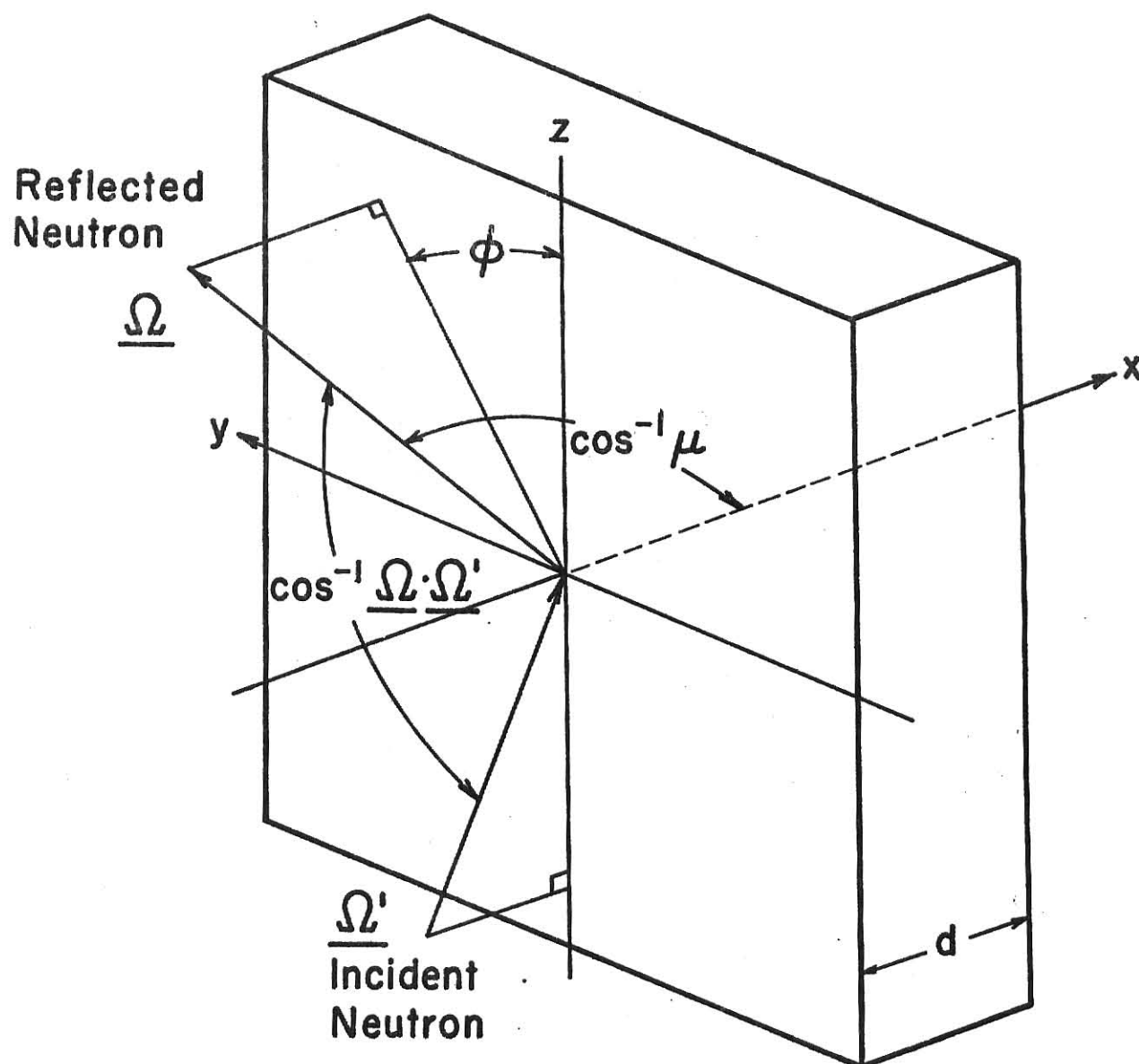


Figure 1. Coordinate for Slab Geometry

$Q(x, \mu, \phi)$ = the particle source strength in direction $\underline{\Omega}$ at position x ,

$\psi(x, \mu, \phi)$ = the angular particle density in direction $\underline{\Omega}$ at position x in the slab,

$\sigma_s(\underline{\Omega}' \cdot \underline{\Omega})$ = the macroscopic scattering transfer cross section from direction $\underline{\Omega}'$ to direction $\underline{\Omega}$.

The scattering transfer cross section, $\sigma_s(\underline{\Omega}' \cdot \underline{\Omega})$, may be thought of in terms of a transfer from one direction defined by μ and ϕ , to another direction defined by μ' and ϕ' . If azimuthal symmetry is assumed, the quantity $\int_0^{2\pi} d\phi \sigma_s(\underline{\Omega}' \cdot \underline{\Omega})$ is independent of ϕ' . Consequently, Eq. (2.1) may be expressed in terms of polar angular dependence as

$$\mu \frac{\partial}{\partial x} \psi(x, \mu) + \sigma_T \psi(x, \mu) = \int_{-1}^{+1} d\mu' \sigma_s(\mu' \rightarrow \mu) \psi(x, \mu') + Q(x, \mu), \quad (2.2)$$

where

$$\psi(x, \mu) \equiv \frac{1}{2\pi} \int_0^{2\pi} d\phi \psi(x, \mu, \phi)$$

is the azimuthally averaged angular density and $\sigma_s(\mu' \rightarrow \mu)$ is the azimuthally averaged elastic scattering cross section from μ' to μ . Similarly, $Q(x, \mu)$ is the azimuthally averaged source in direction μ at position x .

2.1.2 Multigroup Model

It has been pointed out by Davison [5] and others [8,9,7], that a mono-energetic description of neutron transport can be strictly justified only for the case of slightly absorbing media in regions which lie away from sources and boundaries. Division of the energy spectrum into a series of subintervals permits a far more realistic representation of most physical situations, particularly since σ_T and $\sigma_s(\mu' \rightarrow \mu)$ values vary dramatically with energy for many elements [10]. An equation similar to Eq. (2.1) can be written to describe

the source-free, energy-dependent transport of neutrons [5];

$$\mu \frac{\partial}{\partial x} \psi(x, \underline{\Omega}, E) + \sigma_T(E) \psi(x, \underline{\Omega}, E) = \int dE' \int_{\underline{\Omega}'} d\underline{\Omega}' \sigma_s(E' \underline{\Omega}' \rightarrow E, \underline{\Omega}) \psi(x, \underline{\Omega}', E') . \quad (2.3)$$

In this equation, $\sigma_s(E', \underline{\Omega}' \rightarrow E, \underline{\Omega})$ represents the macroscopic scattering transfer cross section from energy E' and direction $\underline{\Omega}'$, to energy E and direction $\underline{\Omega}$.

Before proceeding further, it should be pointed out that for isotropic noncrystalline media, the scattering transfer cross section, $\sigma_s(E', \underline{\Omega}' \rightarrow E, \underline{\Omega})$, may be written in the form $\sigma_s(E' \rightarrow E, \underline{\Omega}' \cdot \underline{\Omega})$. This notation indicates that the scattering probability depends only on the scattering angle rather than on the actual initial and final directions. The scattering cross section can be expressed more formally as the sum of two components; one elastic and the other inelastic. Explicitly,

$$\sigma_s(E' \rightarrow E, \underline{\Omega}' \cdot \underline{\Omega}) = \sigma_{el}(E' \rightarrow E, \mu) + \sigma_{in}(E' \rightarrow E, \mu) , \quad (2.4)$$

where $\mu \equiv \underline{\Omega}' \cdot \underline{\Omega}$, σ_{el} is the elastic scattering cross section, and σ_{in} is the inelastic scattering cross section. Neutrons which undergo inelastic collisions scatter through laboratory angles which are well defined by energy-momentum constraints. Although such constraints differ from those which govern angular distributions for elastically scattered neutrons, the triangular approximating technique developed in this work is equally applicable to the approximation of inelastic group-to-group transfer cross sections. The transition from the approximation of elastic to inelastic scattering distributions can be carried out by replacing the energy-momentum constraints for elastic scattering angular distributions by those constraints for inelastic distributions. Davison [5] points out that for low atomic numbers, inelastic scattering becomes important only at very high energies (higher than the average fission neutron). In most practical situations, inelastic scattering is important

only for elements with large atomic masses. Light element elastic scattering cross section treatment is emphasized in this work with the understanding that inelastic scattering will become an important consideration only for target nuclei with large atomic masses and high energy incident neutrons.

Equation (2.3) may now be used to arrive at a form of the multigroup transport equation. By integrating from E_{g+1} to E_g , the following expression is obtained to describe particle transport in energy group g

$$\mu \frac{\partial}{\partial x} \psi_g(x, \underline{\Omega}) + \sigma_g \psi_g(x, \underline{\Omega}) = \sum_{g'} \int_{\underline{\Omega}'} d\underline{\Omega}' \sigma_{g' \rightarrow g}(\underline{\Omega}' \cdot \underline{\Omega}) \psi_{g'}(x, \underline{\Omega}') , \quad (2.5)$$

where,

$$\psi_g(x, \underline{\Omega}) \equiv \int_{E_{g+1}}^{E_g} dE \psi(x, \underline{\Omega}, E) \quad (2.6)$$

$$\sigma_g \equiv \frac{1}{\psi_g(x, \underline{\Omega})} \int_{E_{g+1}}^{E_g} dE \sigma_T(E) \psi(x, \underline{\Omega}, E) \quad (2.7)$$

$$\sigma_{g' \rightarrow g}(\mu) \equiv \frac{1}{\psi_{g'}(x, \underline{\Omega}')} \int_{E_{g+1}}^{E_g} dE \int_{E_{g'+1}}^{E_{g'}} dE' \sigma_s(E' \rightarrow E, \mu) \psi(x, \underline{\Omega}', E') . \quad (2.8)$$

The group-to-group macroscopic scattering transfer cross section defined by Eq. (2.8) is the portion of the transport equation dealt with most extensively in this work. Therefore, a closer examination of the relationship of $\sigma_{g' \rightarrow g}(\mu)$ to the overall equation, as well as techniques for its numerical determination, are in order.

2.2 Anisotropic Group-to-Group Scattering Cross Sections

To solve the multigroup neutron transport equation, Eq. (2.5), it is necessary to have some analytical expression or numerical method which can be

used to evaluate $\sigma_{g' \rightarrow g}(\mu)$. Although Eq. (2.8) presents one alternative, it is of little use in its present form. One obvious difficulty is that $\psi(x, \underline{\Omega}', E')$ appears explicitly in this equation. If $\psi(x, \underline{\Omega}', E')$ were known, there would be no point in solving the multigroup problem. To free $\sigma_{g' \rightarrow g}(\mu)$ from this explicit dependence upon the angular density, separability of angular and energy components is a common assumption. By allowing $\psi(x, \underline{\Omega}, E)$ to equal $\phi(x, \underline{\Omega}) W(E)$, Eq. (2.8) can be reduced to the following form;

$$\sigma_{g' \rightarrow g}(\mu) = \frac{1}{\Delta_{g'}} \int_{E_{g'+1}}^{E_g} dE \int_{E_{g'+1}}^{E_{g'}} dE' \sigma_s(E' \rightarrow E, \mu) W(E') , \quad (2.9)$$

where,

$$\Delta_{g'} \equiv \int_{E_{g'+1}}^{E_{g'}} dE W(E') . \quad (2.10)$$

By assuming the separability in energy of $\psi(x, \underline{\Omega}, E)$, the evaluation of $\sigma_{g' \rightarrow g}(\mu)$ is no longer contingent upon knowledge of the angular density.

Ginsberg and Becker [11] discuss several possible weighting schemes that might be used for $W(E)$. For the case of an infinite non-absorbing media, the neutron flux is rigorously proportional to the inverse of the neutron energy. This $1/E$ flux weighting is widely used to generate hyperfine multigroup cross section data sets for absorbing and nonabsorbing materials. Actual group averaged cross sections are spatially dependent [12]. However, an underlying assumption behind the use of multigroup methods is that at some level of detail, this inherent spatial dependence can be neglected. For problems where spatial effects are significant, this dependence can be conveniently taken into account when hyperfine group structures are collapsed to few group structures. Whether or not spatial dependence significantly affects few group cross sections depends on the nature of the problem. For example, Becker [13]

points out that for slowing down problems where scattering is predominant and where sources at energies of interest are determined by inscattering, it may be reasonable to assume that spatial dependence is secondary in nature. He points out that spatial dependence is likely to be more significant in problems where absorption is prevalent and scattering is poor. Consequently, evaluation of $\sigma_{g' \rightarrow g}(\mu)$ in this work will be based upon a $W(E) = 1/E$ weighting with the understanding that cross section problems involving significant amounts of absorption (or geometries involving strong flux buckling) may require a modified weighting scheme. Hence, evaluation of angular group-to-group transfer cross sections could be carried out if the elastic scattering transfer cross section, $\sigma_s(E' \rightarrow E, \mu)$, were known.

Odom [3] discusses several computer codes which are currently used to calculate $\sigma_s(E' \rightarrow E, \mu)$ as well as $\sigma_{g' \rightarrow g}(\mu)$. Among those mentioned are SUPERTOG [14], MC**2 [15], and XSDRN [16]. All of these codes make use of conventional Legendre expansion techniques to carry out cross section evaluation.

2.2.1 Legendre Expansion Techniques

Before group-to-group scattering cross sections can be evaluated by Eq. (2.9), empirical data must be obtained for $\sigma_s(E' \rightarrow E, \mu)$. Extensive research over the past twenty years has resulted in detailed tabulations of these data. Common practice has been to express this elastic scattering cross section in a truncated $L+1$ term Legendre polynomial expansion [5,14], namely

$$\sigma_s(E' \rightarrow E, \mu) = \begin{cases} \frac{1}{4\pi} \sum_{\ell=0}^L S_{\ell}(E, E') P_{\ell}(\mu) & \alpha E' \leq E \leq E' \\ 0 & \alpha E' > E \text{ or } E > E' \end{cases}, \quad (2.11)$$

where $\alpha = (A-1)^2/(A+1)^2$. The fact that the elastic scattering cross section is zero for $\alpha E' > E$ or $E' > E$ is derived from collision kinematics for elastic

scattering [7]. This expression for the elastic scattering cross section can now be substituted into Eq. (2.9) to solve for the elastic scattering group-to-group transfer cross section, $\sigma_{g' \rightarrow g}(\mu)$.

Work by Hill [17] and others [3,1], indicate that low order truncation of Legendre expansions for $\sigma_g(E' \rightarrow E, \mu)$ can lead to an inadequate representation of $\sigma_{g' \rightarrow g}(\mu)$. Truncated low order Legendre expansions exhibit particular difficulty in representing the sharply peaked functional behavior of highly anisotropic scattering distributions. Timmons [1] points out that Legendre orders well in excess of 160 terms may be required to eliminate significant oscillations in data sets reduced from DLC2/99G files [18]. The first 26 group-to-group limits for the DLC2 energy structure are given in Table 6. Figures 2 and 3 depict macroscopic angular transfer cross sections for hydrogen scattering between various energy groups in this structure. Results for an eighth order Legendre expansion are compared to exact results computed by BIGD [3]. Note the inability of this low order expansion to represent highly anisotropic behavior of the exact hydrogen cross section. Although sufficient accuracy might be obtained for these cases through use of high order expansions, this approach attains success only at the expense of a dramatic increase in computational time.

2.2.2 Exact Kernel Techniques

The exact kernel approach was applied by Odom [3] to avoid Legendre expansion of the elastic scattering transfer cross section. Subsequent development of a triangular approximation to $\sigma_{g' \rightarrow g}(\mu)$ for hydrogen, as well as other elements, will in part be based upon this approach. Therefore, a brief outline of this technique is presented in this section. Although the development provided here is somewhat different than that presented by Odom, the same results are obtained [19].

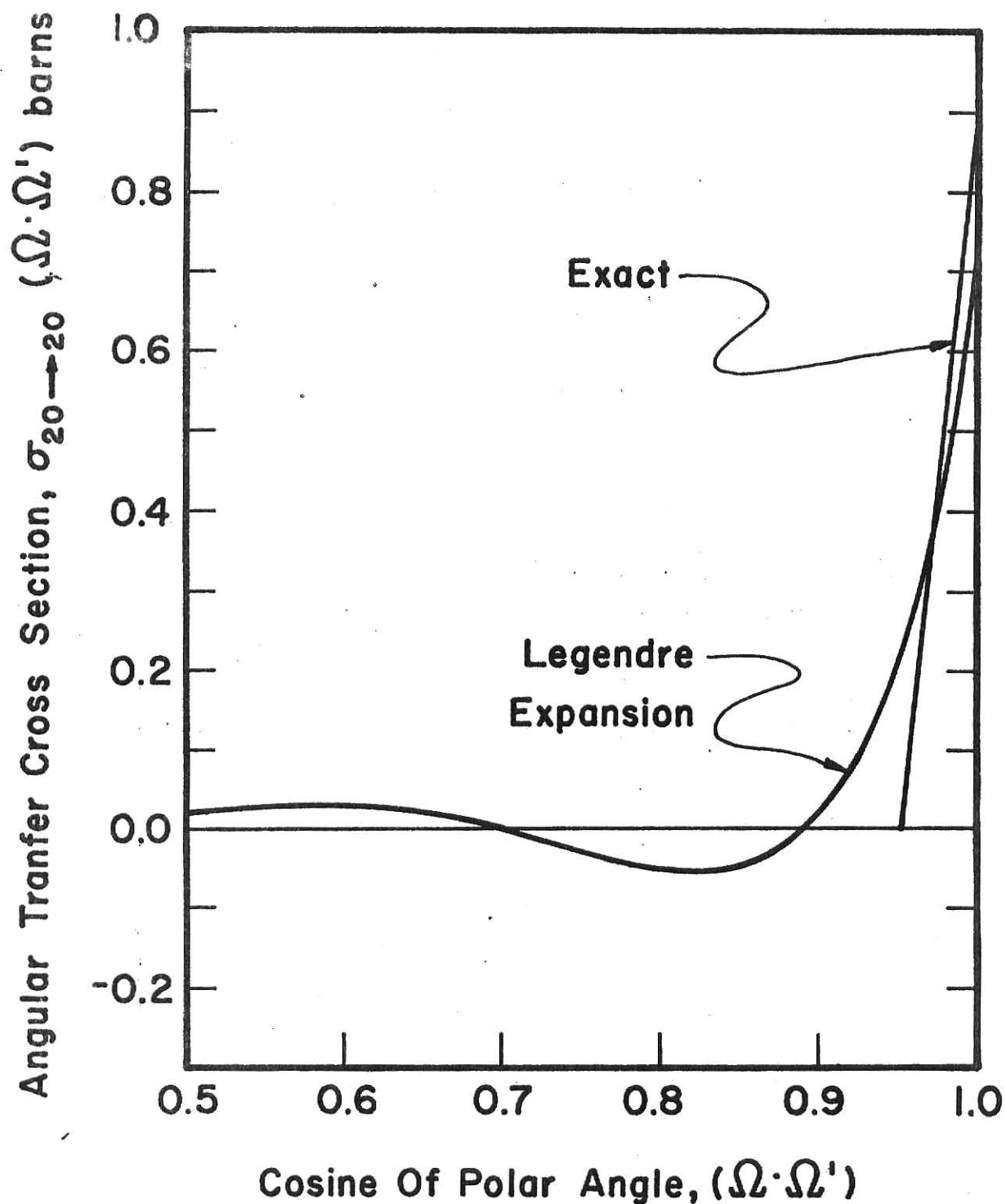


Figure 2. Comparison of the angular transfer cross section for hydrogen DLC/2 group 20 to 20 transfer as calculated exactly by BIGD(3) and by an eighth order Legendre expansion (DLC/2 Group 20 = 2.2313-2.0190 MeV)

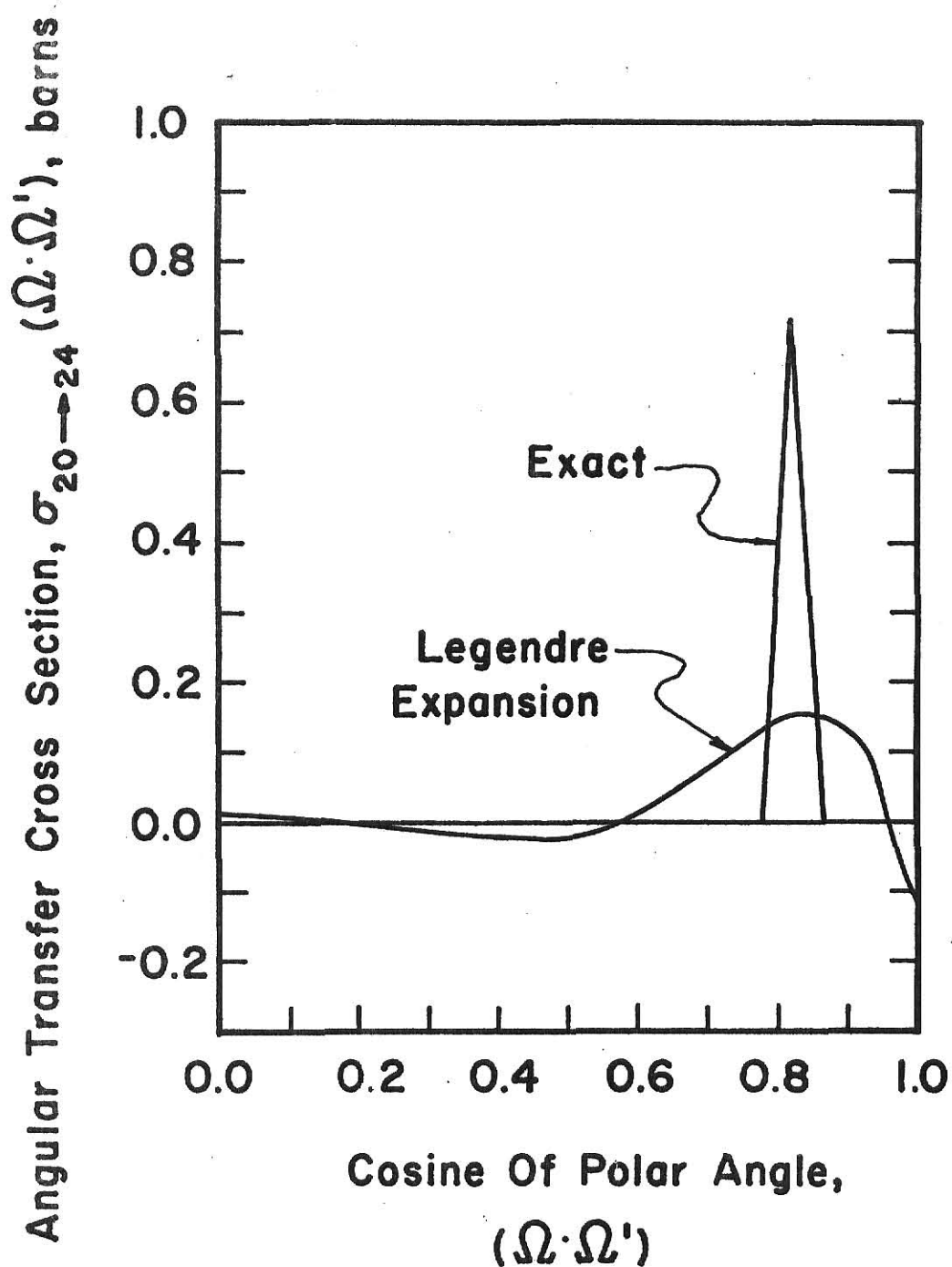


Figure 3. Comparison of the angular transfer cross section for hydrogen DLC/2 groups 20 to 24 transfer as calculated exactly by BIGD(7) and by an eighth order Legendre expansion. (Group 20 = 2.2313-2.0190 MeV, Group 24 = 1.4957-1.3534 MeV)

The general approach to the exact kernel technique is based on the fact that for elastic scattering of neutrons from nuclei of mass number A , the cosine of the scattering angle, μ , is uniquely determined by energy-momentum constraints [6]. Explicitly,

$$\mu = 0.5 [(A+1)\sqrt{E/E'} - (A-1)\sqrt{E'/E}] \equiv S(E, E') \quad (2.12)$$

Because of this relationship the differential elastic scattering cross section, $\sigma_g(E' \rightarrow E, \mu)$, must be proportional to a delta function which imposes the kinematic constraints of Eq. (2.12). In particular, one may write

$$\sigma_g(E' \rightarrow E, \mu) dE = \begin{cases} \sigma_g(E') \sigma(E', \eta) \delta[\mu - S(E, E')] d\eta & \alpha E' < E < E' \\ 0 & \alpha E' > E \text{ or } E > E' \end{cases} \quad (2.13)$$

where $\delta[\mu - S(E, E')]$ expresses the kinematic constraints imposed by conservation of energy and momentum, and η is the cosine of the center of mass scattering angle given by [14]

$$\eta = 1 - \frac{(A+1)^2}{2A} \left(1 - \frac{E}{E'} \right) . \quad (2.14)$$

Most nuclear data sets report differential elastic scattering cross sections, $\sigma(E, \eta)$, in terms of the center of mass scattering angle η . In the center of mass system, this differential scattering cross section is a much smoother function of angle than in the laboratory system. For example, low energy scattering in the center of mass tends toward isotropism, and consequently, $\sigma(E, \eta)$ varies only slightly with η . In the laboratory system, such isotropic trends are difficult to realize.

By combining the expression for η and $\sigma_g(E' \rightarrow E, \mu)$ from Eqs. (2.13) and (2.14) with Eq. (2.9), $\sigma_{g' \rightarrow g}(\mu)$ may be written as follows:

$$\sigma_{g' \rightarrow g}(\mu) = \frac{1}{(1-\alpha)\Delta_{g'}} \int_{E_{g'+1}}^{E_g} dE \int_{E_{g'+1}}^{E_{g'}} \frac{dE'}{E'} \sigma_s(E') \sigma(E', \eta) W(E') \delta[\mu - S(E, E')] . \quad (2.15)$$

Evaluation of this integral can be simplified by examining the region of integration in the (E, E') plane. Figure 4 illustrates the domain of this region. According to Eq. (2.13), the integral is zero unless $(\alpha E' \leq E \leq E')$. Therefore, the area to be integrated must be some subset of region 1 in Fig. 4. Furthermore, since the integral over a delta function is zero unless its range of integration includes the support of the delta function, the double integration of Eq. (2.15) is equivalent to integration along the line defined by $\mu = S(E, E')$ [33]. From Eq. (2.12), this corresponds to an integration in the (E, E') space along the line

$$E' = \frac{E(A+1)^2}{[(A^2 - 1 + \mu^2)^{1/2} + \mu]^2} \equiv E\Gamma(\mu) . \quad (2.16)$$

Since $(-1 \leq \mu \leq 1)$, it is apparent from the above equation that $[1 \leq \Gamma(\mu) \leq (1/\alpha)]$. This means that the line of integration (i.e. $\mu = S(E, E')$ or $E' = E\Gamma(\mu)$) will always lie within region 1 of Fig. 4. From Eq. (2.16), $\sigma_{g' \rightarrow g}(\mu)$ may now be rewritten in the following form

$$\begin{aligned} \sigma_{g' \rightarrow g}(\mu) &= \frac{2}{(1-\alpha)\Delta_{g'}} \int dE \sigma_s(E\Gamma) \sigma(E\Gamma, \eta) W(E\Gamma) \frac{1}{E\Gamma} \\ &\times \int_{E_{g'+1}}^{E_{g'}} dE' \delta[\mu - S(E, E')] \end{aligned} \quad (2.17)$$

The integration over E' is trivial, namely

$$\int_{E_{g'+1}}^{E_g} dE' \delta[\mu - S(E, E')] = |\Gamma'| E \int_{-\infty}^{+\infty} d\mu \delta[\mu - S(E, E')] = |\Gamma'| E \quad (2.18)$$

Substitution of this result into Eq. (2.17) yields

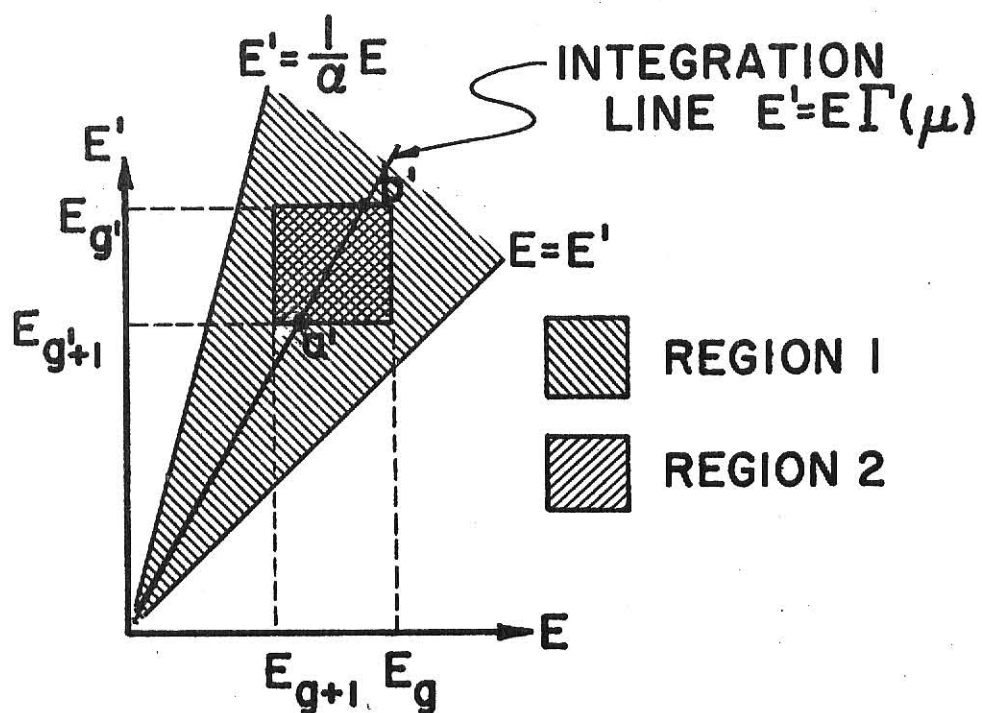


Figure 4. Integral evaluation of $\sigma_{g' \rightarrow g}(\mu)$ in the (E, E') plane

$$\sigma_{g' \rightarrow g}(\mu) = \frac{2}{(1-\alpha)\Delta_{g'}} \int dE \sigma_s(E\Gamma) \sigma(E\Gamma, \eta) W(E\Gamma) \frac{|\Gamma'|}{\Gamma} . \quad (2.19)$$

From Eq. (2.16),

$$\frac{|\Gamma'|}{(\Gamma)^2} = \frac{2}{(A+1)^2} \left(2\mu_o + \sqrt{\mu^2 + A^2 - 1} + \frac{\mu^2}{\sqrt{\mu^2 + A^2 - 1}} \right) \equiv g(\mu) \frac{2}{(A+1)^2} . \quad (2.20)$$

Therefore, the angular group to group scattering cross section may be written as

$$\sigma_{g' \rightarrow g}(\mu) = \frac{g(\mu)}{A\Delta_{g'}} \int_{a'}^{b'} \Gamma dE \sigma_s(E\Gamma) \sigma(E\Gamma, \eta) W(E\Gamma) \quad (2.21)$$

Notice that the range of integration in Eq. (2.21) is from a' to b' as shown in Fig. 4. These limits do not directly correspond to the E_g and E_{g+1} limits of Eq. (2.15). It has already been shown how the region of integration for this equation is a subset of region 1 in Fig. 4. The region of integration is further restricted by integration limits imposed in Eq. (2.15). Figure 4 illustrates how integration along the delta function integration line is constrained to region 2. Hence, integration limits Eq. (2.21) merely become the points at which the delta function integration line intersects the region 2 boundaries, namely

$$a' = \max[E_{g+1}, (E_{g'+1}/\Gamma)] , \quad (2.22)$$

$$b' = \min[E_g, (E_g/\Gamma)] . \quad (2.23)$$

If no intersection exists, the transfer cross section is zero.

Equation (2.21) can be put in a more convenient form by defining the variable $Z \equiv E\Gamma(\mu)$, namely

$$\sigma_{g' \rightarrow g}(\mu) = \frac{g(\mu)}{A\Delta_{g'}} \int_a^b dZ \sigma_s(Z) \sigma(Z, \eta) W(Z) , \quad (2.24)$$

where

$$a = \max(E_{g+1}, E_{g'+1}) , \quad (2.25)$$

$$b = \min(E_g, E_{g'}) , \quad (2.26)$$

$$\Delta_{g'} \equiv \int_{E_{g'+1}}^{E_{g'}} dE W(E) , \quad (2.27)$$

and

$$g(\mu) \equiv 2\mu + \sqrt{\mu^2 + A^2 - 1} + \frac{\mu^2}{\sqrt{\mu^2 + A^2 - 1}} . \quad (2.28)$$

To perform the remaining integration in Eq. (2.24), an explicit form of the differential scattering distribution, $\sigma(Z, \eta)$, must be obtained. For all realistic scattering situations $\sigma(Z, \eta)$ must be determined experimentally [20]; therefore, $\sigma_{g' \rightarrow g}(\mu)$ in Eq. (2.24) must be evaluated numerically.

Finally, it should be noted that the expression for $\sigma_{g' \rightarrow g}(\mu)$ of Eq. (2.24) is considerably simpler in form than the exact results reported by Odom [3]. Consequently, this equation lends itself to a greatly simplified numerical evaluation. However, the two results are equivalent. The same numerical values can be obtained from either formulation.

2.3 Cross Section Approximation

In this section, it is shown that the methods which may be used to approximate anisotropic group-to-group scattering cross sections greatly depend upon the group energy structure under consideration. The general case where a neutron downscatters between two energy groups of arbitrary width is considered first. For this case, it is shown that elastic scattering group-to-group transfer cross sections can be well-approximated by quadrilaterally shaped distributions. If an energy structure based upon equal lethargy widths is used, a simpler triangular shaped distribution can be used to approximate the transfer cross section.

2.3.1 Approximation of $\sigma_{g' \rightarrow g}(\mu)$ for General Multigroup Energy Structures

The development of an approximate form for the group-to-group scattering cross sections begins with the exact result of Eq. (2.24). The integral limits of this equation can be categorized into one of three domains depending upon the exact value of $\Gamma(\mu)$. Figure 5 illustrates the range of the three domains in the (E, E') plane (also refer to Fig. 4). The integral limits for Eq. (2.24) in each of the three domains are:

$$\text{domain 1} \quad \begin{cases} a = E_{g+1} \\ b = E_g, \Gamma(\mu) \end{cases}, \quad (2.29)$$

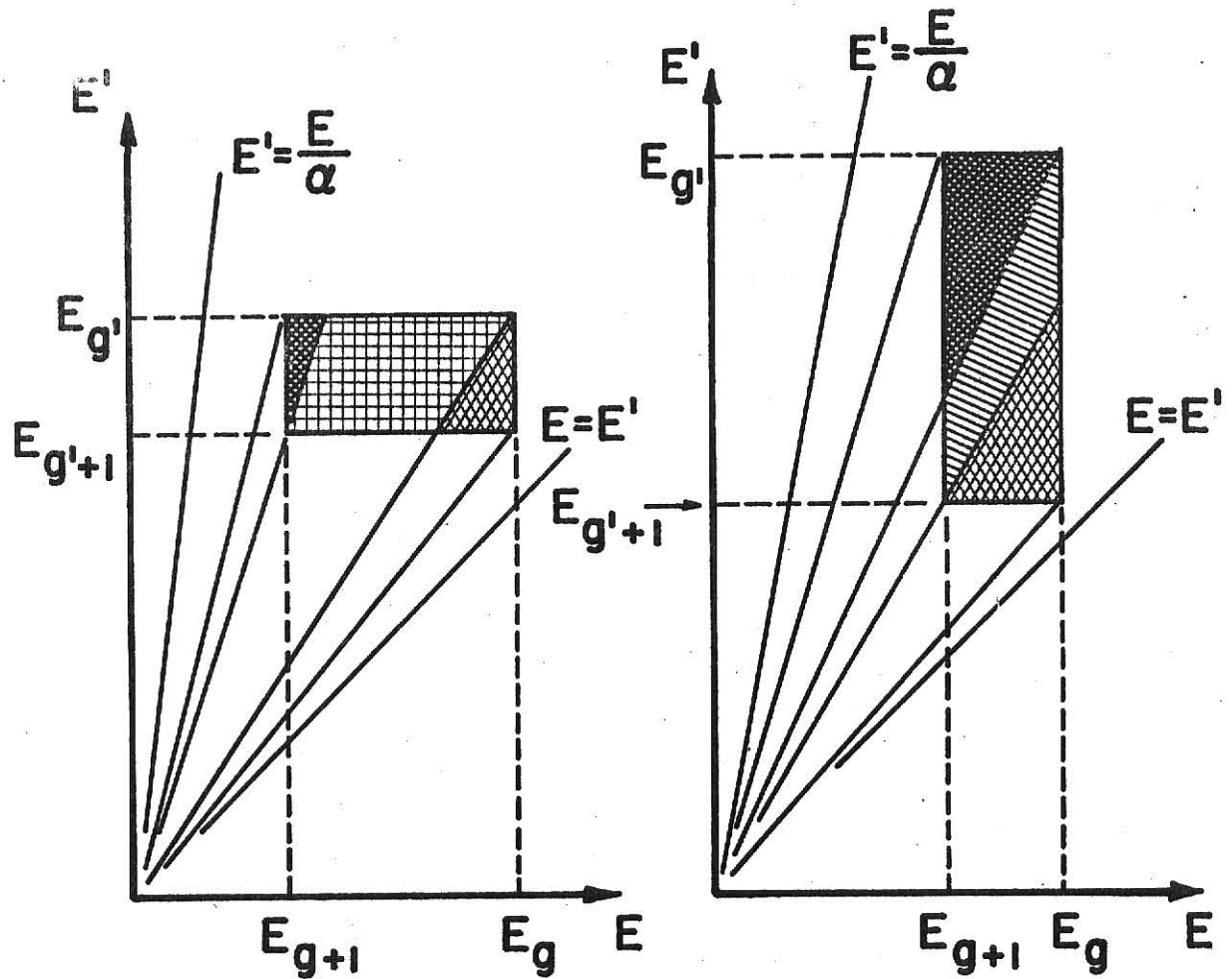
$$\text{domain 2'} \quad \begin{cases} a = E_{g'+1} \Gamma(\mu) \\ b = E_g, \Gamma(\mu) \end{cases}, \quad \text{if } (E_g - E_{g+1}) > (E_{g'} - E_{g'+1}), \quad (2.30)$$





$$\text{domain 2} \quad \begin{cases} a = E_{g+1} \\ b = E_g \end{cases}, \quad \text{if } (E_g - E_{g+1}) < (E_{g'} - E_{g'+1}), \quad (2.31)$$

$$\text{domain 3} \quad \begin{cases} a = E_{g'+1} \Gamma(\mu) \\ b = E_g \end{cases}. \quad (2.32)$$

In order to demonstrate that Eqs. (2.29)-(2.32) may be used for the development of a simple and accurate model for group-to-group cross sections, it is assumed that $\sigma_g(E)$ and $\sigma(E, \eta)$ in Eq. (2.24) are approximately constant over the range $[a, b]$. The assumption that $\sigma(E, \eta)$ is constant implies that center of mass scattering is isotropic; i.e., $\sigma(E, \eta) = 1/4 \pi$. This assumption is strictly valid for the hydrogen case where $A=1.0$ for energies less than about 30 MeV. However, scattering cross sections for $A>1$ are not always isotropic. Buttlar [21] points out that if (k) is the wave number of the incident neutron and (R) is its atomic radius, then when $kR \ll 1$, scattering in the center of mass system will be predominantly isotropic. Since $k \sim \sqrt{E}$ and $R \sim A$, one

Figure 5. Three integral domains in the (E, E') plane for which the integration limits in Eq. (2.24) differ



-  DOMAIN 1 = $(E_{g'+1} \geq E_{g+1} \Gamma')$
-  DOMAIN 2 = $(E_{g'+1} \geq E_{g+1} \Gamma', E_{g'} \geq E_g \Gamma')$
-  DOMAIN 2' = $(E_{g'+1} \leq E_{g+1} \Gamma', E_{g'} \geq E_g \Gamma')$
-  DOMAIN 3 = $(E_{g'} \leq E_g \Gamma')$

would expect to find isotropic center of mass scattering dominant for small A values and low neutron energies. As (kR) approaches one, center of mass scattering ceases to be isotropic. The angular distribution tends to peak in the forward direction. In other words, neutrons most frequently scatter through small angles. Consequently, the assumption of isotropic center of mass scattering for $A > 1$ can be expected to account for some of the differences noted between various approximate and exact group-to-group transfer cross sections values calculated in this section. The second assumption, that $\sigma_s(E)$ is nearly constant over the range $[a, b]$, can be used to account for the remaining portion of the differences. This later assumption is valid for energy group structures in which the nearness of adjacent group limits preclude any dramatic in-group variation of $\sigma_s(E)$. Thus, this assumption is poor for energy ranges which contain many sharp resonance peaks. However, it becomes reasonably accurate for situations involving fine energy structures and relatively smooth cross sections.

Consider the evaluation of Eq. (2.24) for the widely used case of $W(E) = 1/E$. By assuming $[\sigma_s(E)\sigma(\eta, E) = C]$ where C is a constant, the expression for $\sigma_{g' \rightarrow g}(\mu)$ then reduces to

$$\sigma_{g' \rightarrow g}(\mu) = \frac{g(\mu)C}{A\Delta_{g'}} \ln\left(\frac{b}{a}\right) . \quad (2.33)$$

By replacing (a) and (b) with their explicit values in terms of the group limits given by Eqs. (2.29), (2.30), and (2.32), the following expressions result for the three respective regions represented in Fig. 3:

$$\text{Domain 1, } \sigma_{g' \rightarrow g}(\mu) = \frac{g(\mu)C}{A\Delta_{g'}} \ln \frac{E_{g'}}{E_{g'+1} \Gamma(\mu)} , \quad (2.34)$$

$$\text{Domain 2, } \sigma_{g' \rightarrow g}(\mu) = \frac{g(\mu)C}{A\Delta_{g'}} \ln \frac{E_{g'}}{E_{g'+1}} , \quad (2.35)$$

$$\text{Domain 3, } \sigma_{g' \rightarrow g}(\mu) = \frac{g(\mu)C}{A\Delta_{g'}} \ln \frac{E_g \Gamma(\mu)}{E_{g'+1}} \quad (2.36)$$

It is instructive to examine these three equations for two important special cases. The first case of interest is that when $A=1$. For this situation, $g(\mu)=4\mu$ and $\Gamma(\mu)=1/\mu^2$. In this circumstance, it is obvious from Eq. (2.35) that $\sigma_{g' \rightarrow g}(\mu)$ is a linear function of μ for region 2 of Fig. 5. Further examination suggests that Eqs. (2.34) and (2.36) may also be represented by linear functions. This linearity can be seen by taking the derivatives of these two equations. They are

$$\frac{d}{d\mu} [\sigma_{g' \rightarrow g}(\mu)] = \frac{4C}{\Delta_{g'}} \left(\ln \left(\frac{E_g \mu^2}{E_{g'+1}} \right) + 2 \right) \quad (2.37)$$

$$\frac{d}{d\mu} [\sigma_{g' \rightarrow g}(\mu)] = \frac{4C}{\Delta_{g'}} \left(\ln \left(\frac{E_g}{E_{g'+1} \mu^2} \right) - 2 \right) \quad (2.38)$$

Notice from Eq. (2.12) that when $A=1$, μ is constrained between μ_{\max} and μ_{\min} where,

$$\mu_{\max} = \sqrt{E_{g+1}/E_{g'}} \quad \text{and} \quad \mu_{\min} = \sqrt{E_g/E_{g'+1}} \quad (2.39)$$

Furthermore, recall that energy groups have been assumed to be narrow. Consequently, (E_{g+1}/E_g) and $(E_{g'+1}/E_{g'})$ are approximately unity. These conditions can be used to show that the logarithmic term in Eqs. (2.37) and (2.38) tends to zero. Hence, $\frac{d}{d\mu} [\sigma_{g' \rightarrow g}(\mu)]$ is nearly constant for Eqs. (2.34)–(2.36); all three equations may be approximated by linear functions. A similar situation is encountered when these equations are examined for the special case where $A^2 \gg 1$. Under this condition, $\Gamma(\mu) \approx 1$ and $g(\mu) \approx (2\mu+A)$. Substitution of these quantities into Eqs. (2.34)–(2.36) again yields an approximate linear representation in μ for $\sigma_{g' \rightarrow g}(\mu)$.

The purpose for demonstrating approximate piecewise linearity of $\sigma_{g' \rightarrow g}(\mu)$ is not to derive some approximate form of the group-to-group transfer cross section. Rather, the purpose is to justify a low order approximation for the transfer cross section. Figure 6 depicts exact oxygen angular scattering cross sections for three group-to-group energy transfers. Notice how in each case, the exact angular distribution is well approximated by piecewise linear functions. In particular, the cross sections for transfer from groups 18 to 19' and 19' to 20 resemble trapezoidal angular distributions. The area under the distribution is equal to the total scattering cross section from group g' to g , i.e.;

$$\sigma_{g' \rightarrow g}^{\text{tot}} = \int_{\underline{\Omega}} d\underline{\Omega} \sigma_{g' \rightarrow g}(\underline{\Omega} \cdot \underline{\Omega}') \quad . \quad (2.40)$$

The upper vertices of the trapezoid correspond to the values of μ which cause a change of integration limits in Eq. (2.24), (i.e., where the change from domain 1 to 2 or 2 to 3 occurs in Fig. 5). Hence the trapezoid's vertices occur at

$$\mu = S(E_g, E_{g'}) \quad \text{and} \quad \mu = S(E_{g+1}, E_{g'+1}) \quad . \quad (2.41)$$

This trapezoid concept has been applied to approximate two of the exact cross sections illustrated in Fig. 4. Note that in each case, the approximate distribution accurately models the exact oxygen cross section.

Of particular interest in Fig. 6 is the transfer from DLC2 group 18 to 19. Unlike the previous examples for groups 18 to 19' and 19' to 20 where transfer occurred between groups of different lethargy widths, transfer is now between two groups of equal lethargy widths. Consequently, the integration line in Fig. 4 passes through the points $E_g = E_{g'}$ and $E_{g+1} = E_{g'+1}$ simultaneously whenever $\Gamma(\mu)$ equals $(E_g/E_{g'})$ or $(E_{g+1}/E_{g'+1})$. For the case of equal lethargy group

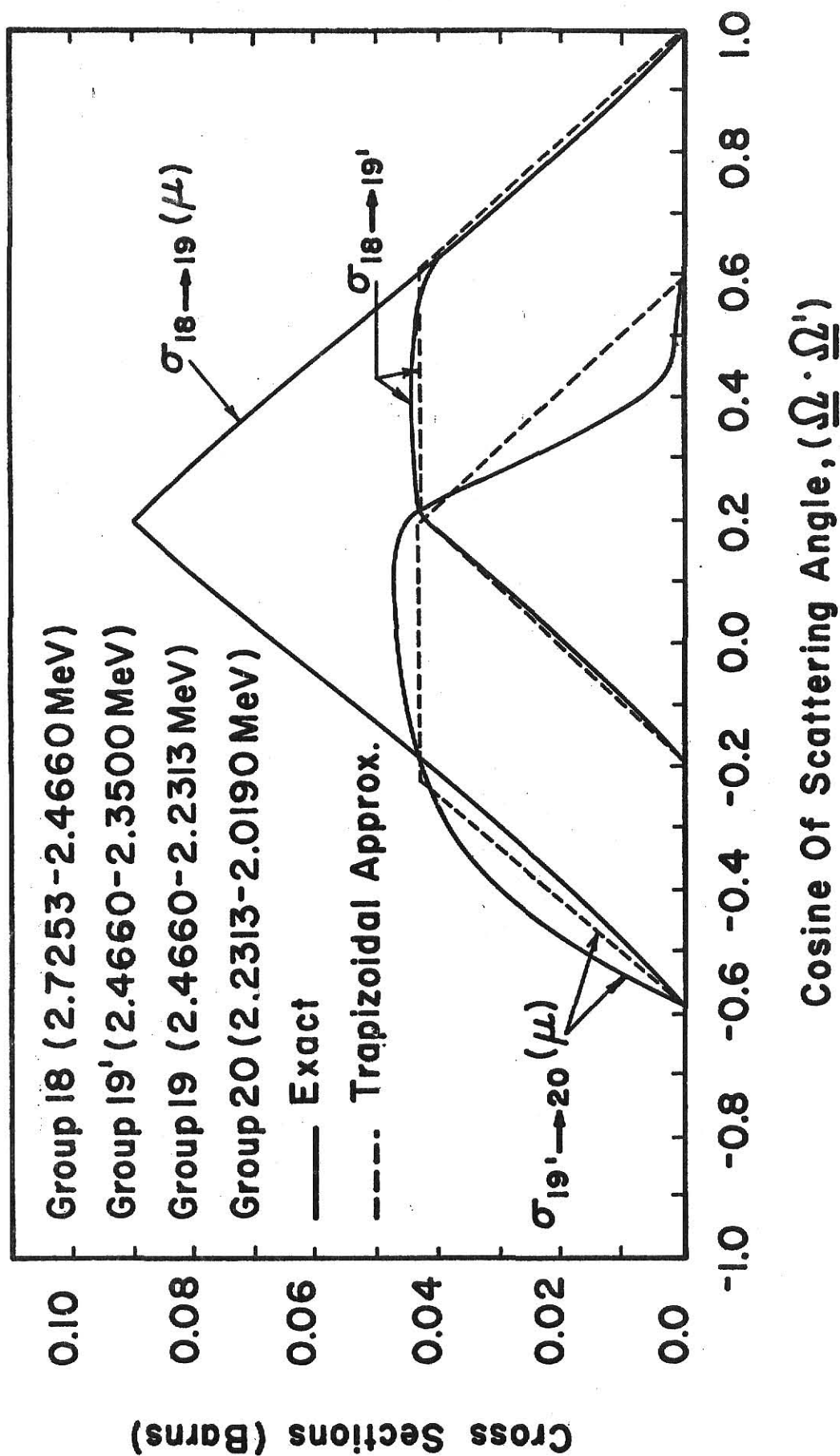


Figure 6. Oxygen angular scattering cross section for scattering between energy groups of unequal lethargy widths

structures, domain 1 in Fig. 5 will directly adjoin domain 3. Domain 2 does not exist; the flat top portions of trapezoidal distributions vanish. Only a triangular representation remains. This is a very simple, but useful, representation since equal lethargy group energy structures are widely used for many multigroup transport calculations [18,22].

2.3.2 Approximation of $\sigma_{g' \rightarrow g}(\mu)$ for Energy Structures Having Equal Lethargy Widths

It has already been pointed out how the approximate trapezoidal representation of a group-to-group scattering cross section reduces to an approximate triangular distribution for energy structures based upon equal lethargy widths. Characteristics of the triangular distribution are easily evaluated. The angular support, or base of the triangular distribution is determined by energy-momentum constraints imposed by Eq. (2.12), i.e., the cosine of the scattering angle, μ , must lie between,

$$\mu_{\max} = \max[-1, S(E_{g+1}, E_{g'})] \quad \text{and} \quad \mu_{\min} = \min[1, S(E_{g'+1}, E_g)] \quad (2.42)$$

where E_g , E_{g+1} , $E_{g'}$, and $E_{g'+1}$ are the group limits for transfer from group g' to g . Note that values of $S(E, E')$ as defined by Eq. (2.12) may lie outside the range $[-1, 1]$. To avoid assigning such meaningless values to the cosine of a scattering angle, μ_{\max} and μ_{\min} are required by Eq. (2.42) to lie on the interval $[-1, 1]$. The apex of the triangle occurs at μ_{mid} where,

$$\mu_{\text{mid}} = S(E_g, E_{g'}) . \quad (2.43)$$

As with μ_{\max} and μ_{\min} , μ_{mid} is also required to lie on the interval $[-1, 1]$.

If μ_{mid} as calculated by Eq. (2.43) lies outside this range, it is set equal to the nearest interval value (i.e., +1 or -1). The height, h , of the triangle at the apex is evaluated from knowledge of the total group-to-group scattering cross section. When $\mu_{\max} = S(E_{g+1}, E_{g'})$ and $\mu_{\min} = S(E_{g'+1}, E_g)$ where $S(E_{g'+1}, E_g)$ and

$S(E_{g+1}, E_{g'})$ are elements of $[-1, 1]$, then

$$h = \frac{2 \sigma_{g' \rightarrow g}^{\text{tot}}}{\mu_{\min} - \mu_{\max}} \quad (2.44)$$

Therefore, the equations which can be used to triangularly approximate anisotropic group-to-group scattering cross sections are

$$\sigma_{g' \rightarrow g}(\mu) = \frac{\mu - \mu_{\max}}{S(E_g, E_{g'}) - \mu_{\max}} h \quad (2.45)$$

when $\mu_{\max} < \mu < S(E_g, E_{g'})$, and

$$\sigma_{g' \rightarrow g}(\mu) = \frac{\mu_{\min} - \mu}{\mu_{\min} - S(E_g, E_{g'})} h \quad (2.46)$$

when $\mu_{\min} > \mu > S(E_g, E_{g'})$.

It is possible when $A > 1$ for values of μ_{\max} to lie beyond the (-1) edge of the $[-1, 1]$ range. Examples of two such cases are illustrated in Figs. 7 and 8. To correctly evaluate $\sigma_{g' \rightarrow g}(\mu)$ for cases such as these, a slight modification of Eq. (2.44) is needed

$$h^* = \frac{2 \sigma_{g' \rightarrow g}^{\text{tot}}}{b_1 + b_2 + \frac{b_2 b_3}{b_2 + b_3}} \quad (2.47)$$

where b_1 , b_2 , and b_3 are defined in Fig. 9.

The computer code LITTLED (Appendix A) calculates triangularly approximated scattering transfer cross sections for elements with $A > 1$. The only inputs required by this code are a multigroup equal lethargy energy structure, and the total group-to-group scattering cross sections (i.e., the zeroth Legendre moments) for the particular element and group structure under consideration. Comparison between exact and triangularly approximated values are discussed in the next section.

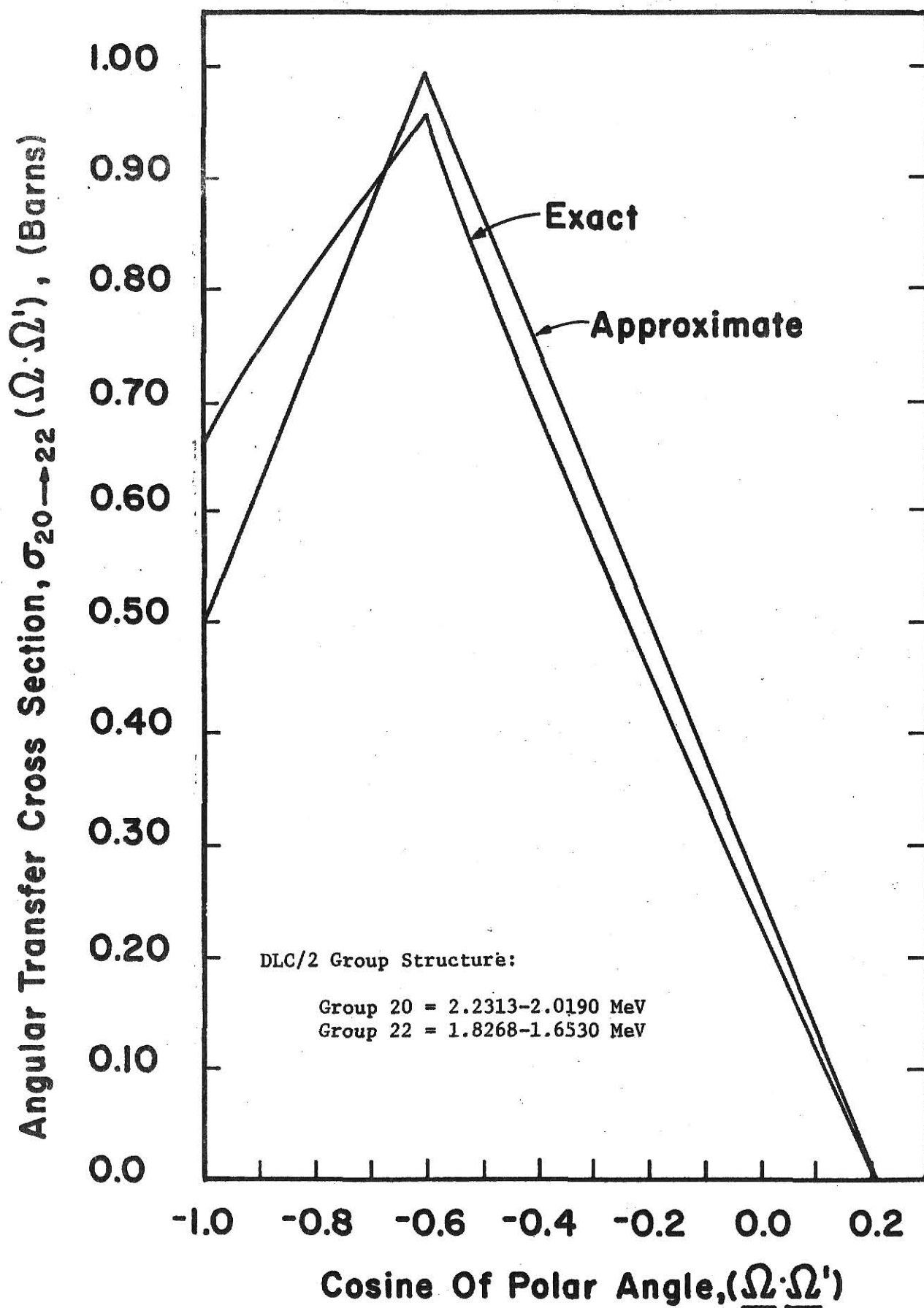


Figure 7. Comparison of the angular transfer cross section for oxygen group 20 to 22 as calculated exactly by BIGD (3)

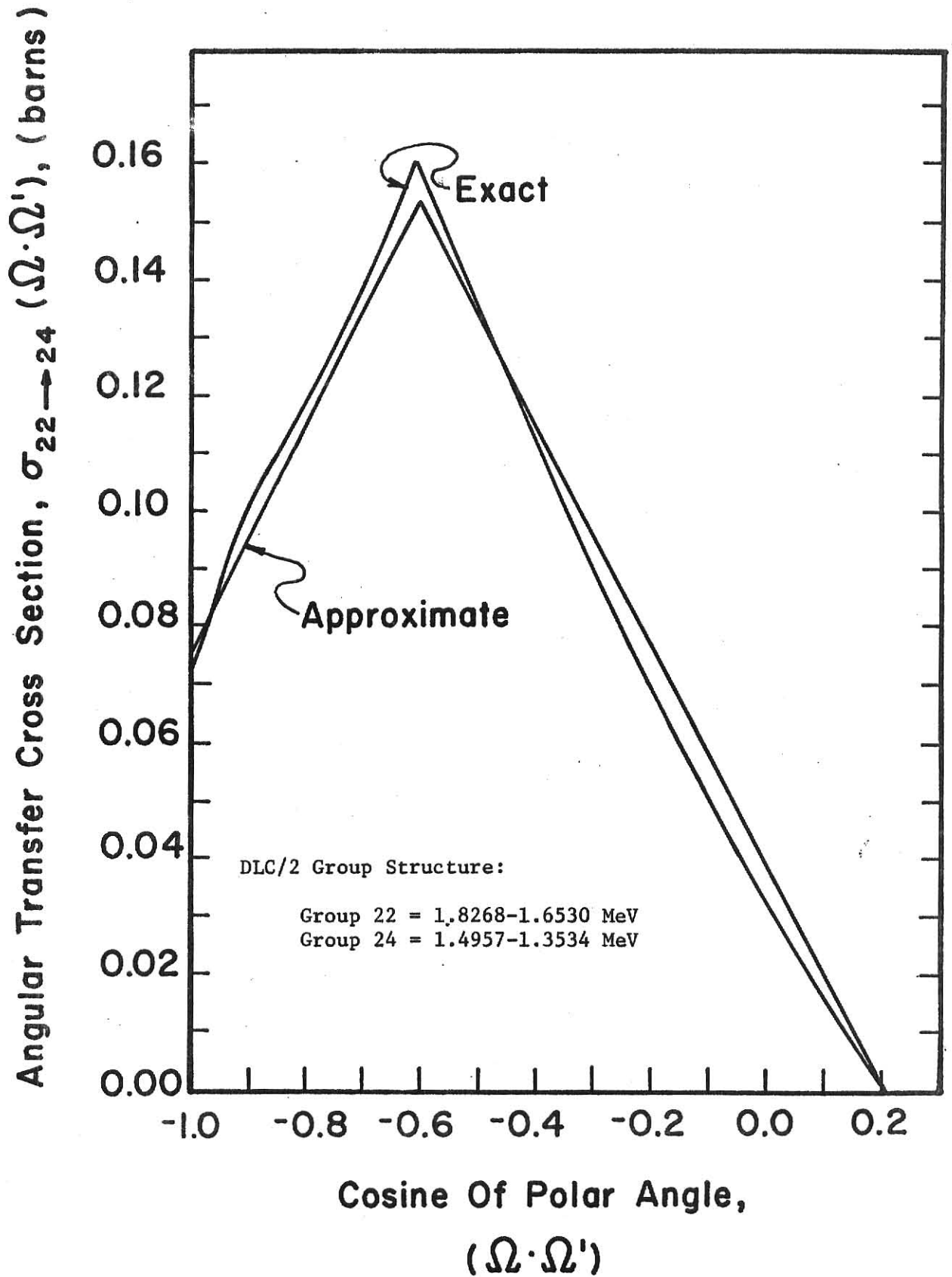


Figure 8. Comparison of the angular transfer cross section for oxygen group 22 to 24 as calculated exactly by BIGD(3) and as triangularly approximated by LITTLED

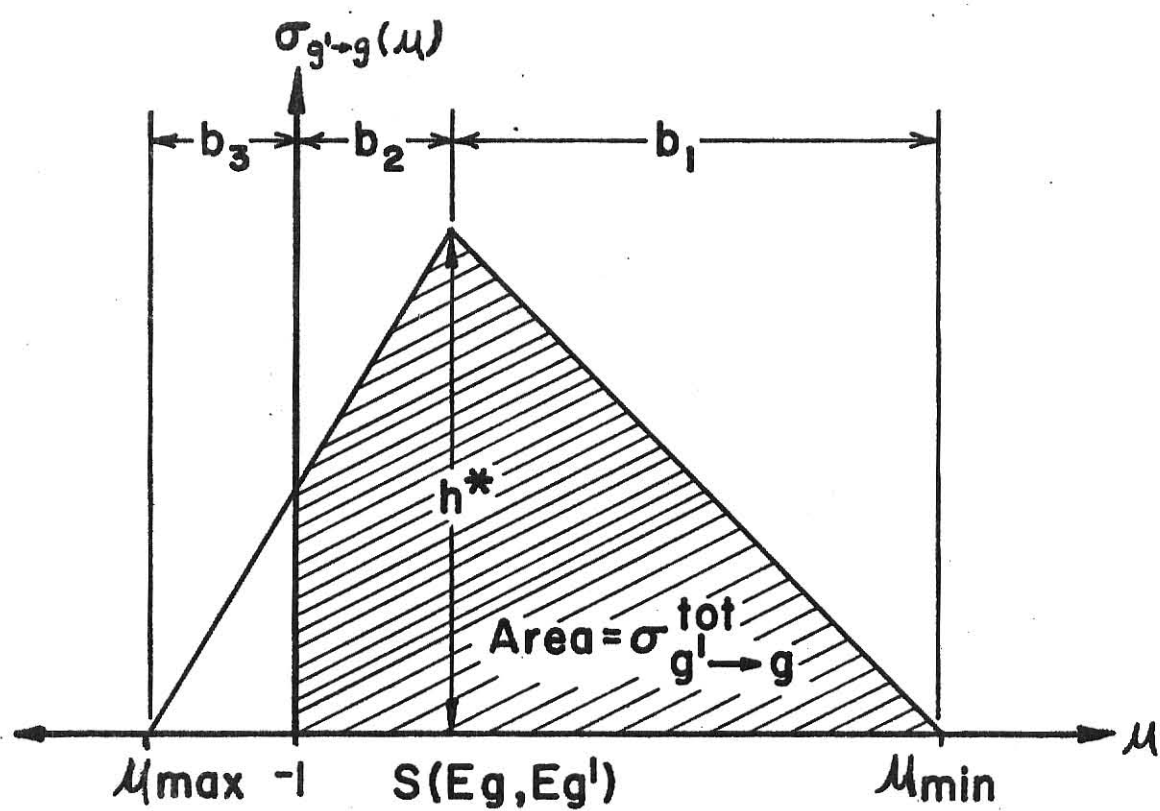


Figure 9. Evaluation of the approximating triangle's height for the case where μ_{\max} lies beyond the (-1) limit

2.3.3 Comparison of Exact and Triangularly Approximated Elastic Transfer Cross Sections

Equations (2.45) and (2.46) suggest simple approximate relations for evaluation of group-to-group scattering cross sections. Before any statements concerning the usefulness of these approximations can be made, some knowledge of their accuracy must be known. In this context, accuracy refers to how well a triangular approximating distribution models the actual transfer cross section. The present work has examined this question for hydrogen and oxygen data.

In Fig. 10 and Table 1, approximated $\sigma_{20 \rightarrow 23}(\mu)$ values for hydrogen are compared to exact results from the computer program BIGD [3]. There is no significant difference in numerical values. Approximated hydrogen transfer cross sections for $\sigma_{20 \rightarrow 20}(\mu)$ and $\sigma_{20 \rightarrow 24}(\mu)$ in Figs. 2 and 3 compare so well with exact values that the discrepancies cannot be shown within the resolutions of the figures. It has been found that the triangular approximation provides an excellent description of hydrogen scattering transfer cross sections for the case of equal lethargy width group structures.

Recall from Section 2.3.1 that the approximation of $\sigma_{g' \rightarrow g}(\mu)$ by a piecewise linear function was developed under the assumption that $[\sigma_g(E)\sigma(E,\eta)]$ is approximately constant over narrow energy intervals. Indeed, hydrogen scattering is isotropic in the center of mass system up to energies of about 35 MeV. It also has an essentially constant elastic scattering cross section, $\sigma_g(E)$, below 100 keV. Above this value this cross section begins to decrease. However, the decrease is relatively slow when compared to the DLC2 group energy width used for cross section evaluations in Figs. 1, 2, and 10. For these reasons, the excellent agreement between triangular and exact hydrogen elastic transfer cross sections is to be expected.

For the case of oxygen, however, $\sigma_g(E)$ does not always vary slowly between group-to-group energy limits. Furthermore, scattering is not isotropic

Table 1. Comparison of Exact and Triangularly
Approximated Transfer Cross Sections
for Hydrogen Group 20 to 23 Transfer
(DLC2/99G Structure).

<u>Scattering Angle, μ</u>	<u>Exact, (barn)</u>	<u>Approximate, (barn)</u>
0.819	0.000	0.000
0.830	0.189	0.197
0.840	0.384	0.395
0.851	0.584	0.592
0.862	0.751	0.752
0.873	0.571	0.564
0.883	0.386	0.376
0.894	0.195	0.189
0.903	0.039	0.038

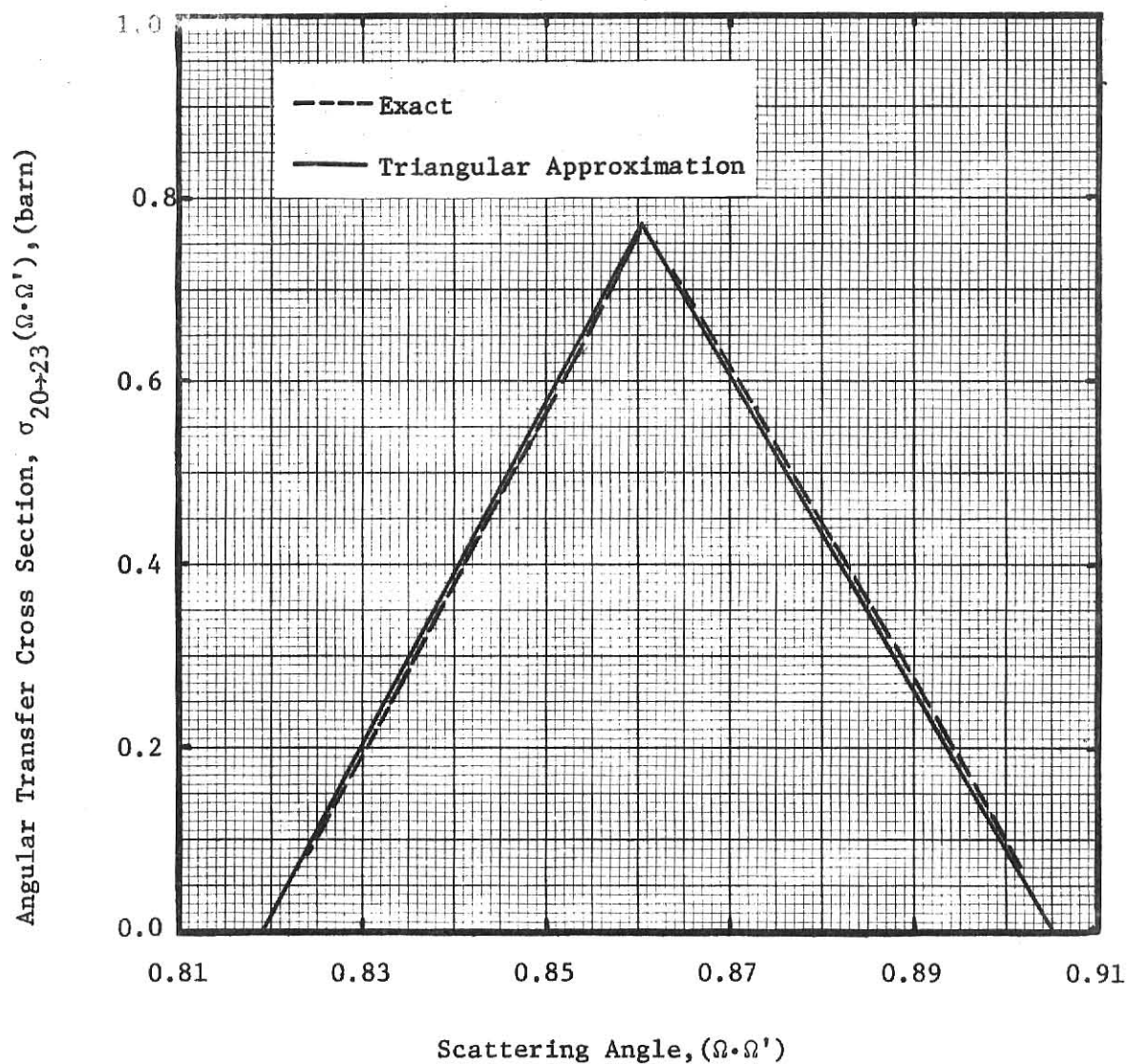


Figure 10. Comparison of hydrogen DLC/2 group 20 (2.2313–2.0190 MeV) to 23 (1.6530–1.4957 MeV) angular transfer cross section as calculated by exact kernel and triangular techniques

in the center of mass, particularly in the resonance energy regions. Consequently slightly poorer agreement of exact and approximate elastic transfer cross section calculation should be expected. Figures 7, 8, and 11 compare triangular approximations with their corresponding exact value from Eq. (2.24). Relative shapes compare favorably; however, more significant deviations are observed than were noted for the similar hydrogen results. Several of the exact cross sections in Fig. 11 exhibit mild curvature between their base point and peak value as well as a shift of the distribution from the mid points. This curvature and distortion of the ideal triangular shape can be attributed to the variation of the differential elastic scattering cross section, $\sigma(E, \eta)$. This cross section is a rapidly varying function of both E and η in the neighborhood of resonances in addition to being highly peaked in the forward scattering direction for large values of E . On Fig. 11, $\sigma_{1 \rightarrow 1}$ is shifted towards the forward scattering angles since $\sigma_s(E, \eta)$ is highly peaked towards $\eta=1$ at the high group 1 energies (14.9-13.5 MeV). The cross sections $\sigma_{12 \rightarrow 14}$, $\sigma_{16 \rightarrow 17}$, and $\sigma_{21 \rightarrow 22}$ all occur for energy intervals near resonances in the oxygen cross section. The value $\sigma_{20 \rightarrow 21}$ is for a relatively flat portion of the oxygen cross section curve where $\sigma_s(E, \eta)$ is much more isotropic in shape. As the group structure becomes finer (as would be needed to perform detailed transport calculation in the neighborhood of a resonance) the group transfer cross sections are even better approximated by the triangular model.

The variation in $\sigma_s(E, \eta)$ can be expected to produce "smooth" variations in the exact group transfer cross sections. However, examination of $\sigma_{16 \rightarrow 17}$ in Fig. 11 shows a relatively rapid oscillation in the transfer distribution. Such oscillations are encountered frequently, particularly for fine group structure and for energy regions near resonances. These oscillations are not physical in origin but arise from discontinuities in the input microscopic

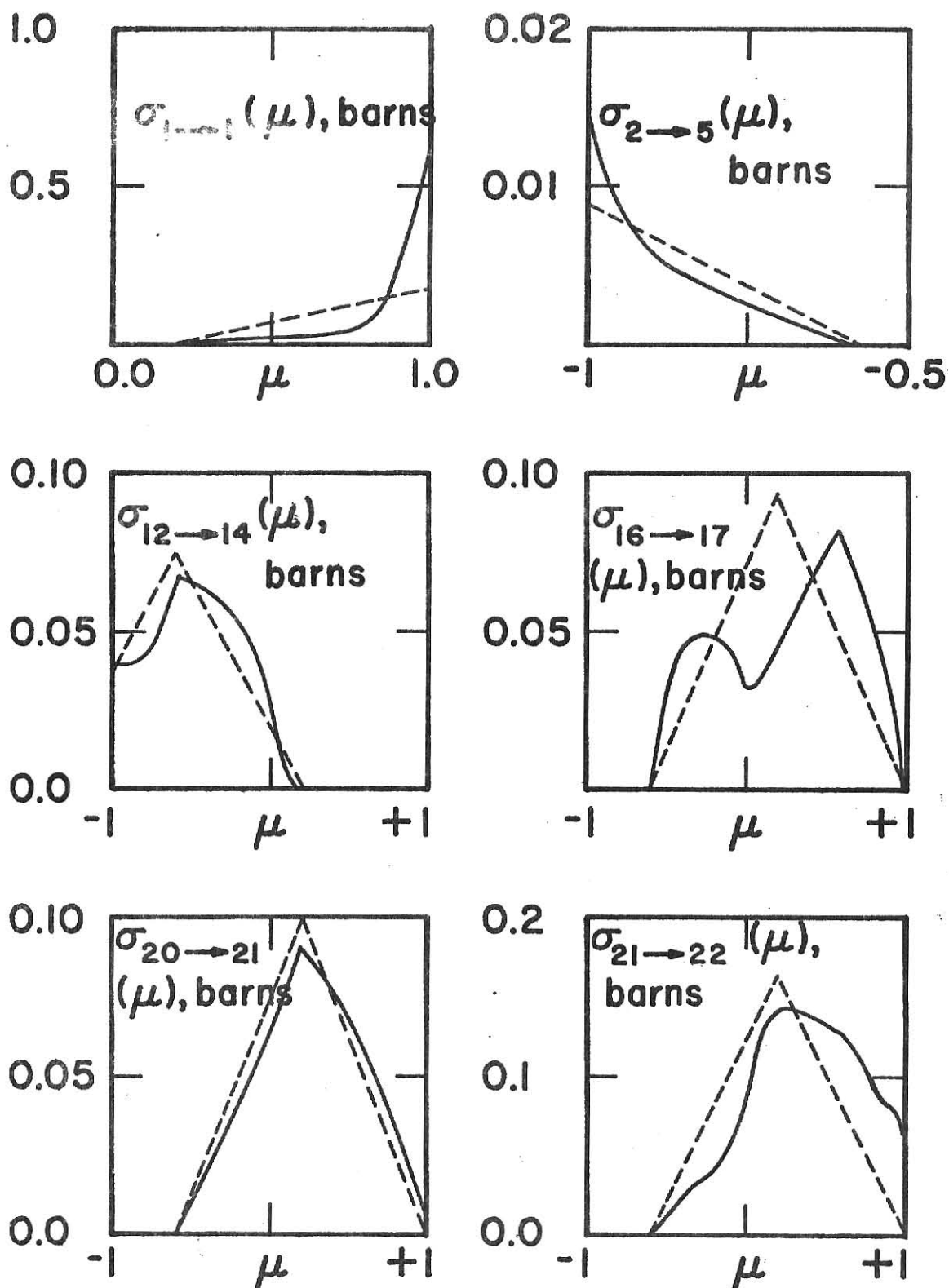


Figure 11. Comparison of exact (solid curves) and triangularly approximated (dashed curves) elastic transfer cross sections for various oxygen DLC/2 group to group transfers (See Table 6 for energy group structure)

data. The initial microscopic cross section data from which the exact group transfer distribution is calculated by BIGD is taken from the ENDF data file. On this file, cross sections and angular distributions are tabulated at discrete energies. The calculation of the transfer distributions often requires cross section values at non-tabulated energies. In BIGD linear interpolation between ENDF tabulated values is used. This linear interpolation as well as statistical error in the tabulated data, produces discontinuities in the microscopic cross section data (see Fig. 12) which in turn produces the spurious oscillations in the calculated transfer distributions.

Although the use of higher order interpolation procedures might tend to mitigate this effect, there would remain the inherent problem of statistical fluctuations in the microscopic data itself which would still lead to non-physical oscillations or structure in the group transfer cross sections. These effects become particularly severe for fine group structure for which the ENDF data file uses a comparatively coarse energy mesh. Consequently, interpolation errors and statistical errors become relatively more important. For such situations the triangular approximation is a crude but effective method for eliminating the spurious structure while maintaining the essential characteristics of the scattering transfer distributions.

In the present work, oxygen scattering cross sections are to be ultimately combined with hydrogen components to produce water cross sections. Table 2 compares the magnitudes of total hydrogen and oxygen cross sections for the first 26 groups of the DLC2/99G energy structure. In nearly all cases, total hydrogen group cross sections exceed those for oxygen. Consequently, the combination of these values to form water cross sections reduces significantly the effect of inaccuracies in triangularly approximated oxygen scattering component.

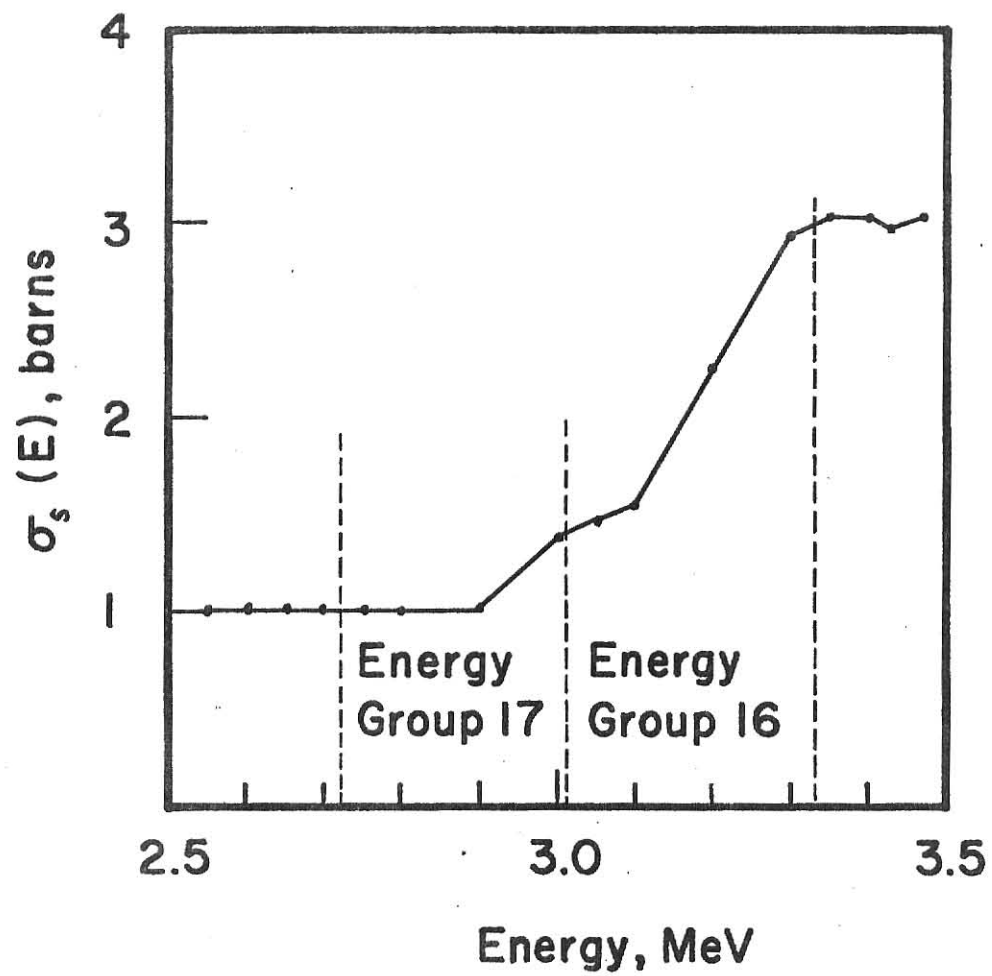


Figure 12. ENDF oxygen point elastic scattering cross section data between the DLC/2 groups 16 and 17 limits

Table 2. Comparison of Total Hydrogen and Oxygen Cross Sections for the First 26 Groups of the DLC/2 Structure.

Group	σ_t^H , (barns)	σ_t^O , (barns)
1	0.684	0.648
2	0.752	0.793
3	0.824	0.878
4	0.901	0.651
5	0.982	0.672
6	1.069	0.778
7	1.160	0.793
8	1.256	0.949
9	1.357	0.883
10	1.463	1.320
11	1.574	1.187
12	1.690	1.164
13	1.810	1.715
14	1.936	2.540
15	2.067	3.009
16	2.203	2.091
17	2.345	1.121
18	2.492	1.035
19	2.645	0.666
20	2.805	1.381
21	2.971	2.127
22	3.145	1.952
23	3.326	1.980
24	3.515	2.467
25	3.714	4.018
26	3.922	2.990

Figure 13 provides a comparison of an exact elastic group-to-group transfer cross section for water with the corresponding Legendre and triangular approximations. Since the triangular representation compares well with the exact result, it is expected that it will produce transport results which would agree well with the use of the exact transfer cross sections. This comparison is the subject of the next chapter.

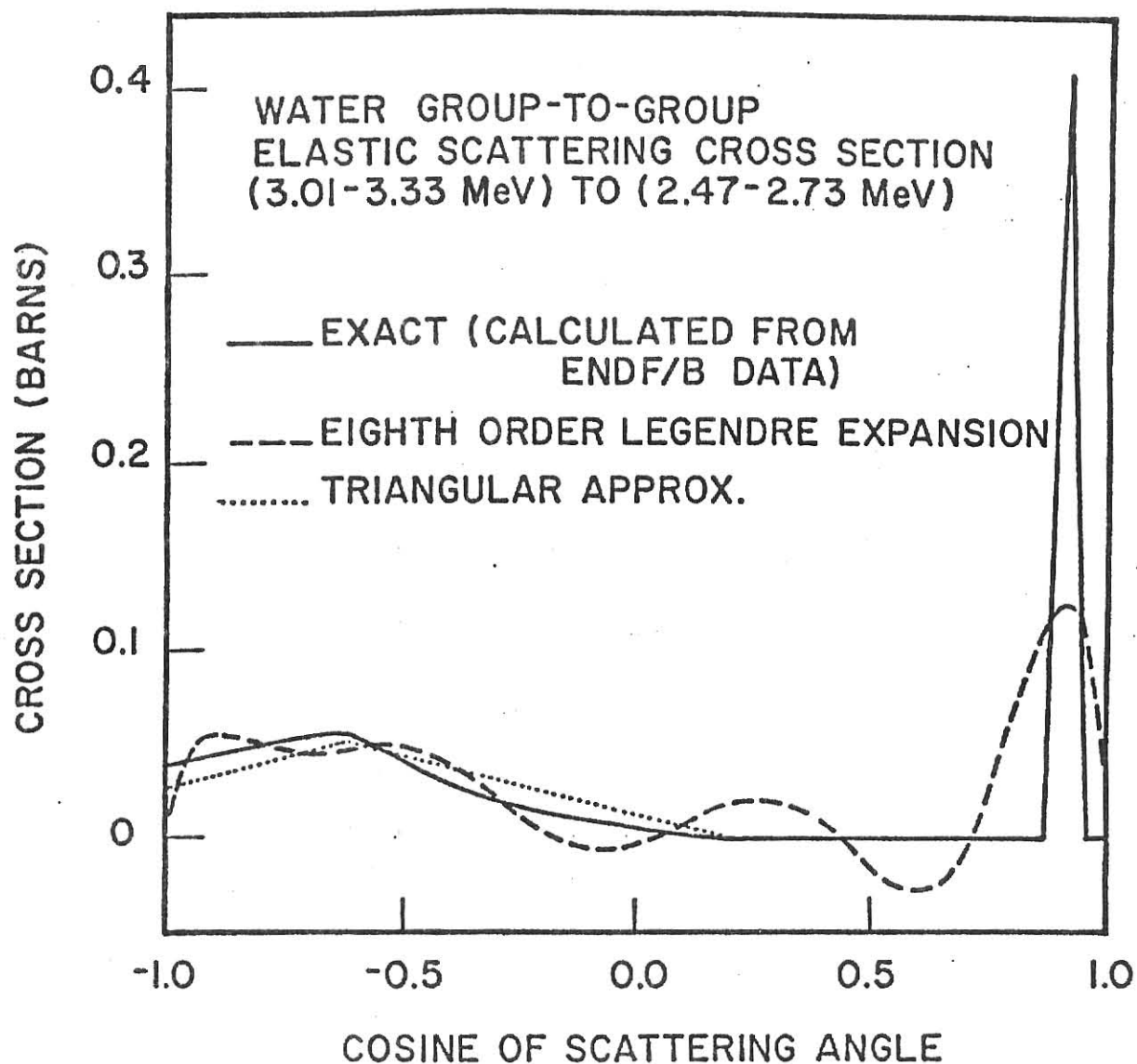


Figure 13. Comparison of approximate triangular and Legendre expansion techniques with an exact water scattering cross section

3.0 Anisotropic Transport Methods and Calculations

The previous section considered a method whereby neutron transfer cross sections for elastic scatters could be approximated by piece-wise linear functions. Brief comments were made as to how well numerical values of exact and approximate cross sections agree. However, such agreement is not only the concern in the development of a useful approximation. The ultimate purpose for evaluation of approximate $\sigma_{g' \rightarrow g}(\mu)$ values is their successful incorporation into transport calculational models.

Standard discrete ordinate transport models in current use (e.g., ONETRAN [23], ANISN [4]) are structured such that Legendre expansions of multigroup transfer cross sections must be used. The advantage of this approach is that cross section computer storage requirements are minimized at the expense of having to perform a Legendre reconstitution. Consequently, most multigroup cross section preparation codes have been written so as to supply only the Legendre expansion coefficients for the group cross sections. For the cross section approximation developed in this work to be of much use, it must be capable of being incorporated into a calculational transport model. It has been shown by Odom [3] that the standard discrete ordinates model can be modified to accept non-expanded group-to-group transfer cross sections. However, Odom did not explore in detail the capabilities and limitations of his approach. In this section an investigation of the accuracy of Odom's *direct S_n model* is presented as it applies to the use of exact and approximate group-to-group elastic transfer cross sections.

When comparing two transport calculations, one using exact scattering transfer cross sections and the other using triangularly approximated values, minor variations are to be expected between calculated values of group angular

fluxes. However, discrepancies among the two sets of results may not be entirely attributable to the differences between exact and approximate transfer cross section values. Differences may also arise as a result of the particular numerical technique used for solution of the transport equation. In this chapter the sources of such differences are investigated.

3.1 Transport Techniques for Evaluating the Utility of Approximated Cross Sections

The usefulness of triangular approximating functions to describe transfer cross sections ultimately depend upon how well they can reproduce transport calculations based upon exact $\sigma_{g' \rightarrow g}(\mu)$ values. To draw this comparison, a method for solving the neutron transport equation must be selected. Several techniques are available. Among them are spherical harmonics [6,24], Fourier transforms [25,17], discrete ordinates [6,5], separation of variables [6], as well as others [6,24].

Discrete ordinates, by far the most common technique used today, is the method employed in the present work. The computer code MGRP[3], which is based upon this technique, has been used for comparative analysis of exact and approximate $\sigma_{g' \rightarrow g}(\mu)$ values. This finite difference discrete ordinates computer program solves the azimuthally symmetric multigroup form of the transport equation. Documentation of this code, as well as supporting cross section preparation codes, can be found in Appendix A. The reason for use of this particular code in the present work is its superior ability to handle highly anisotropic neutron scattering cross sections. This ability results from the fact that MGRP is able to accept group-to-group scattering cross sections which have not been expressed in the form of a Legendre expansion. In this code, the angular particle density is evaluated at a set of discrete

directions and at a set of discrete positions. The spatial derivative term in the transport equation is approximated by a simple finite difference.

Rather than obtaining a transport solution for $\psi_g(x, \mu)$, approximate values of $\psi_g(x_k, \mu_j)$ (where $k=1, 2, \dots, K$ and $j=1, 2, \dots, J$) are obtained from the following set of coupled linear equations

$$\begin{aligned} \mu_j \frac{\psi_g(x_{k+1}, \mu_j) - \psi_g(x_k, \mu_j)}{(x_{k+1} - x_k)} + \sigma_g \psi_g(x_k, \mu_j) \\ = \sum_{g'=1}^G \sum_{i=1}^J w_i \sigma_{g' \rightarrow g}(\mu_i \rightarrow \mu_j) \psi_{g'}(x_{k+1/2}, \mu_i) . \end{aligned} \quad (3.1)$$

By using a sufficiently large spatial mesh set $\{x_k\}$ and angular quadrature set $\{\mu_j\}$, it is possible to produce transport results having any desired degree of accuracy. However, using large spatial and angular sets is not often practical because of the large associated computer cost. Therefore, a compromise between accuracy and computational cost must be made. Table 3 was compiled from a series of water penetration studies done with MGRP. Even for this simple three energy group problem, the effect of quadrature and mesh size are reflected in program execution times.

In general, the maximum mesh size allowed in discrete ordinates calculations is governed by the specific quadrature set used for polar discretization. This interdependence is necessary to maintain the convergence stability criterion inherent in discrete ordinate equations [3]. Common practice is to first select a quadrature set for the polar angle. Once this choice has been made, mesh size is adjusted so as to provide reasonably accurate results with a minimum amount of computational time. The selection of a particular quadrature set to describe the polar angular dependence of the angular flux is a key step in any discrete ordinates calculation. Its importance is emphasized here since improper or inadequate selection of this set can lead to erroneous

Table 3. Computer execution times* for a 3 group transport problem. Calculations were done by MGRP on the Kansas State University IBM 370/158 computer.

Number of Quadrature Points	Number of Mesh Points		
	76	101	131
14	6.5	7.9	9.3
16	7.2	9.5	11.4
18	9.2	12.1	14.9
22	---	27.9	----

*Time in seconds.

transport results. As is pointed out in the next section, selection considerations are important when comparing the effect of exact and/or approximate $\sigma_{g' \rightarrow g}(\mu)$ values with each other or with experimental results.

3.2 Discrete Ordinate Quadrature Set Selection

Equation (3.1) shows how, in the discrete ordinate calculations, the integral over polar angle μ is replaced with a quadrature summation over index (i). By making this approximation, certain concessions are made which limit the flexibility of the calculated results.

One concession of lesser consequence is that values for $\psi_g(x, \mu)$ are only available at specific quadrature angles. If calculated results are to be compared with experimental data at fixed polar angles, these experimental source and exit angles must be included in the quadrature set. There are two ways by which this may be accomplished. The first is to generate an angular quadrature set on the interval -1 to +1 which contains these angles. Such an approach can possibly lead to negative quadrature weights for certain discrete directions. Bell [6] indicates that such sets are unacceptable for transport calculations. The second approach is to modify a standard quadrature set. Two common standard quadratures are the Gaussian and Lobatto sets [26]. To evaluate $\psi_g(x, \mu)$ at desired quadrature angles, a common practice is to modify these standard sets by including the desired quadrature directions with zero weights [17].

There is however, a more serious concession which results from the numerical quadrature approximation in Eq. (3.1), particularly when highly anisotropic scattering prevails. To grasp the significance of this concession, one must first understand how the azimuthally symmetric form of the discrete ordinates transport equation is typically used. Odom [3] and others [12,27]

have used the azimuthally symmetric form of the transport equation to analyze neutron slab penetration distributions for normally incident spectra. It should be pointed out that aside from the case of an isotropic neutron source, normal slab incidence is the only situation for which the azimuthally symmetric equation holds any promise of being physically realistic. Since the polar angle has been discretized, a neutron source may mathematically be selected only at one or more of the discrete directions in the quadrature set. For example, if a monodirectional azimuthally symmetric source at $\mu_{\text{source}} = \mu_1$ were selected, this implies the presence of a conical neutron beam at one edge of the slab. While there is nothing mathematically wrong with this implication, conical neutron sources seldom occur in realistic situations.

3.2.1 Incident Direction Considerations

As μ_{source} approaches +1.0, an azimuthally symmetric conical neutron beam becomes more like that of a normally incident neutron spectra. This brings to mind the question of how close to unity must μ_{source} be to adequately depict normal incidence. Figures 14 and 15 show two one-speed transport calculations which were carried out for isotropic scattering through a one mean free path slab. The scattering ratios were $c \equiv \sigma_s / \sigma_t = 0.6$ and $c = 1.0$ respectively. Results for these calculations are shown to compare well with exact values calculated using the X-Y Functions¹ of radiative transfer. In both the reflected and transmitted distributions a minor deviation in μ_{source} from +1.0 seems to have little effect. Such results suggest that a quadrature set as small as DP-5 ("Double Gauss" 5 point quadrature, i.e. 5 point Gauss quadrature on both polar intervals $(-1, 0)$ and $(0, 1)$), whose maximum quadrature ordinate is $\mu_1 = 0.95308$ (17.6°), might adequately describe normal incidence for the case of isotropic scattering. However, multigroup elastic scattering for light elements is often quite anisotropic. Figure 16 depicts the diffuse penetration spectra from group 1 to 1 (See Table 6

¹In one speed transport problems involving slabs of finite thickness, the angular distribution of the emergent flux can be expressed in terms of two rational functions, the so-called X and Y functions [28]. If $c \equiv \sigma_s / \sigma_t$ and $\mu_s \equiv$ the input source direction at one edge of the finite optical media, then the transmitted and reflected angular distributions for isotropic scattering in the media are given by

$$\psi_R(-\mu_1) = \frac{c\mu_s}{2(\mu_1 + \mu_s)} [X(\mu_1) X(\mu_s) - Y(\mu_1) Y(\mu_s)] \quad , \quad \mu_1 > 0$$

and

$$\psi_T(\mu_1) = \frac{c\mu_s}{2(\mu_1 - \mu_s)} [Y(\mu_1) X(\mu_s) - X(\mu_1) Y(\mu_s)] \quad , \quad \mu_1 > 0$$

Values of $X(\mu)$ and $Y(\mu)$ are tabulated by Carlstedt and Mulliken [29] for various optical thicknesses and values of c .

Figure 14. Transmitted angular density for isotropic scattering through 1 mean free path for a unit neutron source when $c=0.6$

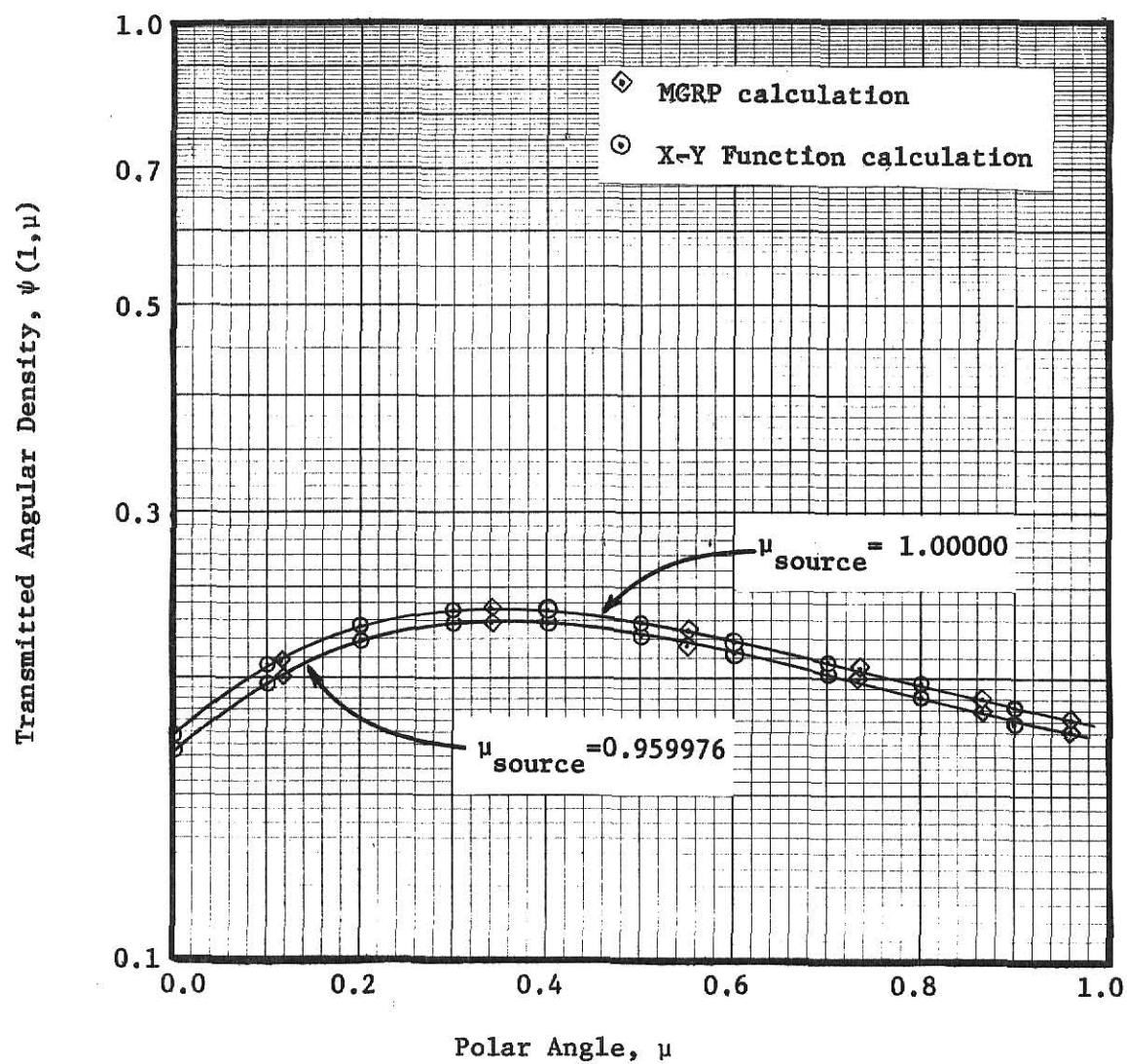
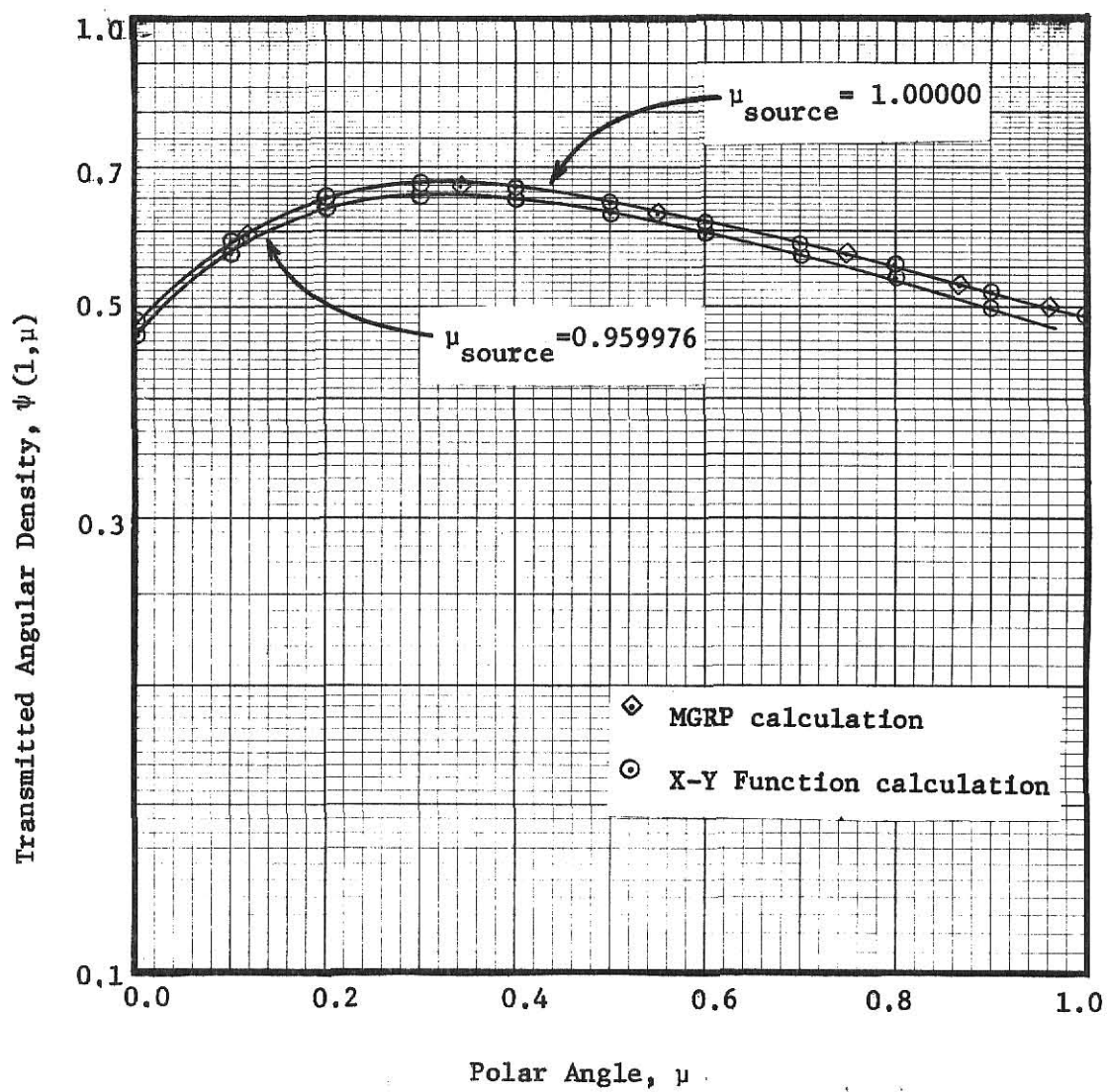


Figure 15. Transmitted angular density for isotropic scattering through 1 mean free path for a unit neutron source when $c=1.0$



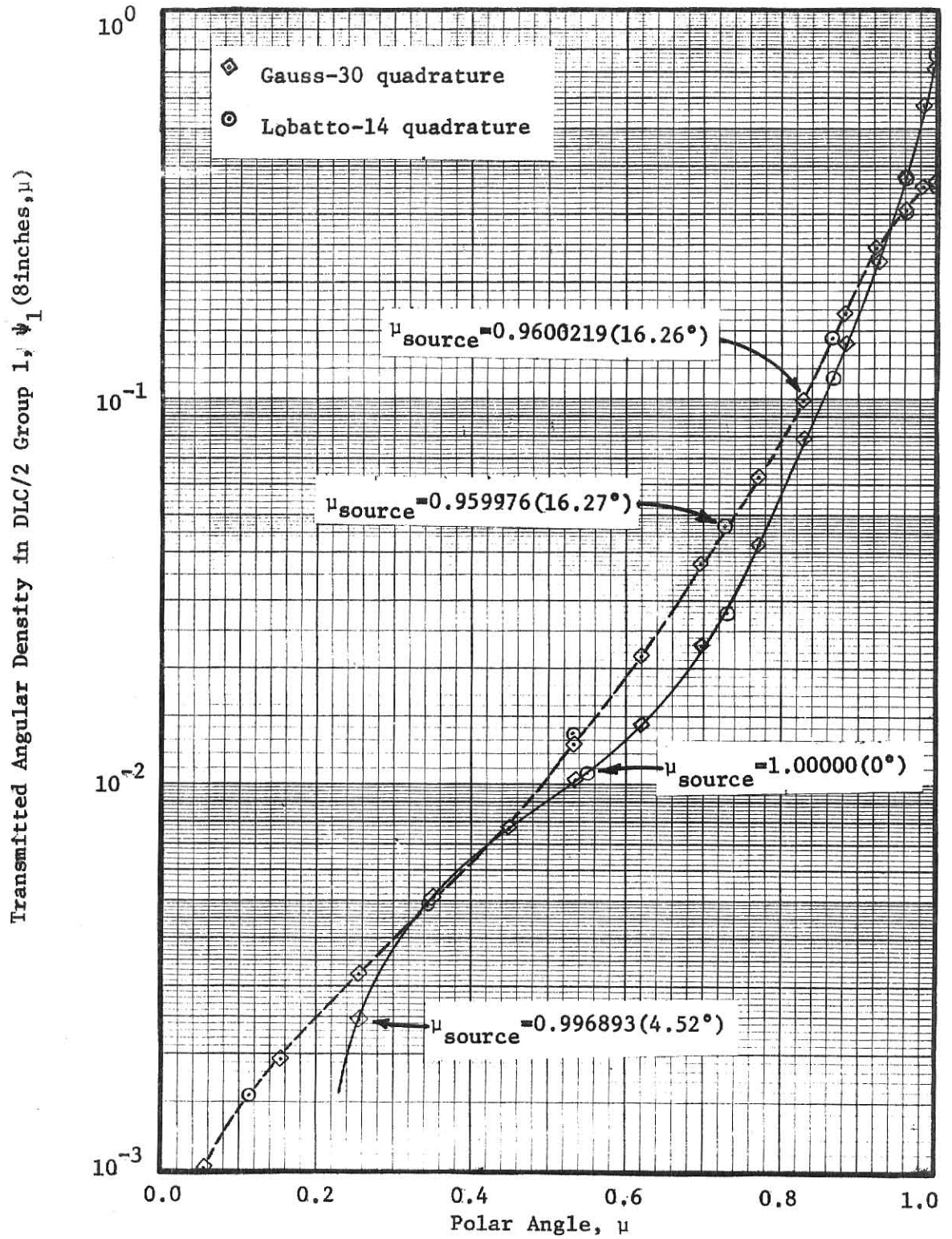


Figure 16. Transmitted angular density from DLC/2 group 1 to 1 through 8 inches of water for a unit source in group 1 (DLC/2 group 1 = 14.918-13.499 MeV)

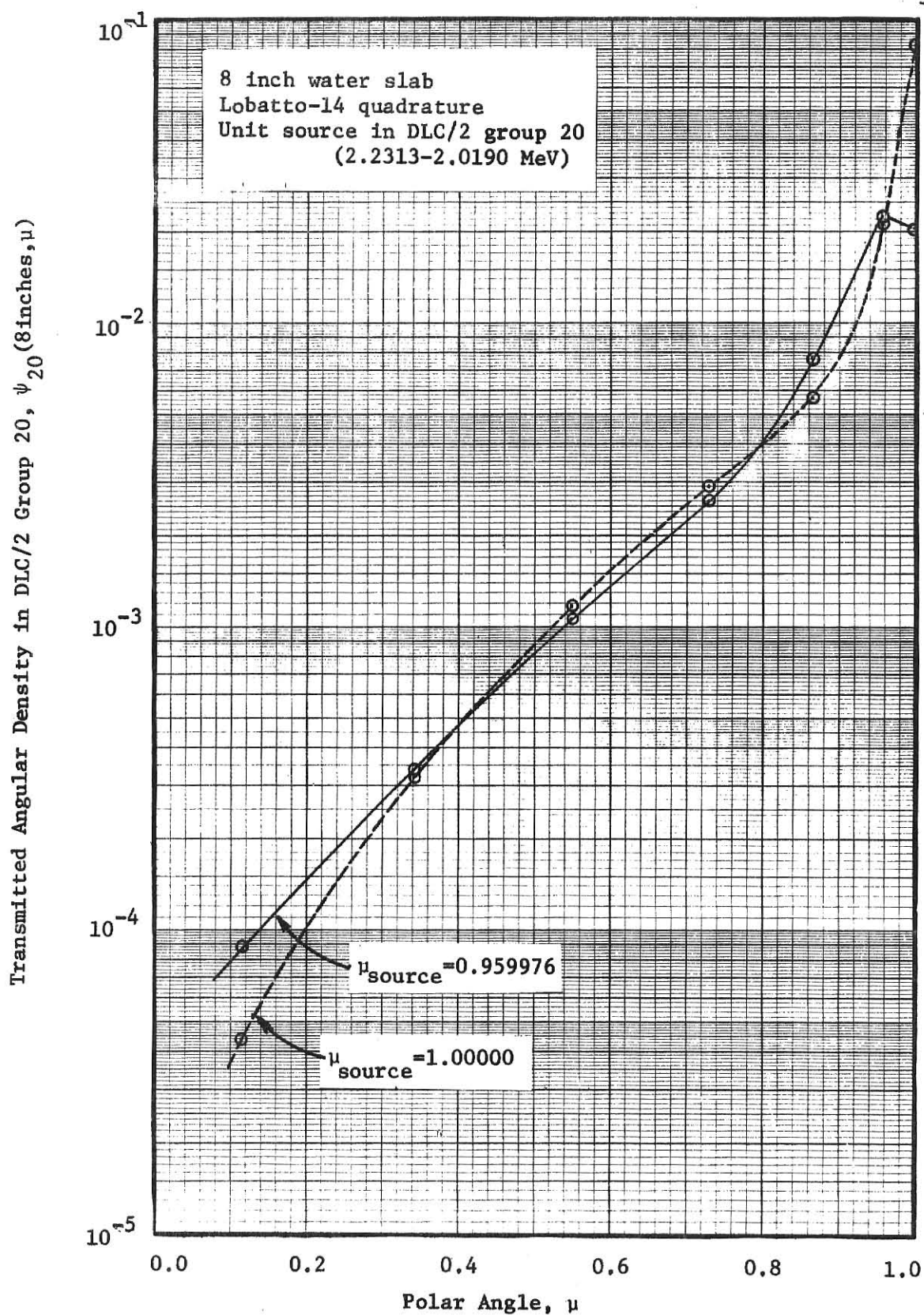


Figure 17. Comparison of transmitted angular densities in DLC/2 group 20 through 8 inches of water for $\mu_{\text{source}} = 0.959976$ and $\mu_{\text{source}} = 1.00000$

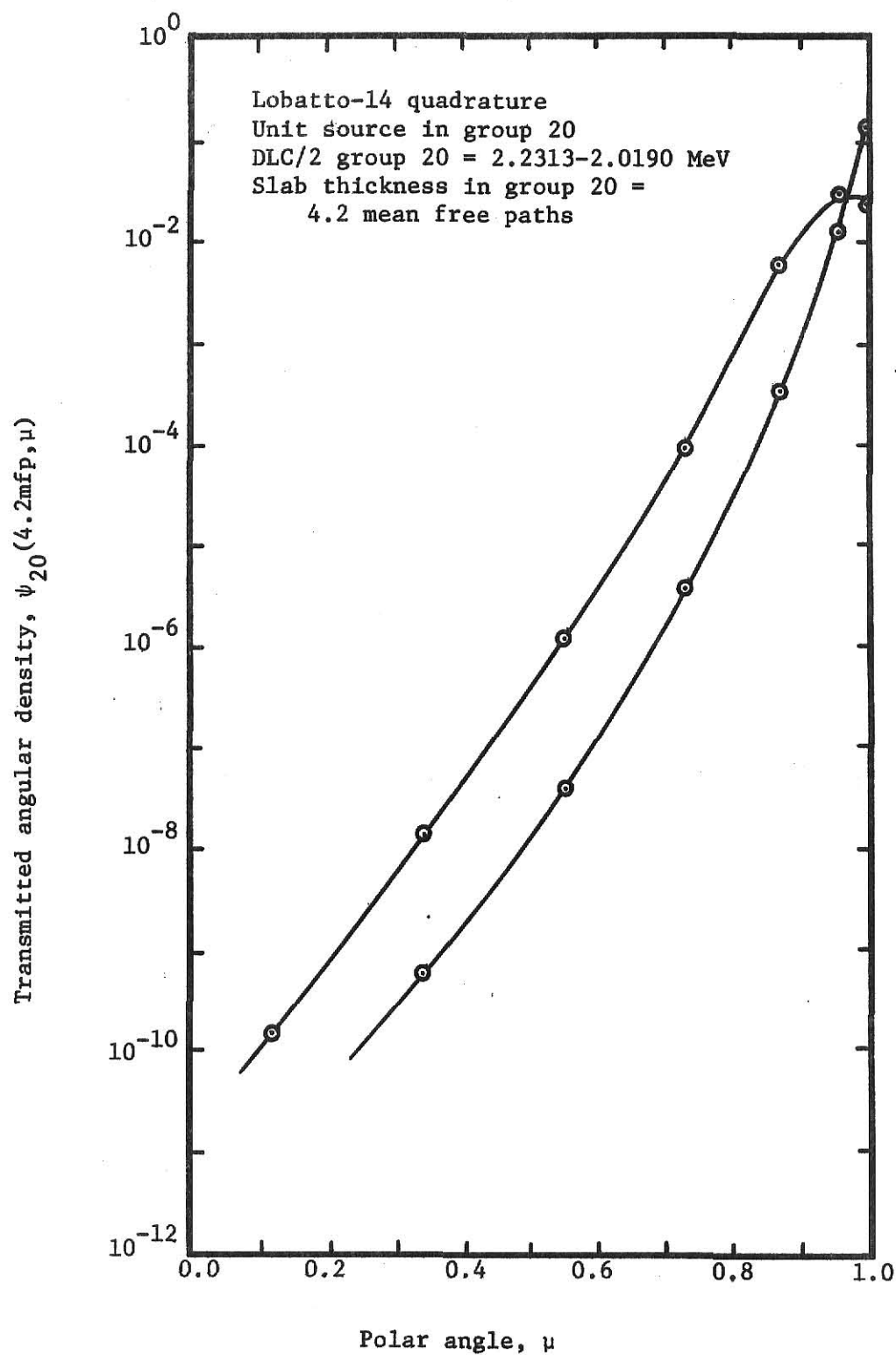


Figure 18. Comparison of transmitted angular densities through a 4.2 mean free path hydrogen slab for $\mu_{source} = 1.0000$ and $\mu_{source} = 0.959976$

for energy limits) through eight inches of water. In this figure calculations using $\mu_{\text{source}} = 0.959976$ (16.27°) and $\mu_{\text{source}} = 1.000$ (0°) from a Lobatto-14 quadrature set are compared. Also shown are calculations resulting from a Gauss-30 discretization of the polar angle where $\mu_{\text{source}} = 0.9600219$ (16.26°) and $\mu_{\text{source}} = 0.996893$ (4.52°). Unlike the isotropic case, significant differences are noted near the ends of the angular range. Note that when $\mu_{\text{source}} = 0.996893$ (4.52°), the 30 point quadrature appears to adequately describe a normally incident neutron spectra. However, this improvement over the 14 point quadrature was accomplished at the expense of a significant increase in program execution time. For the 30 point Gauss results, program execution time was nearly three times that required for the corresponding 14 point Lobatto data. Results similar to those shown in Fig. 16 are presented in Fig. 17 for a group 20 to 20 transfer. These two figures suggest that neutron energy has little to do with the disparity between results calculated using incrementally different values of μ_{source} .

One further comparison is made to demonstrate that significant differences can be obtained when angles other than $\mu_{\text{source}} = 1.0$ are used to approximate normally incident source neutrons. Figure 18 illustrates the difference between diffuse neutron penetration results when $\mu_{\text{source}} = 0.959967$ and $\mu_{\text{source}} = 1.0000$ for a 4.2 mean free path hydrogen slab. This plot displays deviations between $\psi_{20}(4.2 \text{ mfp}, \mu)$ values in excess of one decade for some values of μ . Hence, whenever possible Lobatto quadratures should be employed to describe normally incident source neutrons. This is particularly true when highly anisotropic scattering prevails.

3.2.2 Angular Scattering Quadrature Coverage

As indicated by the previous section, use of Lobatto quadrature sets are preferred when normally incident source neutrons are used with the azimuthally symmetric transport equation. However, the use of Lobatto quadrature sets is not as straight forward as it may seem. Complications are uncovered upon examination of the ability of such sets to adequately describe normally incident anisotropic neutron transport. Table 4 displays results from a transport calculation through 4.2 mean free paths of hydrogen with a unit source at $\mu_{\text{source}}=1.0$ in group 20. Obvious differences are observed between calculations carried out with Lobatto-12 and -14 quadrature sets. The reason for these differences can be seen from Eq. (3.1). The right hand side of this equation attempts to describe the transfer of neutrons from all directions and energies to a specific direction and specific energy. The zero values of $\psi_{20}(4.2, \mu)$ for the Lobatto-12 calculation result from failure of this term in the numerically approximated transport equation to adequately model the angular transfer. This section discusses the mathematical model used by Eq. (3.1) to describe angular neutron transfer. A mathematical relation which links the inherent degree of scattering anisotropy for a given element to the minimum order of angular quadrature required to adequately describe angular transport is developed.

In the azimuthally symmetric form of the transport equation, Eq. (2.2), transfer of neutrons from all directions μ' to direction μ is evaluated by the following term:

$$\int_{-1}^{+1} d\mu' \sigma_s(\mu' \rightarrow \mu) \psi(x, \mu') \quad (3.2)$$

The S_n (discrete ordinates) model replaces this source term by the following numerical approximation:

Table 4. Group 20 transmission spectra through
a 4.2 mean free path hydrogen slab with
a unit source at $\mu_{\text{source}}=1.0$ in Group 20.

<u>Lobatto-12 Quadrature</u>		<u>Lobatto-14 Quadrature</u>	
μ	$\psi_{20}(1.5, \mu)$	μ	$\psi_{20}(1.5, \mu)$
0.136496	0.0	0.115954	0.0
0.399402	0.0	0.342012	5.23 E-10
0.632755	0.0	0.550201	4.026 E-8
0.819209	0.0	0.728792	4.069 E-6
0.944876	0.0	0.867866	3.518 E-4
1.000000	0.132	0.959976	2.463 E-2
		1.000000	1.391 E-1

$$\sum_{i=1}^J w_i \sigma(\mu_i \rightarrow \mu_j) \psi(x, \mu_i) . \quad (3.3)$$

To carry out transport calculations, one must first have some knowledge of the azimuthally symmetric scattering transfer cross section, $\sigma(\mu_i \rightarrow \mu_j)$. This value is typically obtained by averaging $\sigma_s(\underline{\Omega} \cdot \underline{\Omega}')$ over all azimuthal directions, namely

$$\sigma(\mu_i \rightarrow \mu_j) = \frac{1}{2\pi} \int_0^{2\pi} \sigma_s(\underline{\Omega}' \cdot \underline{\Omega}) d\phi' = \frac{1}{2\pi} \int_0^{2\pi} \sigma_s(\mu_i, \phi' \rightarrow \mu_j, \phi) d\phi' \quad (3.4)$$

The angle $\mu_o \equiv \underline{\Omega} \cdot \underline{\Omega}'$ can be expressed in terms of μ_i , μ_j , ϕ' , and ϕ as (6)

$$\mu_o = \mu_i \mu_j + \sqrt{1-\mu_i^2} \sqrt{1-\mu_j^2} \cos(\phi-\phi') . \quad (3.5)$$

Scattering transfer cross sections can be obtained by approximating the integral over ϕ' in Eq. (3.4) by numerical quadrature. In the present work, a computer program named QUAZ [3] was employed to carry out this integration using a 32 point Gauss quadrature. Explicitly,

$$\sigma(\mu_i \rightarrow \mu_j) = \frac{1}{2\pi} \sum_{\ell=1}^{32} \sigma_s(\mu_o) w_\ell , \quad (3.6)$$

where

$$\mu_o = \mu_i \mu_j + \sqrt{1-\mu_i^2} \sqrt{1-\mu_j^2} \cos\phi_\ell . \quad (3.7)$$

Values of $\{\phi_\ell\}$ and $\{w_\ell\}$ are the ordinates and weights for numerical integration of $(\phi-\phi')$ over $(0, 2\pi)$.

Once $\sigma(\mu_i \rightarrow \mu_j)$ values are known, they may be incorporated into transport calculations. The question of how well these calculated cross sections actually represent transfer from directions μ_i to directions μ_j remains to be determined. Odom used reciprocity relations to establish whether or not calculated values of $\sigma(\mu_i \rightarrow \mu_j)$ were sufficiently accurate, i.e.

$$\int_{-1}^{+1} \sigma(\mu_1 \rightarrow \mu') d\mu' = \int_{-1}^{+1} \sigma(\mu_l \rightarrow \mu') d\mu' . \quad (3.8)$$

Since the above equation is strictly valid, its numerical approximation can be used to estimate the accuracy of $\sigma(\mu_1 \rightarrow \mu_j)$ values in the discrete ordinate equations. For all values of l and j does

$$\sum_{j=1}^J \sigma(\mu_1 \rightarrow \mu_j) w_j = \sum_{j=1}^J \sigma(\mu_l \rightarrow \mu_j) w_j ? \quad (3.9)$$

If J is the order of angular quadrature being used then $\sum_{j=1}^J \sigma(\mu_1 \rightarrow \mu_j) w_j$ should theoretically be equal for all μ_1 in the set if the quadrature is sufficiently fine. Table 5 draws this comparison for the previous example of Table 4 which used Lobatto-12 and -14 quadrature sets to study neutron transport in hydrogen. Notice that values computed by the 12 point quadrature are in moderate disagreement with each other as well as with the exact cross section value. These deviations become significant as the $\mu_1 = \pm 1$ directions are approached. At this point it often becomes a judgment decision as to whether or not such a quadrature would yield reasonable transport results. The question could be resolved by actually carrying out the calculation. Use of this 12 point quadrature in transport calculations has already been demonstrated to yield questionable results (see Table 4).

Application of reciprocity relations to justify use of a particular quadrature set is only quantitative in nature. No knowledge is gained about individual $\sigma(\mu_1 \rightarrow \mu_j)$ values. Table 5 fails to explain why the 12 point set produced zeros for all scattering transfers in Table 4. A more involved study of the scattering transport mechanism leads not only to an explanation of why this set failed to produce non-zero values for angular densities in Table 4, but also a criterion which enables one to judge the adequacy of any given quadrature set.

Table 5. Calculated total transfer cross sections for 12 and 14 point Lobatto quadratures used with calculations in Table 5. (Also shown are calculations based on a 30 point Gauss quadrature)

Lobatto-12			Lobatto-14			Gauss-30		
μ_i	$\sum_{j=1}^{12} \sigma(\mu_i \rightarrow \mu_j) w_j$	μ_i	$\sum_{j=1}^{14} \sigma(\mu_i \rightarrow \mu_j) w_j$	μ_i	$\sum_{i=1}^{30} \sigma(\mu_i \rightarrow \mu_j) w_j$	μ_i	$\sum_{i=1}^{30} \sigma(\mu_i \rightarrow \mu_j) w_j$	μ_i
+ 1.000	0.085	+ 1.000	0.126	+ 0.997	0.133	+ 0.997	0.133	0.133
+ 0.945	0.119	+ 0.960	0.133	+ 0.984	0.134	+ 0.984	0.134	0.134
+ 0.819	0.122	+ 0.868	0.134	+ 0.960	0.133	+ 0.960	0.133	0.133
+ 0.633	0.122	+ 0.729	0.136	+ 0.926	0.133	+ 0.926	0.133	0.133
+ 0.399	0.123	+ 0.550	0.135	+ 0.883	0.133	+ 0.883	0.133	0.133
+ 0.136	0.121	+ 0.342	0.134	+ 0.830	0.134	+ 0.830	0.134	0.134
		+ 0.116	0.134	+ 0.768	0.133	+ 0.768	0.133	0.133
				+ 0.698	0.133	+ 0.698	0.133	0.133
				+ 0.621	0.134	+ 0.621	0.134	0.134
				+ 0.537	0.134	+ 0.537	0.134	0.134
				+ 0.447	0.133	+ 0.447	0.133	0.133
				+ 0.353	0.132	+ 0.353	0.132	0.132
				+ 0.255	0.132	+ 0.255	0.132	0.132
				+ 0.154	0.132	+ 0.154	0.132	0.132
				+ 0.051	0.132	+ 0.051	0.132	0.132

Exact = 0.135

From Eq. (2.42) it is apparent that $\sigma_{g' \rightarrow g}(\mu' \rightarrow \mu)$ will take on non-zero values only over certain $(\mu' \rightarrow \mu)$ ranges. This fact has significant implications when an attempt is made to approximate the transfer cross section using a discrete quadrature set. This limitation can be seen diagrammatically in Fig. 19. The figure illustrates a three dimensional scattering cone into which neutrons initially traveling in azimuthal direction ϕ' and polar direction μ_1 may scatter. An important conclusion can be drawn from this figure. Whether or not the azimuthally symmetric transfer cross section, $\sigma(\mu_1 \rightarrow \mu_j)$, is zero depends upon the polar spacing between adjacent quadrature values of μ_1 . If the spacing between adjacent μ_1 values is too large, neutrons initially headed in direction μ_1 will never scatter into other directions. This inability of particles to redistribute angularly remains even after multiple scatters. If transfer from any direction μ_1 to another direction μ_j is to take place, then $\sigma(\mu_1 \rightarrow \mu_j)$ must at least be non-zero for some value $j \neq 1$. In other words, the azimuthally symmetric scattering shell shown in Fig. 20 (obtained by rotating the three dimensional neutron scattering cone of Fig. 19 about the x-axis) should at least overlap some polar directions other than μ_1 .

The problem now becomes one of determining how many discrete directions other than μ_1 lie within the polar bounds of the conical azimuthally symmetric scattering shell. The polar bounds on this scattering shell can be expressed in terms of two angles β_{\max} and β_{\min} . The value β_{\max} defines the maximum angle of scatter between the positive x-axis and all possible scattering rays in the azimuthally symmetric scattering shell. Similarly, β_{\min} defines the minimum angle of scatter between the positive x-axis and all possible scattering rays in the azimuthally symmetric scattering shell (see Fig. 20). Hence, in order for transfer from all initial directions μ_1 to other possible directions μ_j to take place, there must exist a polar quadrature ordinate $\theta_j \equiv \cos^{-1} \mu_j$ such that

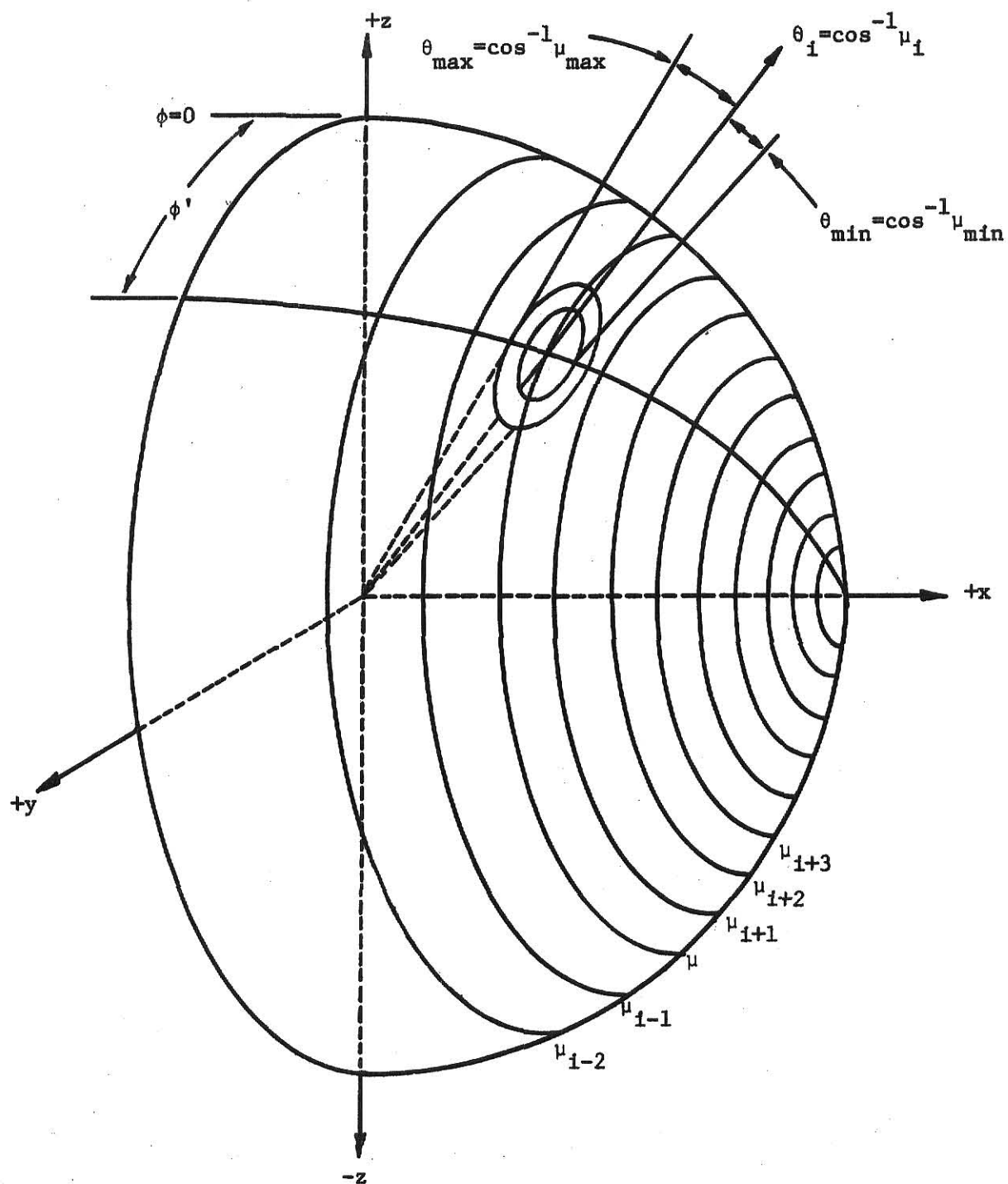


Figure 19. Neutron scattering cone into polar direction μ_i and azimuthal direction ϕ'

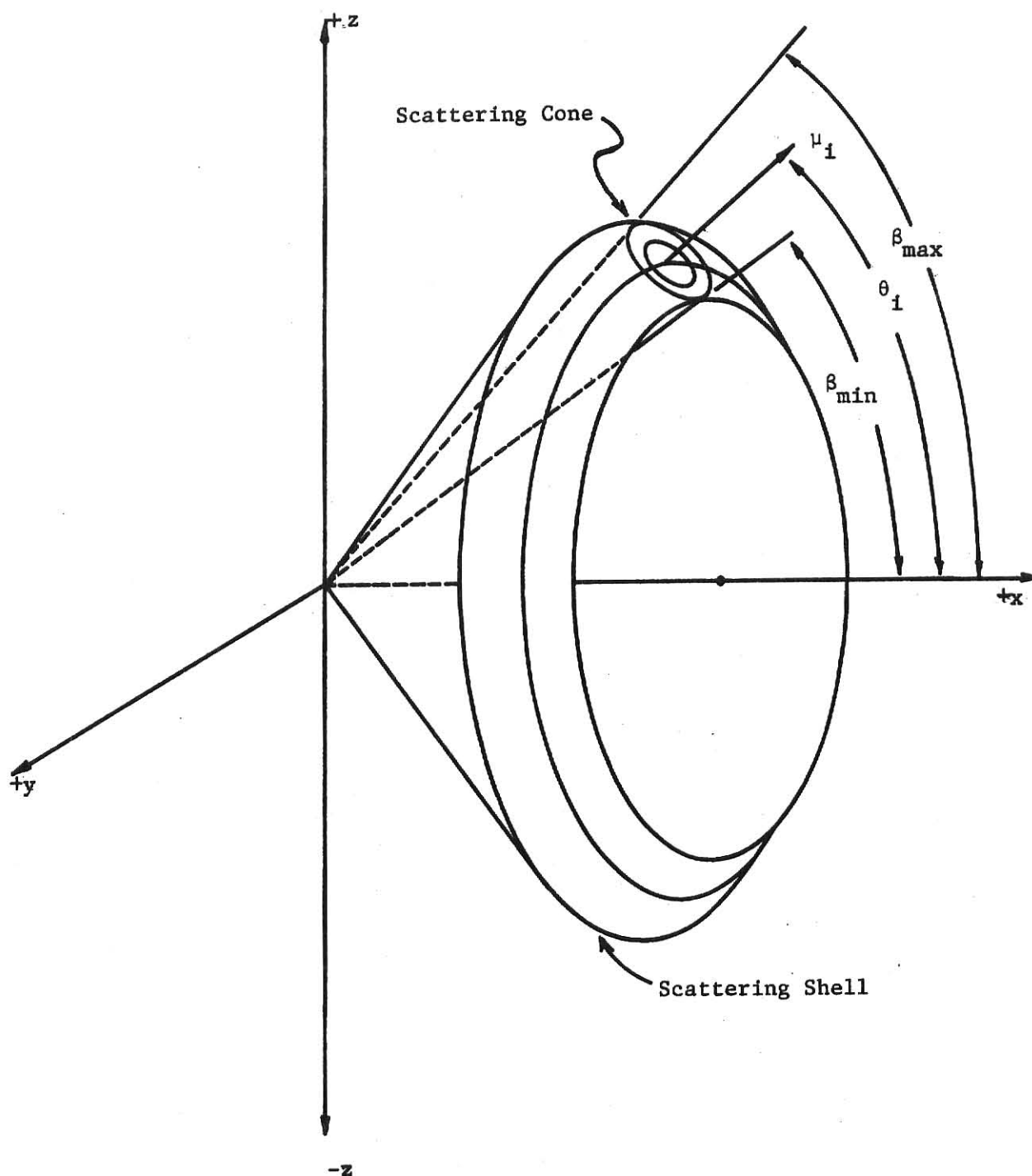


Figure 20. Azimuthally symmetric neutron scattering shell

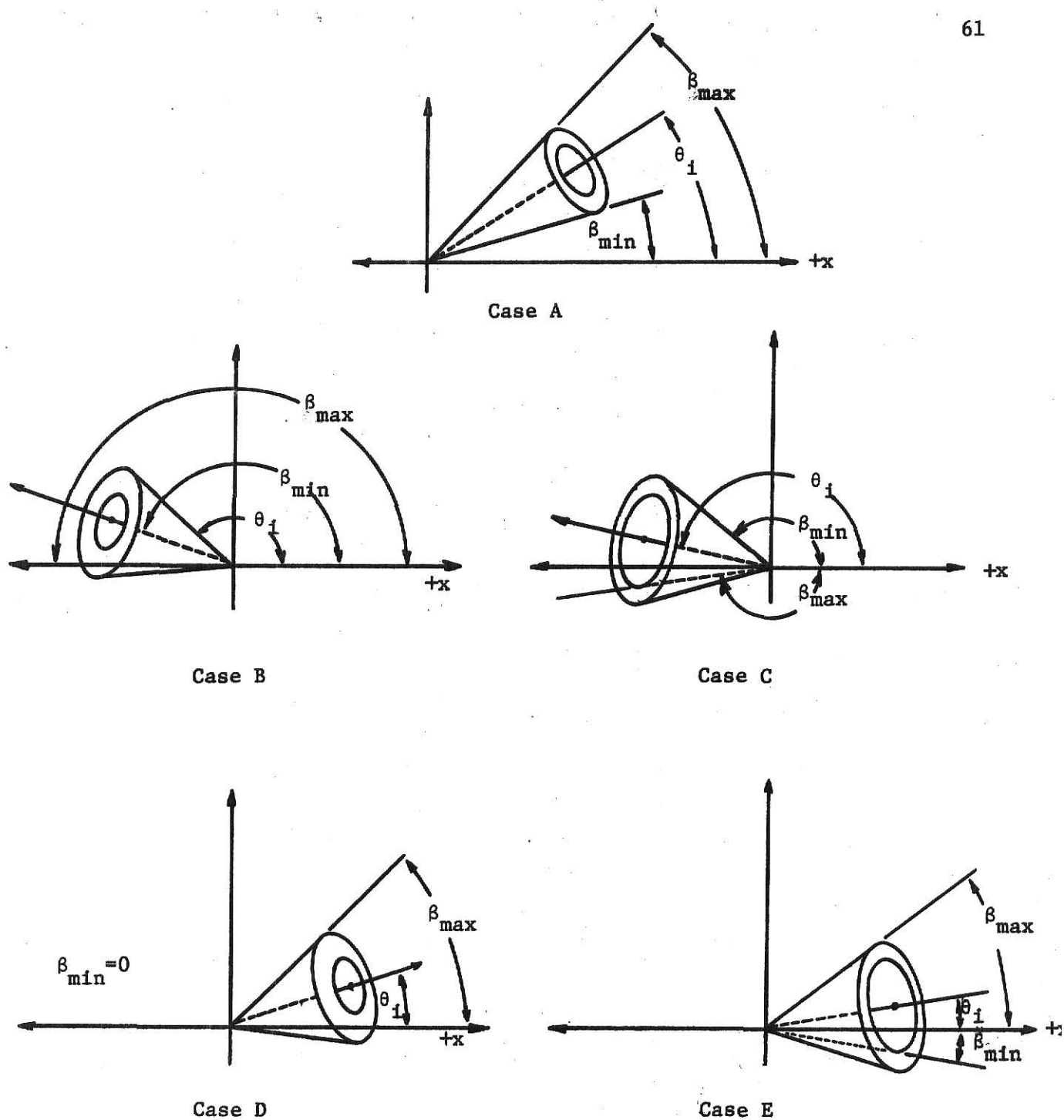


Figure 21. Various positionings of the neutron scattering cone with respect to the positive x-axis

$$\beta_{\min} \leq \theta_j \leq \beta_{\max} \quad (3.10)$$

for each value of i in the quadrature set (where $j \neq i$). From Figs. 19 and 20 it is apparent that angles β_{\max} and β_{\min} are in some way related to $\theta_{\max} \equiv \cos^{-1} \mu_{\max}$ and $\theta_{\min} \equiv \cos^{-1} \mu_{\min}$. Values of θ_{\max} and θ_{\min} are in turn related to elastic scattering energy-momentum constraints through Eqs. (2.12) and (2.42). Thus, once the bounds in Eq. (3.10) are known, the ability of a given quadrature set to describe angular particle transfer for a particular set of energy-momentum constraints can be evaluated (i.e., the order of angular quadrature needed to describe a given degree of scattering anisotropy can be determined).

First consider the relationship between β_{\max} and the neutron scattering cone. By considering the various possible orientations of the three dimensional neutron scattering cone in Fig. 19, one finds that there are only three values which β_{\max} may take on depending upon the exact values of θ_i , θ_{\max} , and θ_{\min} . When $(\theta_i + \theta_{\max} \leq \pi)$, the maximum possible angle of azimuthally symmetric neutron scatter away from the positive x-axis is $\beta_{\max} = \theta_i + \theta_{\max}$ (see Fig. 21, Case A). For cases where $(\theta_i + \theta_{\max} > \pi)$ but $(\theta_i + \theta_{\min} < \pi)$, Case B in Fig. 21 illustrates how the maximum angle of scatter away from the positive x-axis is merely $\beta_{\max} = \pi$. Finally, when $\theta_i + \theta_{\min} > \pi$, Case C of Fig. 21 illustrates how the $\beta_{\max} = (2\pi - \theta_i - \theta_{\min})$. Therefore,

$$\beta_{\max} = \begin{cases} \theta_i + \theta_{\max} & \text{when } \theta_i + \theta_{\max} \leq \pi, \\ \pi & \text{when } \theta_i + \theta_{\min} < \pi < \theta_i + \theta_{\max}, \\ 2\pi - \theta_i - \theta_{\min} & \text{when } \theta_i + \theta_{\min} > \pi. \end{cases} \quad (3.11)$$

This expression can be written more concisely as

$$\beta_{\max} = \begin{cases} \min[(\theta_i + \theta_{\max}), \pi] & \text{when } \theta_i + \theta_{\min} \leq \pi, \\ 2\pi - \theta_i - \theta_{\min} & \text{when } \theta_i + \theta_{\min} > \pi. \end{cases} \quad (3.12)$$

A similar approach may be used to evaluate β_{\min} . As with β_{\max} , there are three possible values which β_{\min} may take on depending upon the exact values of θ_i , θ_{\max} , and θ_{\min} . When ($\theta_i > \theta_{\max}$), the minimum possible angle of azimuthally symmetric neutron scatter away from the positive x-axis is $\beta_{\min} = \theta_i - \theta_{\max}$ (see Fig. 21, Case A). Case D of Fig. 21 illustrates how the initial quadrature ordinate θ_i is contained on the interval ($\theta_{\min}, \theta_{\max}$), the angle of minimum approach to the positive x-axis is zero. Finally, Case E of Fig. 21 illustrates how when $\theta_i \leq \theta_{\min}$, the angle of minimum approach between azimuthally symmetric scattering shell and the positive x-axis is $\beta_{\min} = (\theta_{\min} - \theta_i)$. Therefore,

$$\beta_{\min} = \begin{cases} \theta_i - \theta_{\max} & \text{when } \theta_{\max} < \theta_i, \\ 0 & \text{when } \theta_{\min} \leq \theta_i \leq \theta_{\max}, \\ \theta_{\min} - \theta_i & \text{when } \theta_i < \theta_{\min}. \end{cases} \quad (3.13)$$

This expression can be written more concisely as

$$\beta_{\min} = \begin{cases} \max[(\theta_i - \theta_{\max}), 0] & \text{when } \theta_i \geq \theta_{\min}, \\ \theta_{\min} - \theta_i & \text{when } \theta_{\min} > \theta_i. \end{cases} \quad (3.14)$$

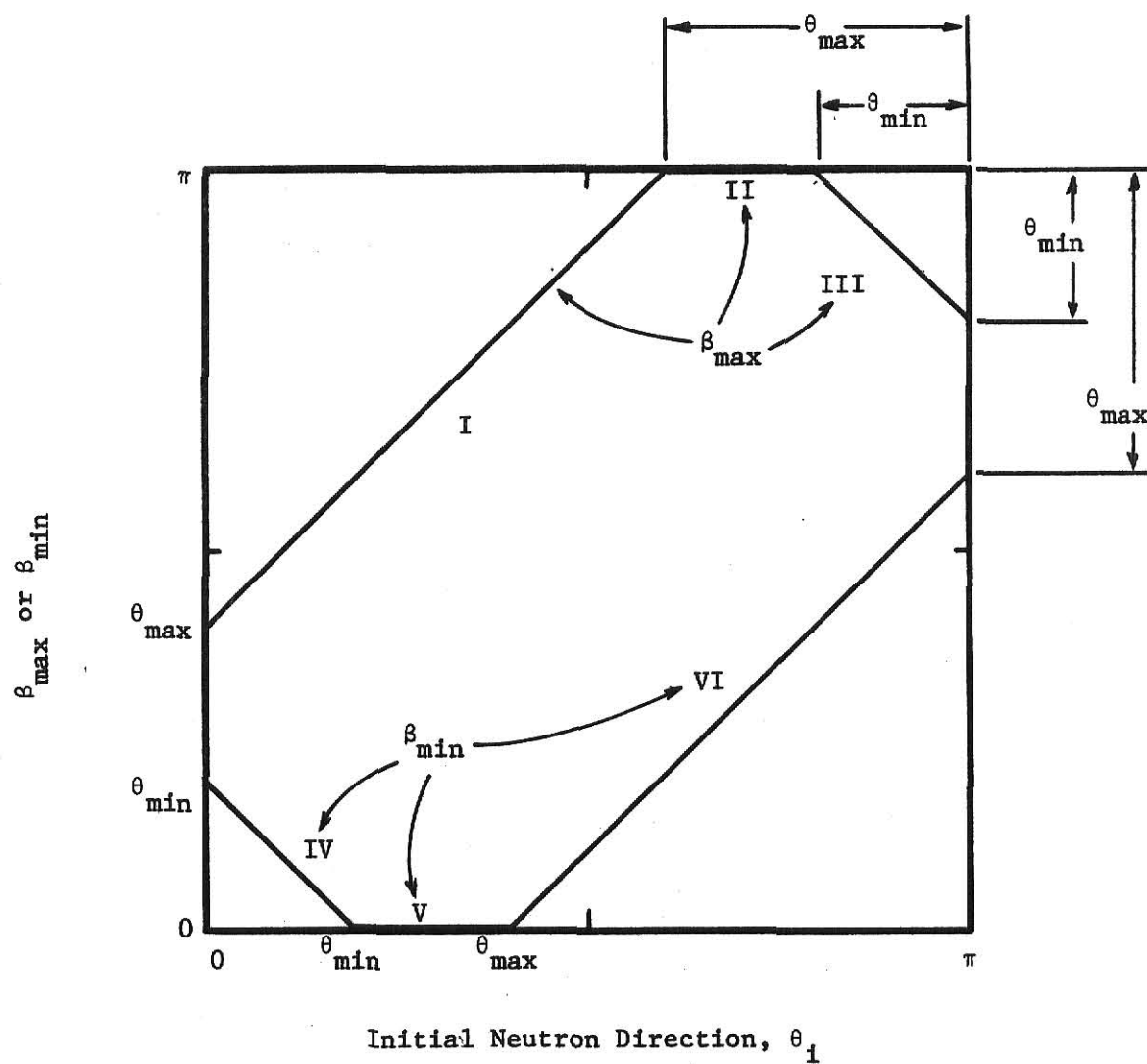
Once β_{\max} and β_{\min} have been defined, it is of interest to graphically represent the range of discrete polar value defined by Eq. (3.10) which will yield non-zero group-to-group transfer cross sections after scattering from an initial direction θ_i (where $j \neq i$). Figure 22 illustrates a plot of β_{\max} and β_{\min} versus incident direction θ_i for some hypothetically fixed values of θ_{\max} and θ_{\min} . Of course, θ_{\max} and θ_{\min} are readily determined for a given group-to-group energy transfer by Eqs. (2.12) and (2.42). Thus, for a given initial neutron direction θ_i , the range of θ_j directions which will render $\sigma(\theta_i \rightarrow \theta_j)$ non-zero are found by simply carrying out the projections from θ_i to the appropriate curves for β_{\max} and β_{\min} in Fig. 22. It is often convenient

to express initial directions, θ_i , and final directions, θ_j , in terms of polar quadrature ordinates ranging between -1 and +1. By merely taking the cosine of all abscissa and ordinate values found on Fig. 22, Fig. 23 is obtained.

Figure 23 (or 22) can be used directly to evaluate the ability of a given numerical quadrature set to represent angular transfer. As an illustration consider a neutron in the energy range 2.0190-2.2313 MeV which scatters with hydrogen to an energy between 1.3534-1.4975 MeV. From Eqs. (2.12) and (2.42) the values of μ_{\max} and μ_{\min} for this scatter are calculated to be 0.77815 (38.85°) and 0.860705 (30.60°) respectively. Furthermore, assume that this neutron is initially traveling in some polar direction $\mu_i = 0.82$ (34.92°) with respect to the positive x-axis, where 0.82 represents a particular ordinate value of a discrete numerical quadrature. Therefore, for a given numerical quadrature set to permit transfer from the assumed initial direction $\mu_i = 0.82$, the quadrature must contain at least one ordinate value other than $\mu_j = 0.82$, between $\cos(\beta_{\max}) = +1$ and $\cos(\beta_{\min}) = 0.60$ (see Fig. 24).

The concept behind Figs. 22-24 becomes useful when trying to analyze the ability of a particular quadrature set to describe anisotropic scattering transport. Note how in Figs. 22-24 that the range of non-zero $\sigma(\mu_i \rightarrow \mu_j)$ values on the ordinate is greater than the magnitude of the laboratory scattering range ($\mu_{\max} \leftrightarrow \mu_{\min}$) for all values of μ_i except ± 1 . For the case where $\mu_i = +1$, the non-zero range for $\sigma(\mu_i \rightarrow \mu_j)$ values is merely equal to the range between μ_{\max} and μ_{\min} . This equality is of utmost importance when selecting numerical quadrature sets for use with the azimuthally symmetric transport equation.

Consider the normal source problem of Section 3.2.2 in which Lobatto-12 and -14 quadrature sets were used (see Table 4). Transport calculations



- | | |
|---|---|
| I. $\beta_{\max} = \theta_i + \theta_{\max}$ | IV. $\beta_{\min} = \theta_i - \theta_{\max}$ |
| II. $\beta_{\max} = \pi$ | V. $\beta_{\min} = 0$ |
| III. $\beta_{\max} = 2\pi - \theta_i - \theta_{\min}$ | VI. $\beta_{\min} = \theta_{\min} - \theta_i$ |

Figure 22. Plot of β_{\max} and β_{\min} verses θ_i

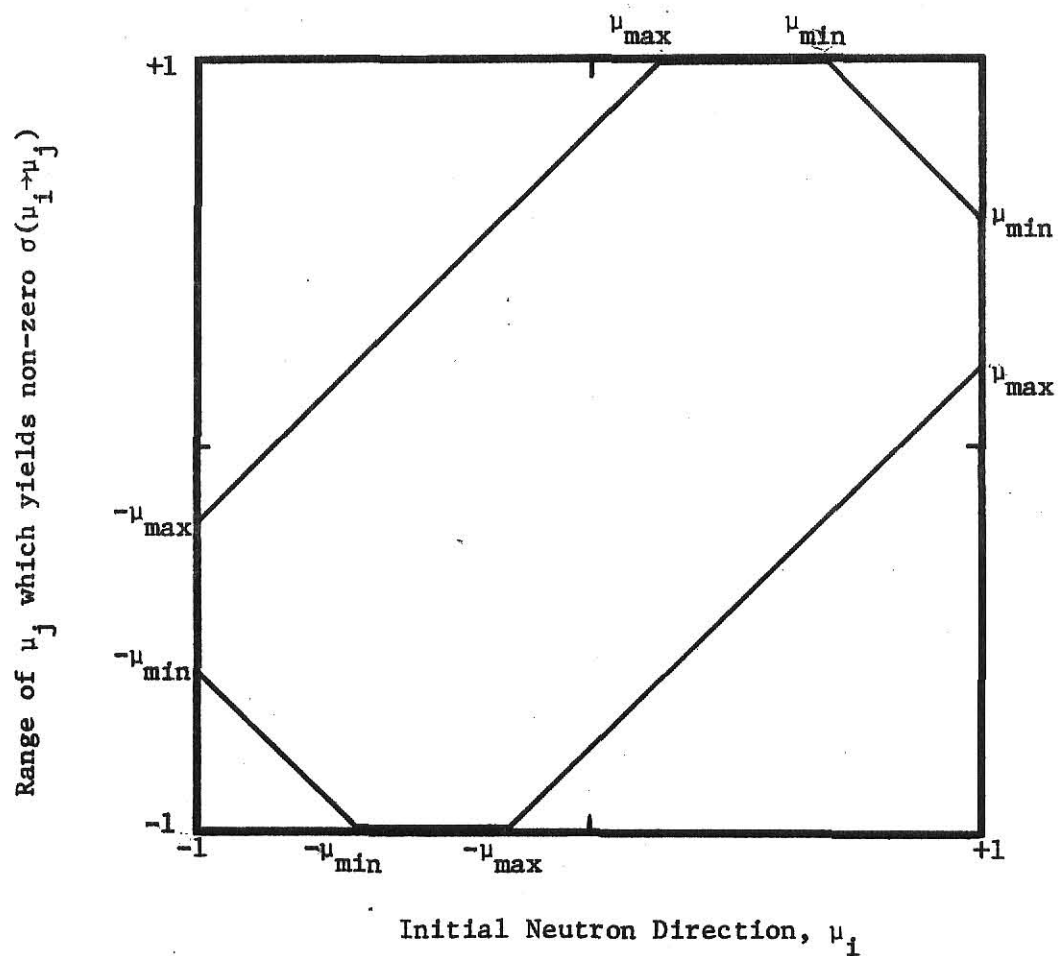


Figure 23. Plot for range of μ_j which will render a non-zero value of $\sigma(\mu_i \rightarrow \mu_j)$ for an initial neutron direction of μ_i

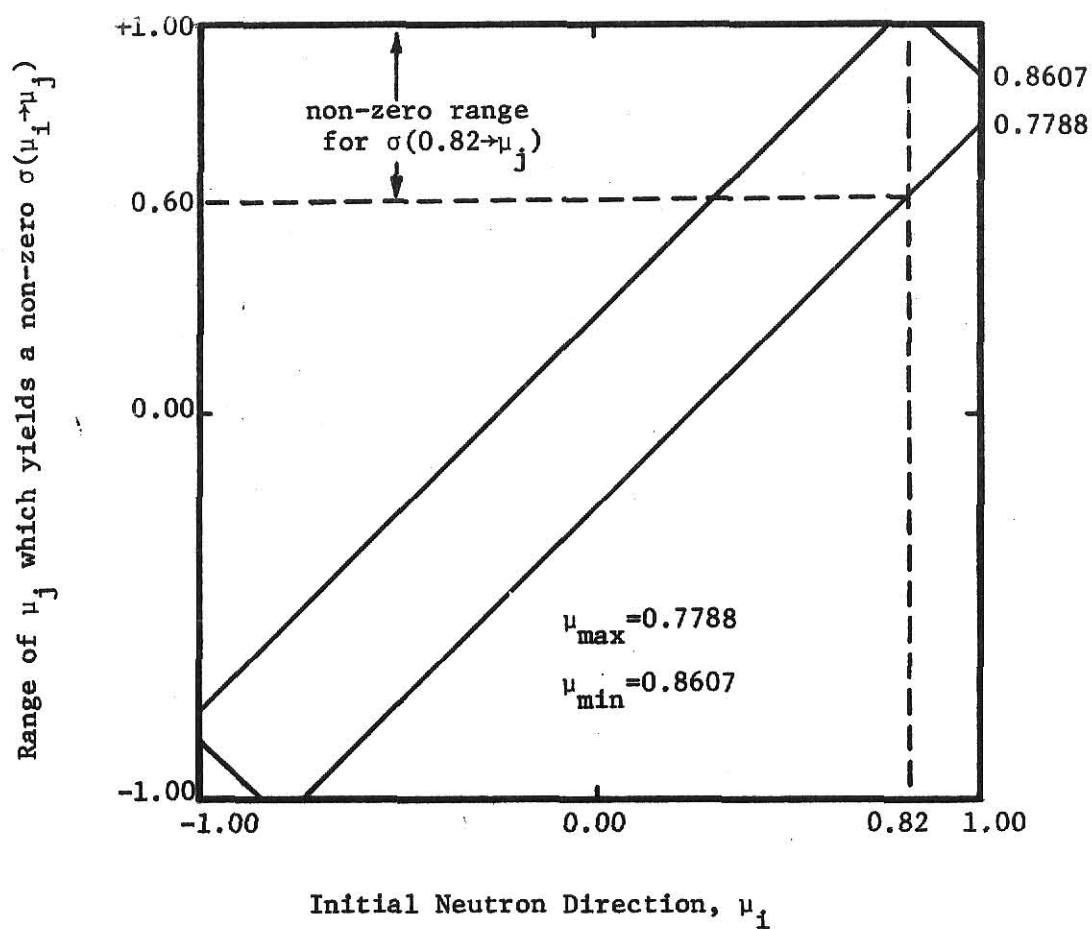


Figure 24. Example which determines the range of μ_j values which yield a non-zero $\sigma(0.82 \rightarrow \mu_j)$ value when $\mu_{\max} = 0.7788$ and $\mu_{\min} = 0.8607$

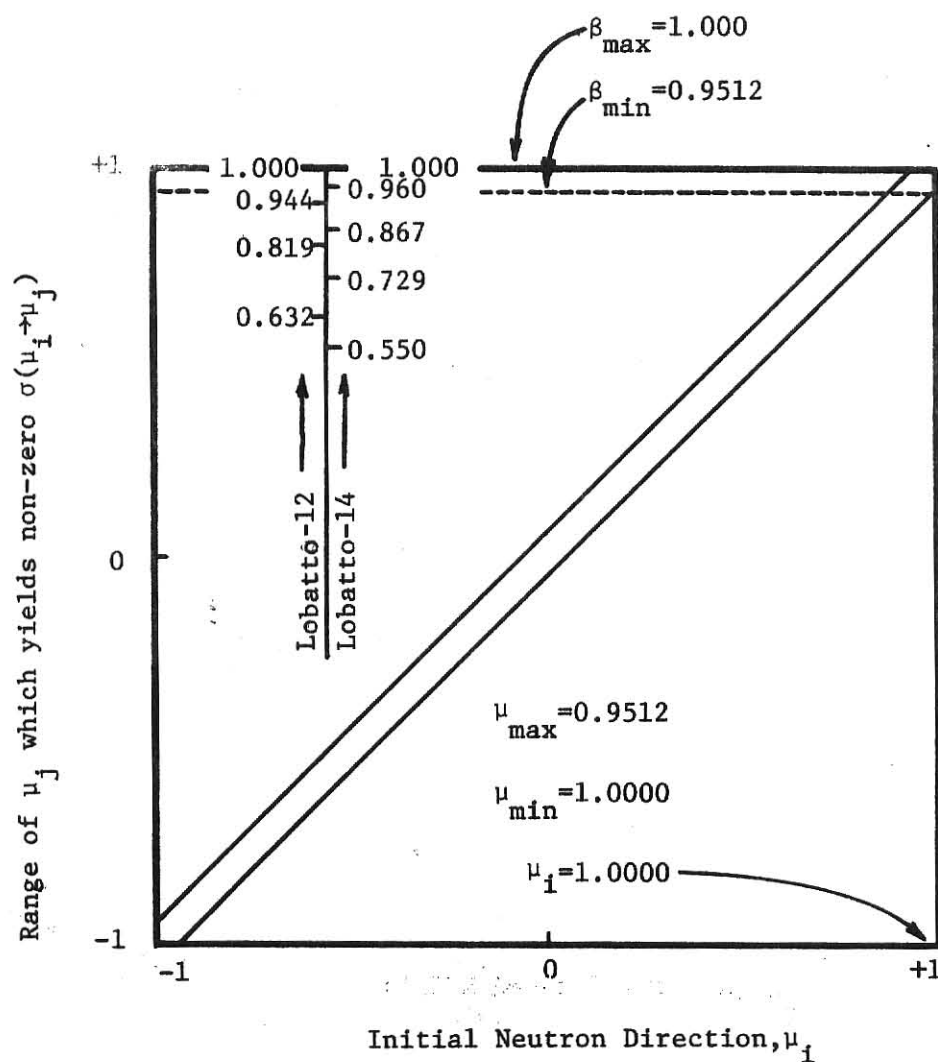


Figure 25. Lobatto 12 and 14 quadrature sets are examined for possible use with a normally incident neutron source on a hydrogen slab

carried out for a normally incident neutron spectra through 4.2 mean free paths of hydrogen show no angular transfer within the source group when the Lobatto-12 set was used. However, source group angular transfer occurred when the 12 point set was replaced by a Lobatto-14 set. The reason for this improvement is illustrated in Fig. 25. For both quadrature sets, the incident neutron source was placed in DLC/2 group 20 (2.0190-2.2313 MeV) at $\mu_{\text{source}} = \mu_1 = +1$. Values of μ_{min} and μ_{max} for transfer from group 20 to 20 can be calculated from Eq. (2.42). These values are 0.9512 (18.0°) and 1.0000 (0°) respectively. Thus, one observes from Fig. 25 that $\sigma(1.000 \rightarrow \mu_j)$ will only take on non-zero values when μ_j lies between 0.9512 and 1.0000. It is now apparent why no group 20 to 20 angular transfer occurred when the 12 point quadrature set was used; unlike the Lobatto-14 set, the Lobatto-12 set had no value of μ_j within the required range. Had scattering been slightly less anisotropic, i.e. if $\mu_{\text{max}} < 0.944$, the 12 point set could have been used with greater success.

3.3 Transport Calculations Using Triangularly Approximated Cross Sections

It has been pointed out that the usefulness of triangularly approximated transfer cross sections depends upon how well they reproduce transport results obtained with exact cross section values. In this section, comparisons are drawn between transport calculations carried out with exact and triangularly approximated cross sections. Also, some extensive calculations are presented which attempt to compare transport results to experimental data.

3.3.1 Comparison of Emergent Angular Densities

A series of computer codes developed by Odom [3] which solve the multi-group azimuthally dependent neutron transport equation for slab geometry were

used to analyze the utility of triangularly approximated scattering cross sections (see Appendix A). Figures 26 through 35 illustrate the results of such calculations. In these figures, BIGD was used to evaluate cross sections for the curves labeled "exact". LITTLED was used to evaluate these values for curves labeled "approximate". In all other respects calculations are identical. Figures 26, 27, and 28 compare transmitted angular densities through 4 inches of water. Similar comparisons are made by Figs. 29, 30, and 31 for 8 inch water slabs. Figures 32, 33, and 34 compare reflected angular densities through 8 inches of water. In all the cases, a unit neutron source was placed in group 20 with an incident direction of $\mu_{\text{source}}=0.5$. All transport calculations for Figs. 26-34 were carried out using a DP-7 (Double Gauss-7 point) numerical quadrature set for approximating the polar integration.

For all cases shown in Figs. 26 through 34, transport calculations using approximate cross sections agree favorably with data calculated from exact cross sections. A slight deviation of the curves as the polar angle approaches ± 1.0 is noted. This discrepancy is mainly attributable to the triangularly approximated oxygen component in the water cross section. This conjecture can be justified since Table 1 and Figs. 2, 3, and 10 show no significant differences between exact and approximate hydrogen cross sections. However, Figs. 7, 8, and 11 indicate that the triangular approximation is not always a reasonable one when applied to oxygen data.

It is interesting to note that the approximate water calculations for the group 20 to 20 reflected angular density in Fig. 32 shows a much larger deviation from the exact values than do similar calculations from groups 20 to 22 to 24 (see Figs. 33 and 34). This result is to be expected since for hydrogen to take any significant part in the shape of the reflected distribution, neutrons would have to undergo multiple in-group scatters. On the other hand,

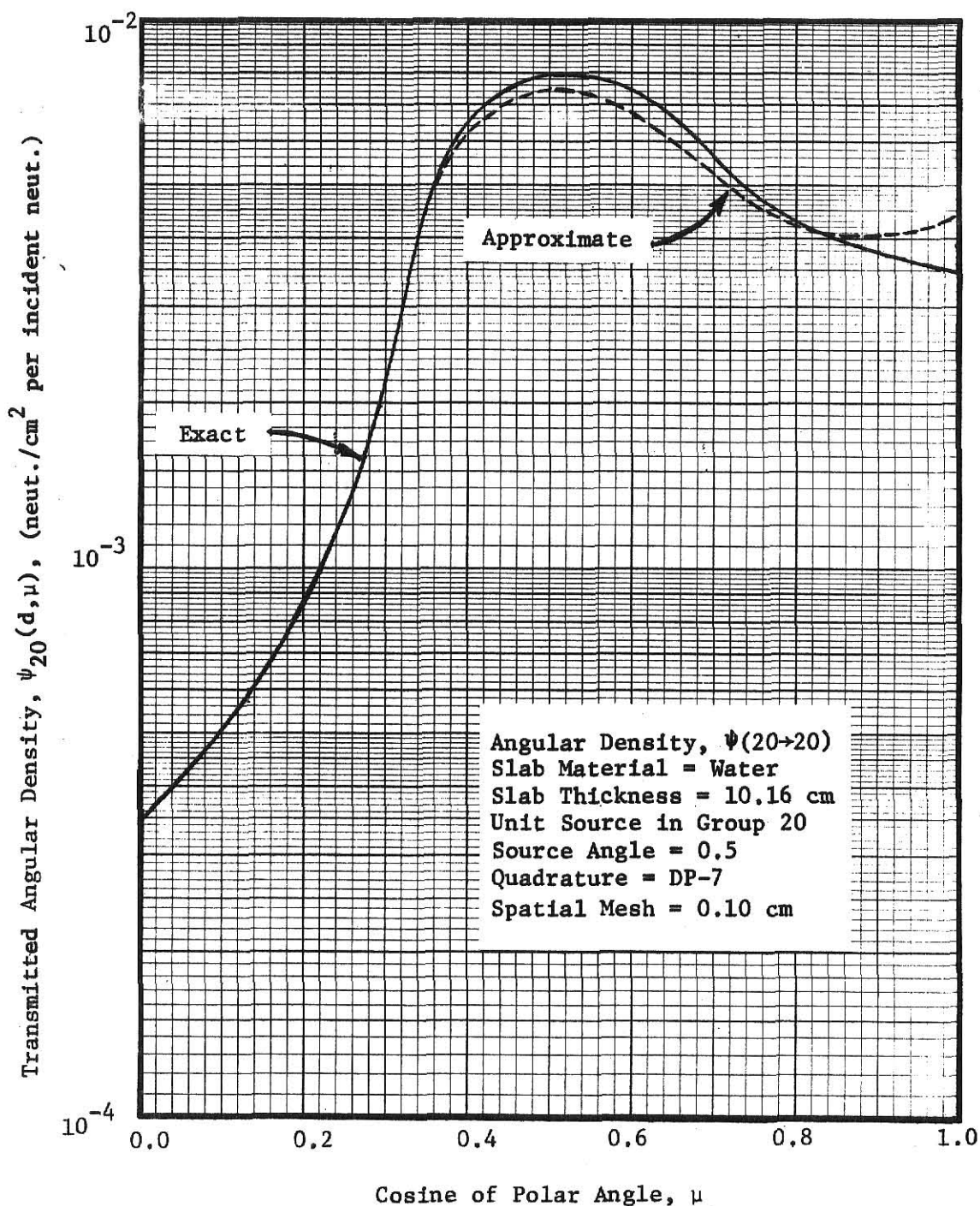


Figure 26. Transport calculations using exact and approximate angular transfer cross sections are compared for group 20 to 20 transfer through a 4 inch water slab (DLC/2 group 20 = 2.2313→2.0190 MeV)

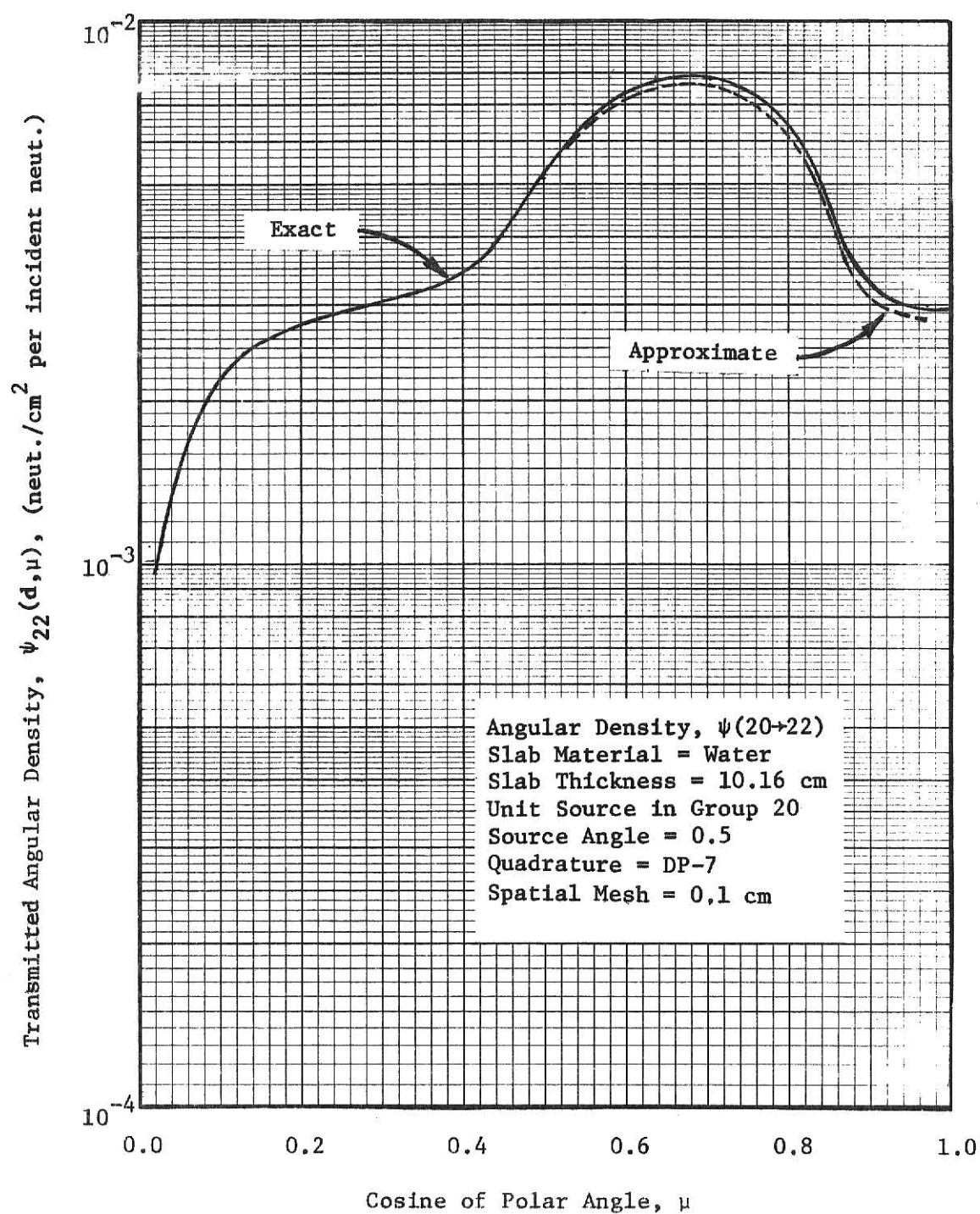


Figure 27. Transport calculations using exact and approximate angular transfer cross sections are compared for group 20 (2.2312-2.0190 MeV) to 22 (1.8268-1.6530 MeV) transfer through a 4 inch water slab

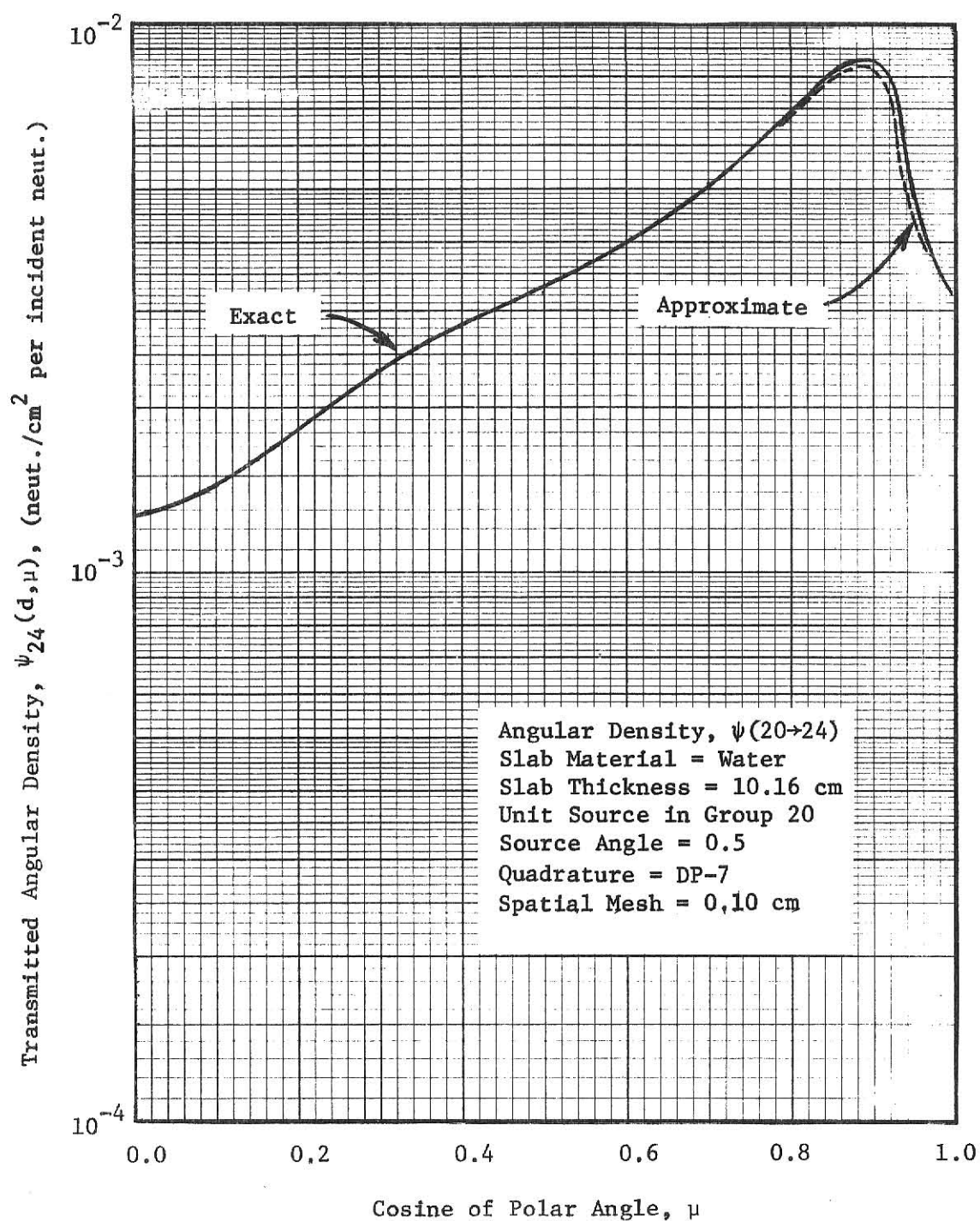


Figure 28. Transport calculations using exact and approximate angular transfer cross sections are compared for group 20 (2.2313-2.0190 MeV) to 24 (1.4957-1.3534 MeV) transfer through a 4 inch water slab

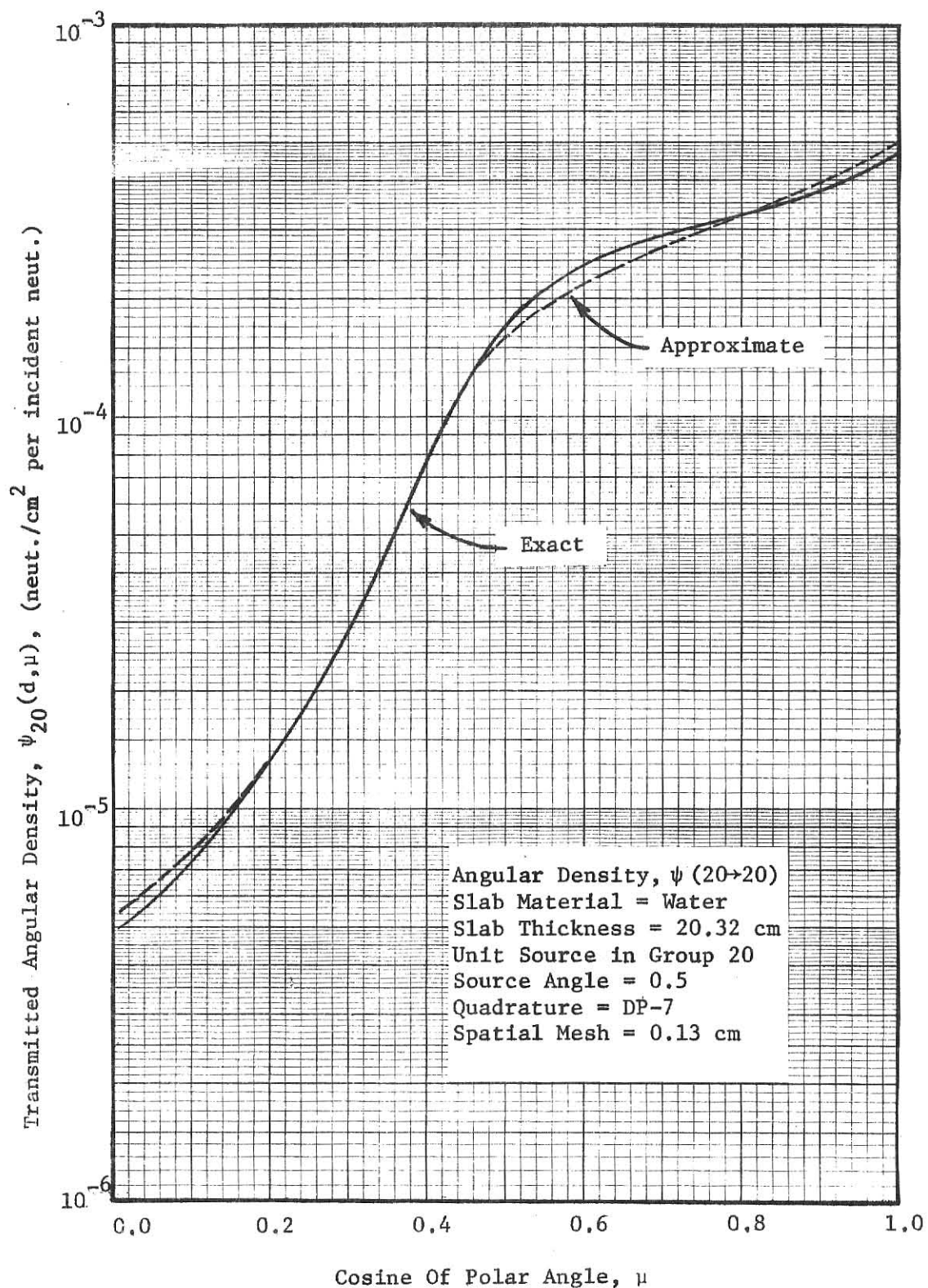


Figure 29. Transport calculations using exact and approximate angular transfer cross sections are compared for group 20 to 20 transfer through an 8 inch water slab (DLC/2 group 20 = 2.2313-2.0190 MeV)

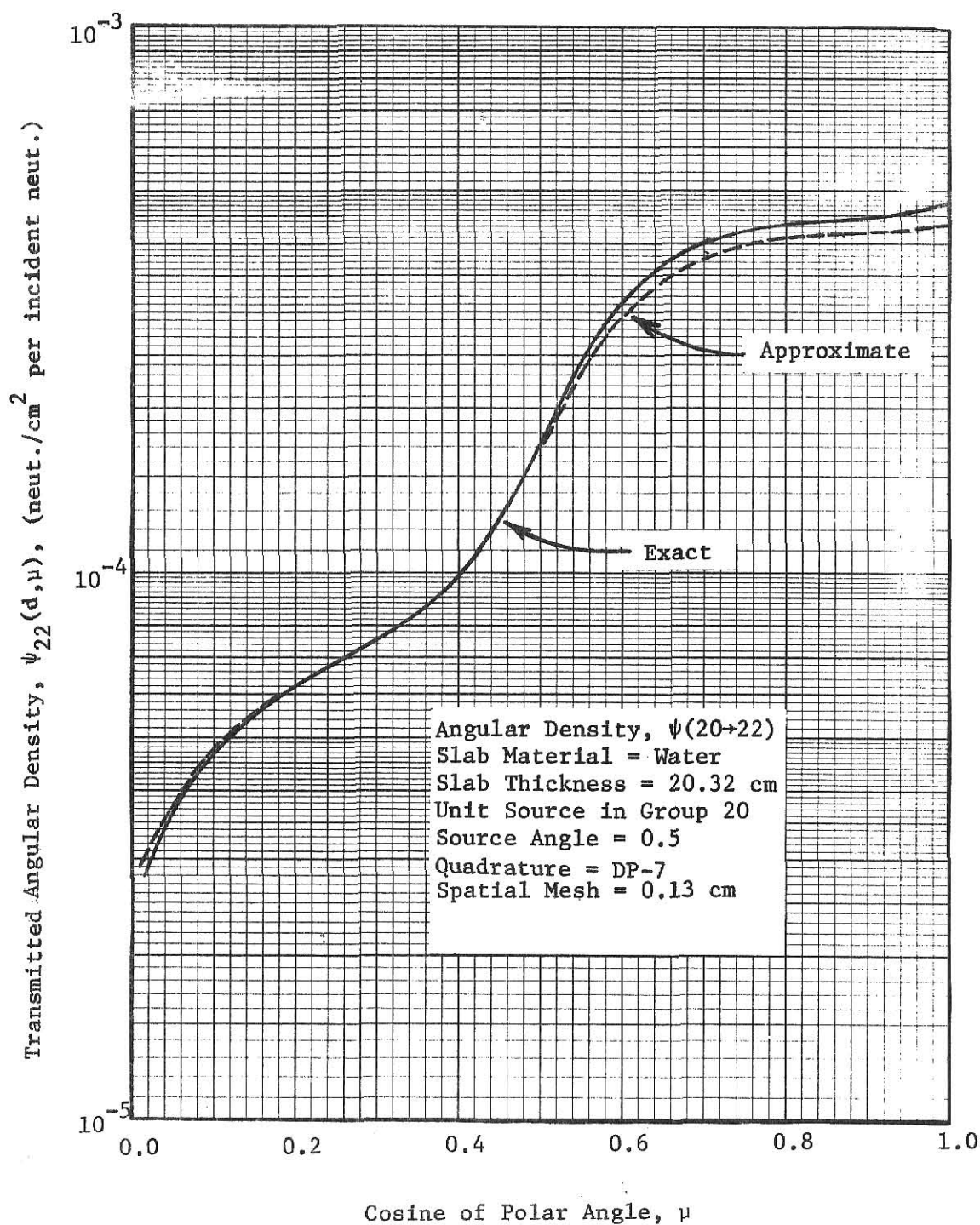


Figure 30. Transport calculations using exact and approximate angular transfer cross sections are compared for group 20 (2.2313-2.0190 MeV) to 22 (1.8268-1.6530 MeV) transfer through an 8 inch water slab

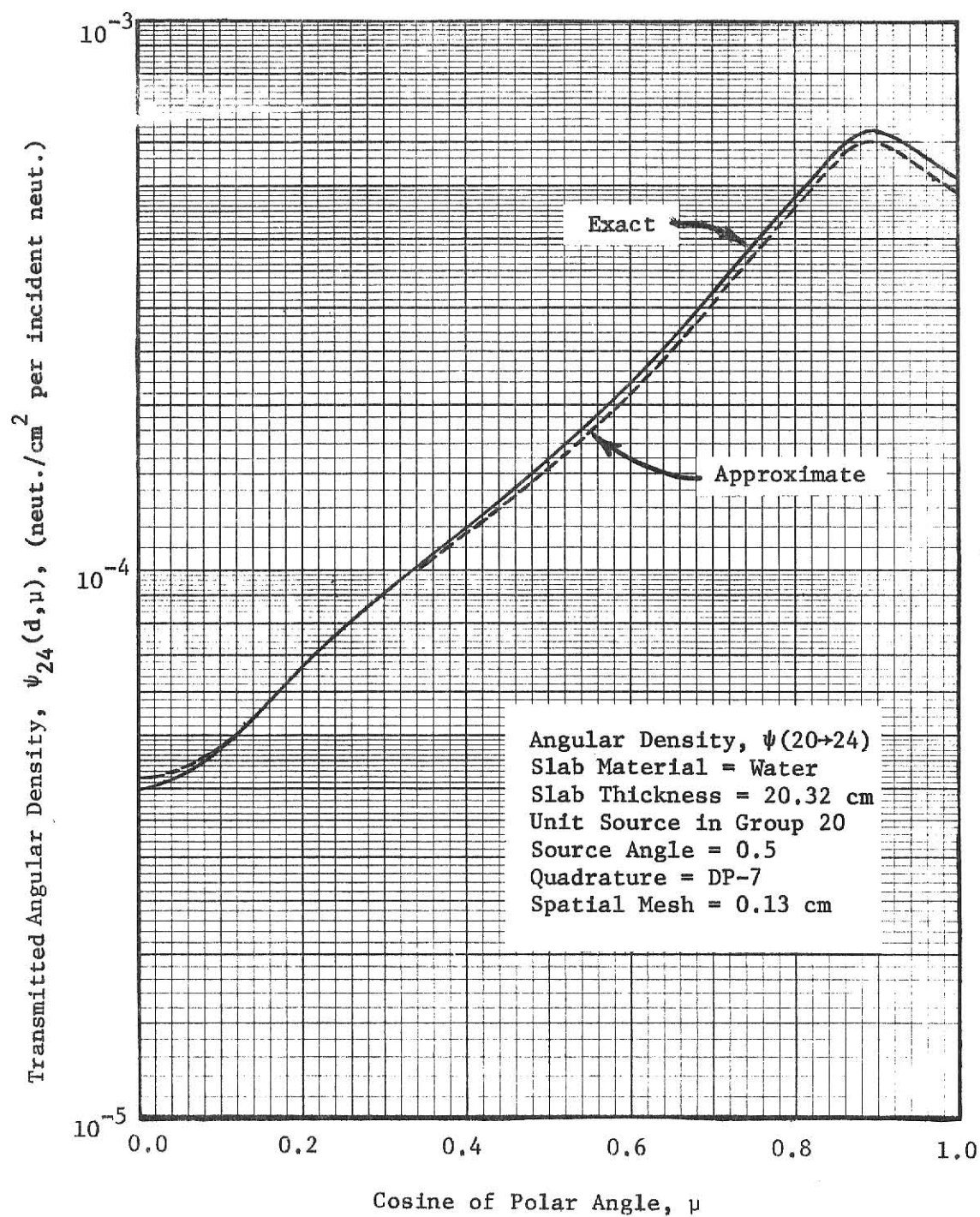


Figure 31. Transport calculations using exact and approximate angular transfer cross sections are compared for group 20 (2.2313–2.0190 MeV) to 24 (1.4957–1.3534 MeV) transfer through an 8 inch water slab

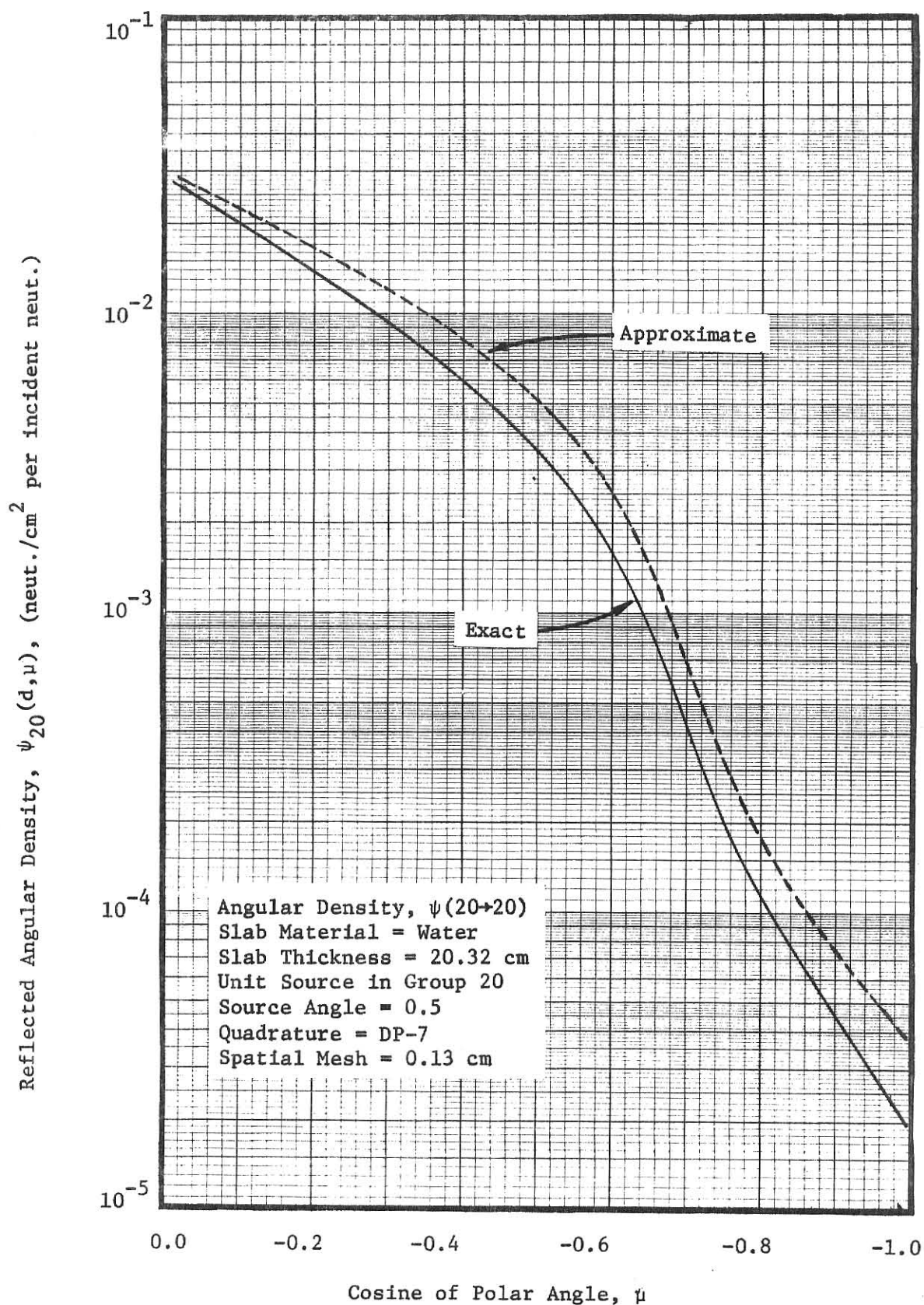


Figure 32. Transport calculations using exact and approximate angular transfer cross sections are compared for a DLC/2 group 20 to 20 transfer through an 8 inch water slab (DLC/2 group 20 = 2.2313-2.0190 MeV)

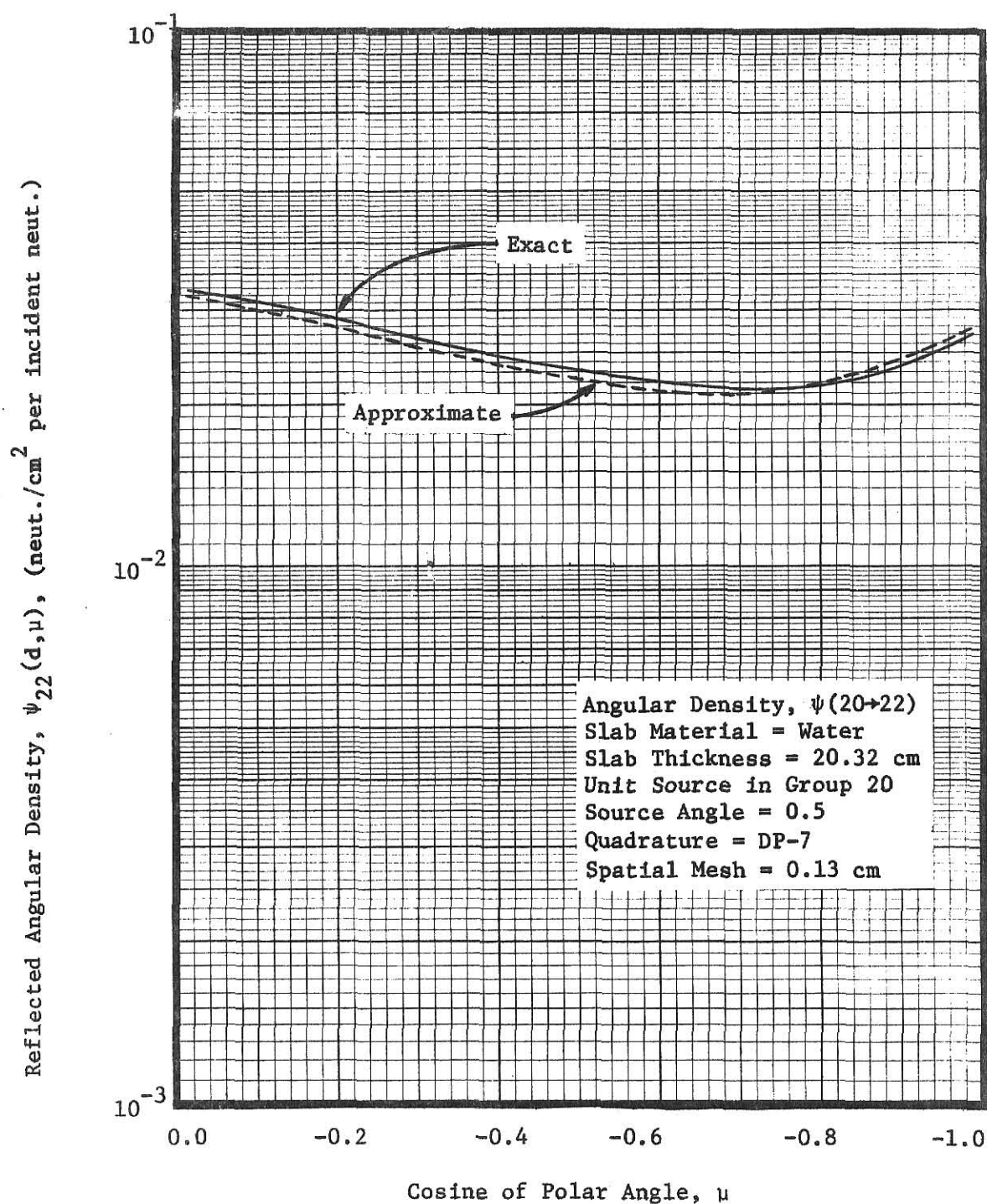


Figure 33. Transport calculations using exact and approximate angular transfer cross sections are compared for group 20 (2.2313-2.0190 MeV) to group 22 (1.8268-1.6530 MeV) for transfer through an 8 inch water slab

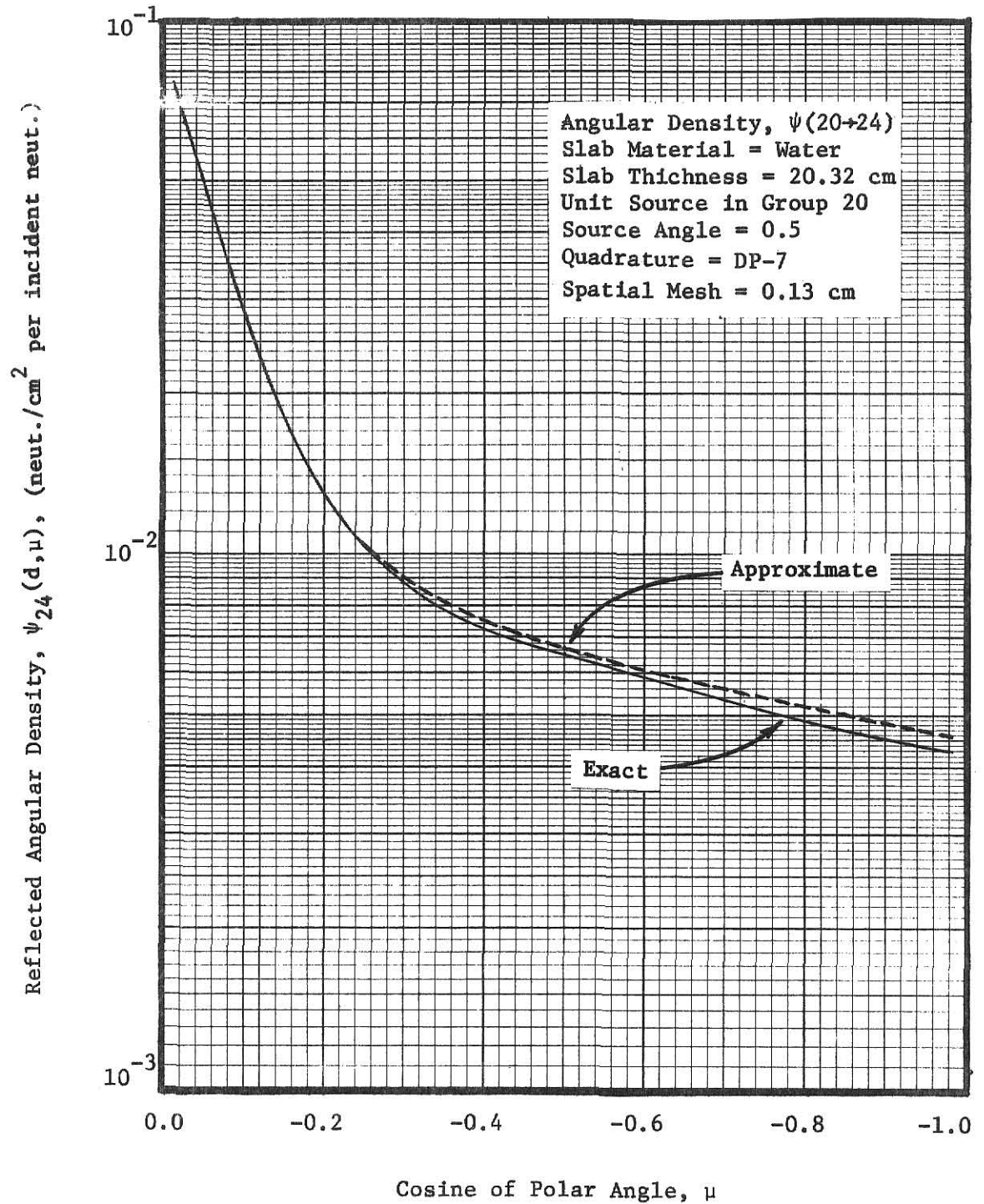


Figure 34. Transport calculations using exact and approximate angular transfer cross sections are compared for group 20 (2.2313-2.0190 MeV) to group 24 (1.4957-1.3534 MeV) transfer through an 8 inch water slab

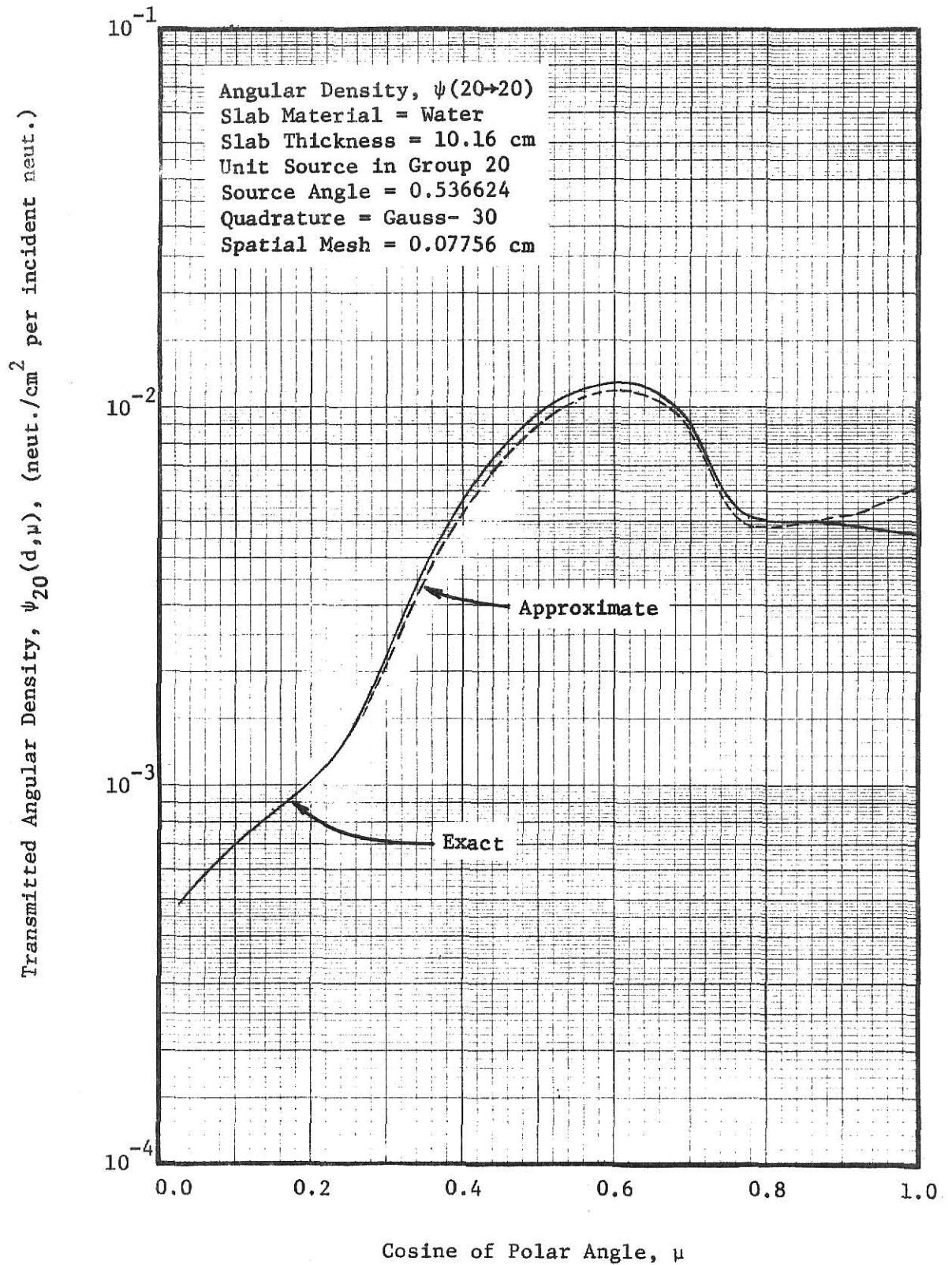


Figure 35. Transport calculations using exact and approximate angular cross sections are compared for a group 20 to 20 transfer through a 4 inch water slab using a Gauss-30 quadrature (DLC/2 group 20 = 2.2313-2.0190 MeV)

neutrons which scatter only once or twice with oxygen would quickly reach reflected directions. Since the triangular approximation for the oxygen cross sections show moderate deviation from exact cross section values, the in-group reflected angular density is expected to show more significant differences from results which use exact cross sections.

The possibility does exist that discrepancies in Figs. 26 through 34 result from minor differences in the way approximate cross sections respond to the DP-7 quadrature used for transport calculations. However, Fig. 35 illustrates similar deviations when a 30 point Gaussian quadrature is employed to calculate the transmitted density through 4 inches of water.

3.3.2 Comparison of Calculated and Experimental Results

Transport calculations presented thus far have only examined the ability of approximate cross sections to represent exact values over a small energy decrement. The greatest down scatter case has been that of Figs. 28, 31, and 34 which show transfers from group 20 to 24. To evaluate the usefulness of triangular transfer cross sections for more general transport applications, a problem involving a larger number of energy groups was studied. Experimental data for water slab penetrations were obtained from Meyer [30]. In his experiment a neutron beam approximately 1.25 inches in diameter was directed normally onto an 8 inch water slab. The incident beam spectrum is given in Table 6, and some of the experimental data are plotted in Fig. 36.

Exact and triangularly approximated transfer cross sections were used with the incident beam spectrum from Table 6 in the previously mentioned transport model named MGRP. A 14 point Lobatto quadrature was selected to discretize the polar angle. Figure 36 gives experimental results for $\psi_g(x, \mu)$ only at 11.2° , 33.6° , and 45.0° . Since these angles are not part of the standard Lobatto set, dummy angles with a quadrature weight of zero were inserted at 11.2° and 45.0° .

Table 6. Incident neutron spectrum for experimental water data[†] (Ref. 30).

<u>DLC/2 Group</u>	<u>Energy Range</u>	<u>Neu/cm² sec</u>
1	14.9180 - 13.4990	0.230
2	13.4990 - 12.2140	0.245
3	12.2140 - 11.0517	0.178
4	11.0517 - 10.0000	0.809
5	10.0000 - 9.0484	1.730
6	9.0484 - 8.1873	2.602
7	8.1873 - 7.4082	3.728
8	7.4082 - 6.7032	5.385
9	6.7032 - 6.0653	6.150
10	6.0653 - 5.4881	6.084
11	5.4881 - 4.9659	6.015
12	4.9659 - 4.4933	7.109
13	4.4933 - 4.0657	8.111
14	4.0657 - 3.6788	8.577
15	3.6788 - 3.3287	8.448
16	3.3287 - 3.0119	9.978
17	3.0119 - 2.7253	13.196
18	2.7253 - 2.4660	17.751
19	2.4660 - 2.2312	23.033
20	2.2313 - 2.0190	28.101
21	2.0190 - 1.8268	34.146
22	1.8268 - 1.6530	40.031
23	1.6530 - 1.4957	43.379
24	1.4957 - 1.3534	44.525
25	1.3534 - 1.2246	44.526
26	1.2246 - 1.1080	42.335

[†] The experimental neutron spectrum obtained from Meyer [30] was numerically integrated over the DLC/2 energy structure to produce this table. It should be pointed out that energy group 1 contains only those neutrons which have energies between 14.918 and 13.499 MeV. If high energy neutrons from 19.4 to 14.918 MeV are included in the first group, then the group 1 sum would read $(0.2302 + 0.8527) = 1.0829$ neut/cm²sec. Meyer points out that spectral data above 12 MeV is somewhat unreliable. However, this is of little consequence since low energy transport calculations carried out using the spectrum as shown in this table could not be appreciably affected by significant errors in the first few high energy groups. These groups constitute only a small fraction of the total energy spectrum.

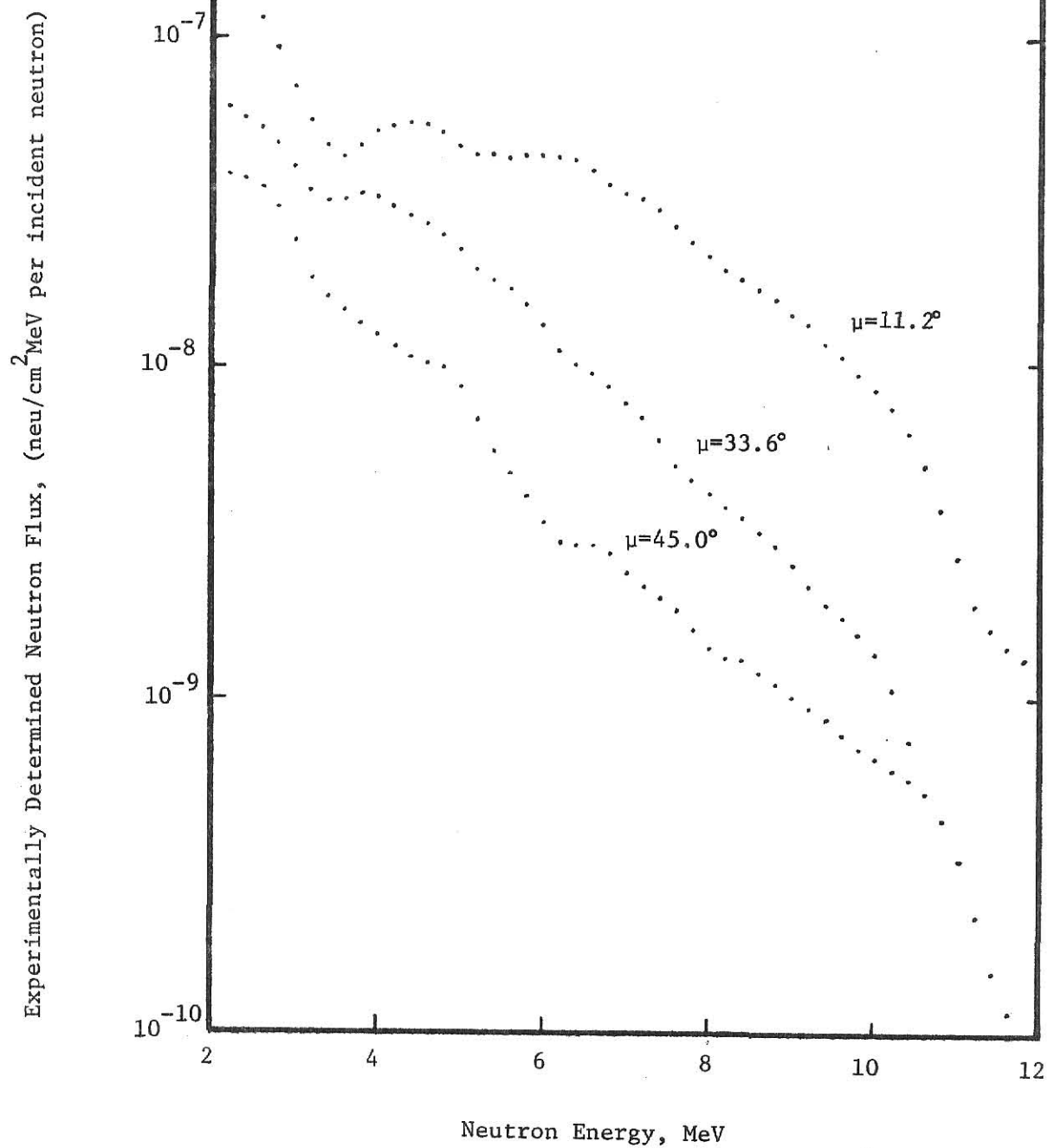
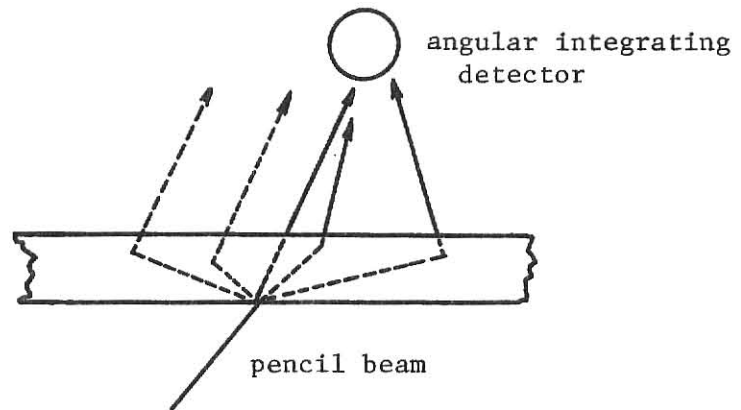


Figure 36. Experimental penetration data from Meyer(30) for normal incidence of a 1.25 cm neutron beam upon an 8 inch water slab

One noteworthy difference should be pointed out between the experimental configuration and the transport model used in MGRP. The transport model used by MGRP applies only to a slab system illuminated by a uniformly distributed slant source. However, the experimental transmission spectrum is for a slab that has been illuminated by a small diameter neutron beam (sometimes referred to as a "pencil beam"). The experimental data were obtained from a detector that responded to fast neutrons which hit it regardless of their polar and azimuthal angles; whereas, the transport model's calculated angular flux refers to neutrons traveling in well-defined directions (see Fig. 37). Nevertheless, the angular transmitted flux for the pencil beam experiment can be expected to agree with the calculated results from the uniform illumination problem under certain circumstances. The transport model calculates, for a uniformly illuminating slant source, the total flux of neutrons which exit per unit area of the slab face in a fixed direction. The same value (with an appropriate source normalization) could be measured experimentally using an incident pencil beam source by sweeping a collimated detector across the face of the slab. This procedure would integrate the total number of neutrons which exit the slab in a fixed direction from all possible incident beam locations (see Fig. 38).

Movement of the detector creates difficulties in the design of such experiments. Odom [3] and Hill [17] use the computer code TWOTRAN to demonstrate that for thin slabs the angular flux decreases very rapidly as one moves laterally away from the uncollided pencil beam in the slab. Thus, for large lateral distances, the probability of a neutron being emitted at an angle which would strike an angularly integrating detector becomes exceedingly small. Consequently, a stationary angularly integrating detector placed a large distance away from the exit slab face will detect essentially all



MGRP TRANSPORT MODEL CONFIGURATIONS

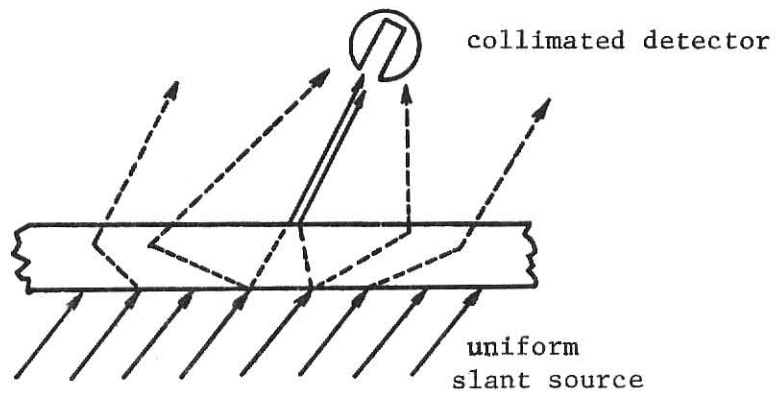
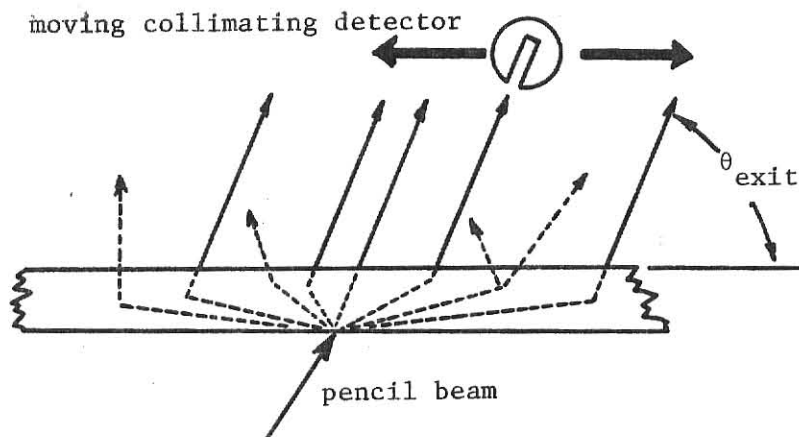


Figure 37. Experimental and transport model comparison



APPROXIMATE EXPERIMENTAL EQUIVALENCE TO
UNIFORM ILLUMINATION TRANSPORT MODEL

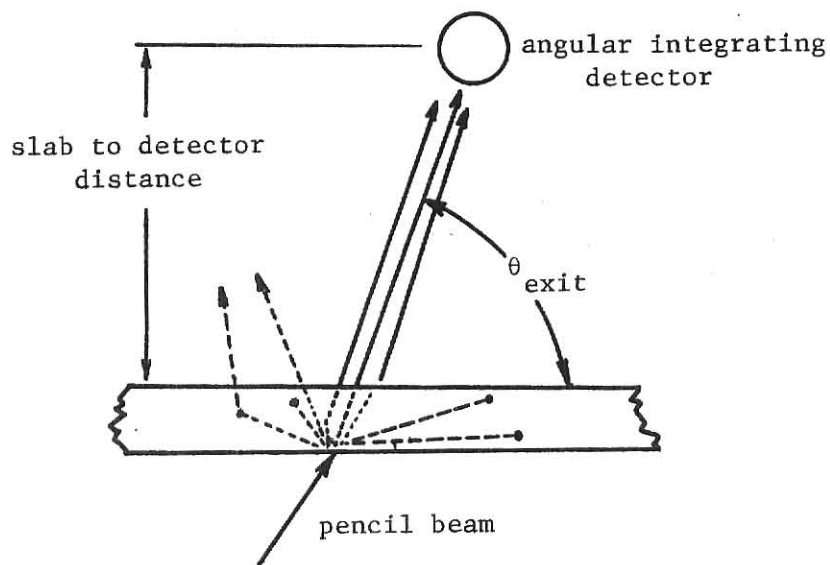


Figure 38. Exact and approximate experimental equivalence to the uniform illumination source

neutrons transmitted through the slab at approximately the same exit angle. This occurs since all neutrons hitting the detector come from roughly the same area of the exit face. This approximate equivalence is illustrated in Fig. 38. This approximation should become more accurate for thin slabs since beam spread would be minimized. Accuracy of the approximation should also increase with increases in slab to detector distances since then, neutrons which significantly deviate from θ_{exit} would not be picked up by the angularly integrating detector.

Data from Meyer [31] tend to support the source equivalence between the two configurations of Fig. 38 only at high neutron energies and for small scattering angles. These data suggest that high energy neutrons which scatter only a few times at shallow angles undergo little energy loss. These neutrons are transmitted through the slab and exit very near their extrapolated entry point. However, some low energy neutrons that undergo multiple scatters are observed to exit the far side of the slab at great distances from their extrapolated entry point (and consequently may not be "seen" by the detector). This phenomena causes transport calculations for the angular flux in a discrete direction at low energies to overestimate the experimentally determined value for that same direction. Hence, from experimental data for a 6.6° exit angle and an 8 inch water slab, Meyer concludes that the approximate source equivalence in Fig. 38 breaks down below about 3.5 MeV.

Angular densities calculated by MGRP (using exact cross section values) and by the Monte Carlo computer code MORSE [30] (using eighth order Legendre expanded cross section values) are compared to experimental data in Fig. 39. Transmitted angular densities appear to compare well for the 11.2° exit direction down to about 6.5 MeV (note that this is a logarithmic plot). Past

this point calculated angular densities slightly exceed experimental results; the validity of the source equivalence suggested by Fig. 38 appears to dwindle. Transmitted densities in the 45° direction compare poorly for all neutron energies. These results are to be expected. There appears to be a direct relationship between the energy and deflection angle for transmitted neutrons, and the validity of the hypothesized point versus uniform source illumination equivalence. The smaller the exit angle for transmitted neutrons, the lower the energy is for which the source equivalence remains valid.

From the preceeding comments, it is evident that only limited comparisons are possible between the calculations from MGRP and experimental results. Despite these limitations, calculations using triangularly approximated cross sections were carried out for the experimental spectrum in Table 6. Although these calculations may not be readily comparable to the experimental data, the information does serve as a check on how well triangularly approximated cross sections perform in general transport applications. Such an analysis is important since transport results produced from exact cross section data can never be expected to exactly coincide with results based upon approximate cross sections.

Figure 40 compares transport calculations based upon exact and approximate angular scattering cross sections. Both sets of calculations were carried out using the experimental spectrum from Table 6. In Fig. 40 there is general agreement in shape between the two sets of results. However, results using approximate cross sections tend to underpredict values obtained from exact cross sections. This outcome is to be expected since for all cases of neutron downscattering in Figs. 26 through 34, the transport calculations using approximate cross sections underpredicted the exact results. It is important to note that Figs. 26 through 34 all indicate better agreement between exact

and approximate results as μ decreases. Consequently, deviations between exact and triangularly approximated values in Fig. 40 would be expected to decrease as μ decreases. Such was found to be the case. Figure 41 illustrates transport results analogous to those of Fig. 40 for a slightly smaller μ value. The deviations between approximate and exact results are indeed smaller.

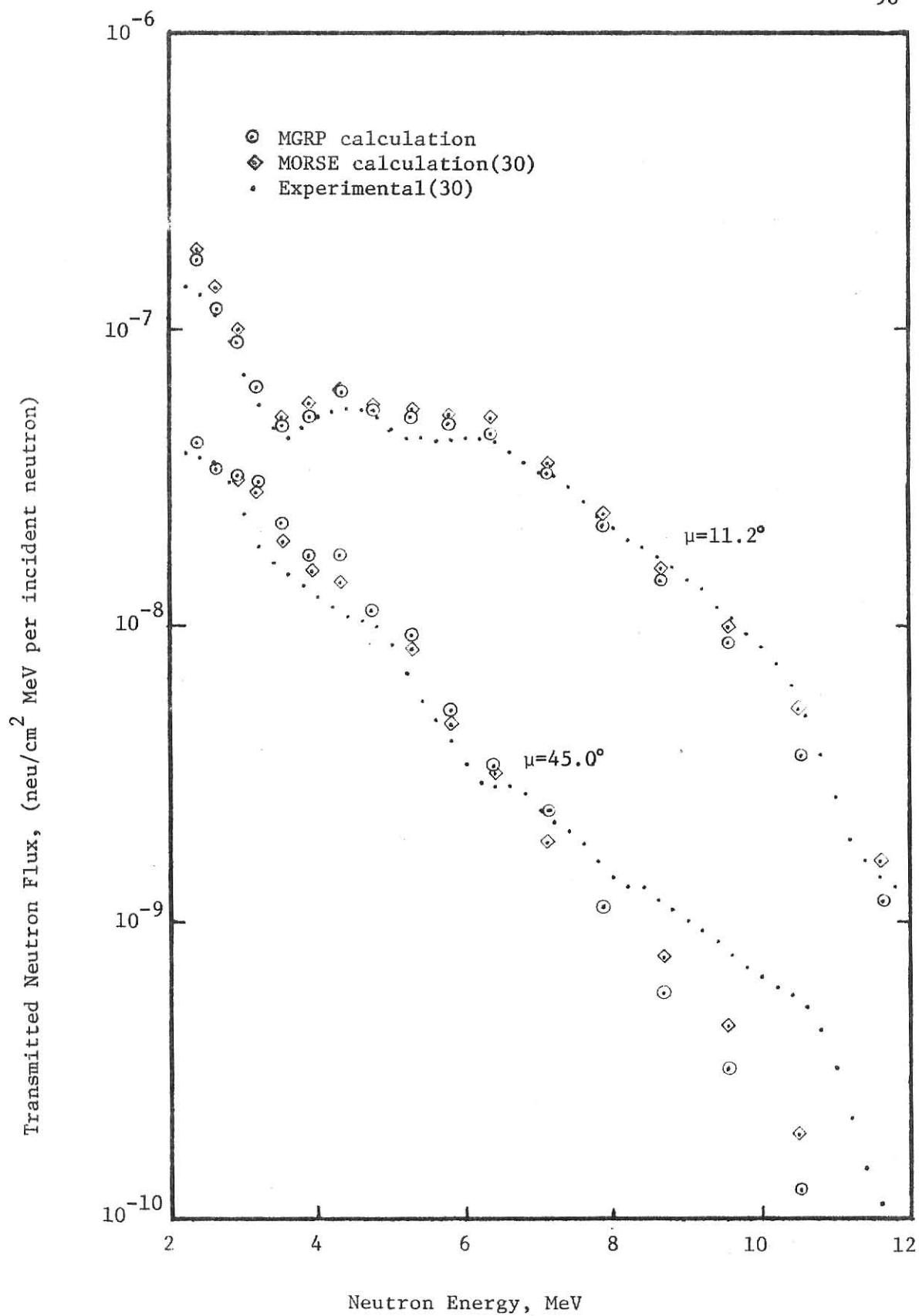


Figure 39. Comparison of calculated and experimental results for an 8 inch water slab

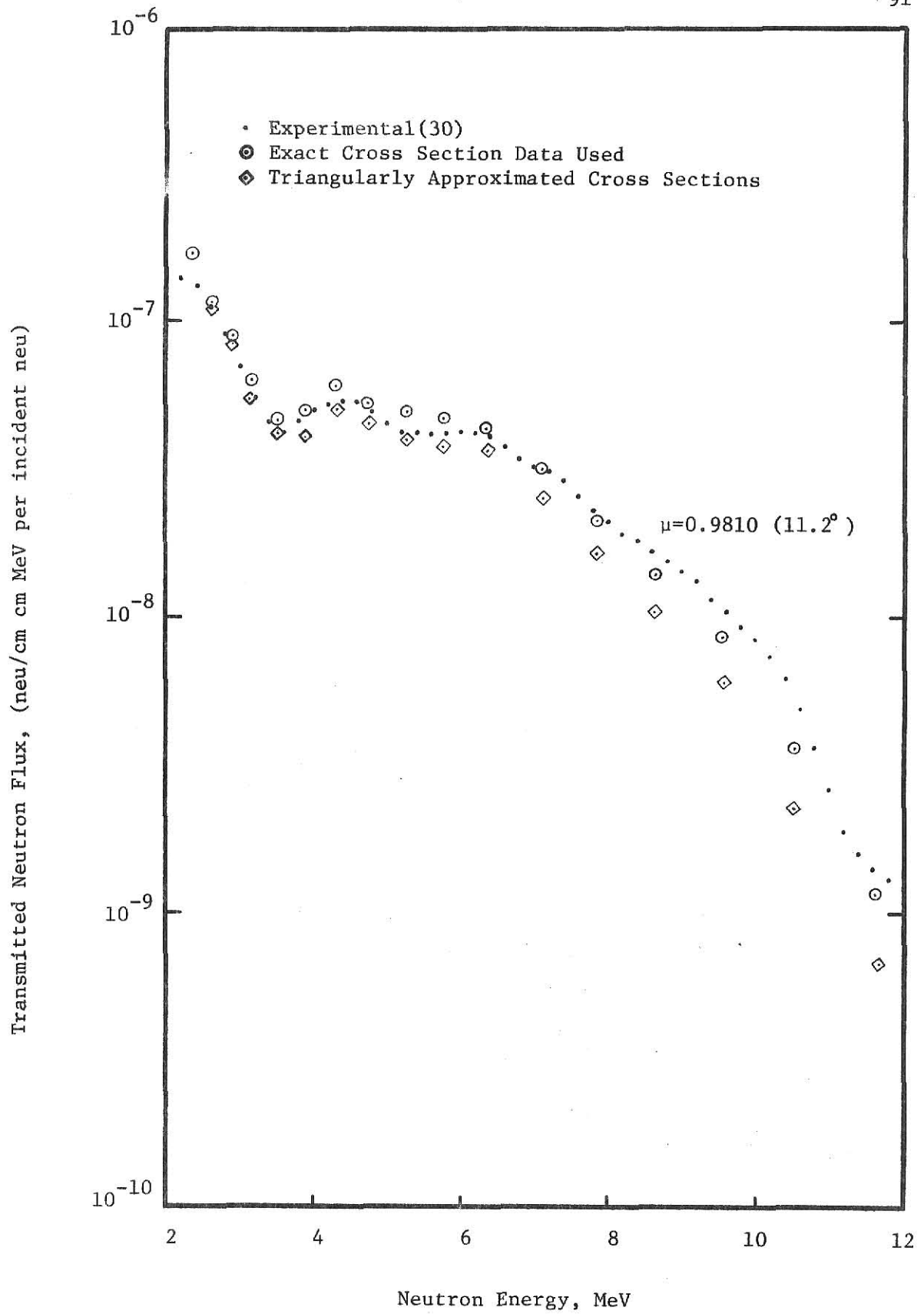


Figure 40. Comparison of transmitted fluxes for an exit angle of 11.2° through 8 inches of water

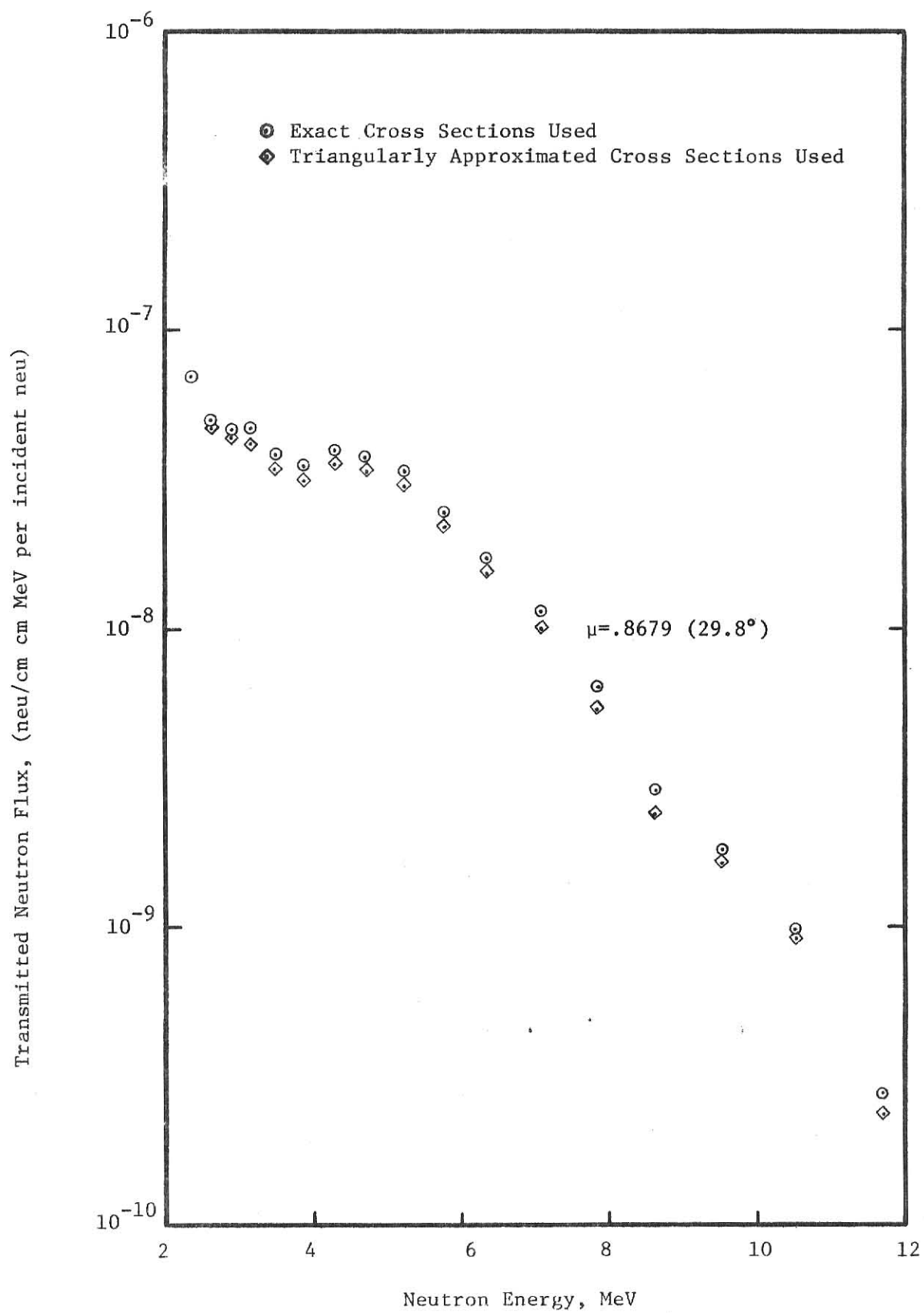


Figure 41. Comparison of transmitted fluxes for an exit angle of 29.8° through 8 inches of water

4.0 Conclusions

In this work, simple numerical techniques have been studied which aid in the analysis of azimuthally-symmetric multigroup neutron transport problems involving anisotropic scattering. Particular attention has been focused upon the use of elastic group-to-group transfer cross sections for light element scattering in transport calculations. These cross sections tend to be highly anisotropic in the scattering angle because of elastic scattering energy-momentum constraints. As finer multigroup structures are used, angular support of the scattering cross section becomes increasingly small. Consequently, the anisotropy of the multigroup scattering cross sections become more pronounced. Use of conventional Legendre expansion techniques to represent such highly anisotropic cross sections often introduce serious oscillatory errors into transport calculations.

It has been shown in this work that many highly anisotropic group-to-group transfer cross sections may be represented by simple piecewise linear functions. The exact nature of these functions depend upon the type of multigroup energy structure used. In the general case, a group-to-group transfer cross section may be approximated by a quadrilaterally shaped distribution. However, when an equal lethargy width energy structure is employed, many transfer cross sections can be well-approximated by triangularly shaped distributions. Such an approximation is excellent for hydrogen scattering. Since hydrogen scatters isotropically in the center of mass coordinate system and its elastic scattering cross section is a relatively smooth function of energy. The approximation becomes less useful for other elements which scatter anisotropically in the center of mass system and whose elastic scattering cross section exhibits numerous resonance peaks. Such is the case for oxygen. Although the triangular approximation of oxygen group-to-group cross sections

does not provide an extremely accurate representation for all group transfers of the relatively broad DLC/2 group structure, it does constitute a definite improvement over customary Legendre expansion techniques. Use of a fine group structure, such as would be employed to study the transmission of neutrons in the oxygen antiresonance region, would considerably improve the triangular method's ability to represent exact transfer cross sections.

The approximate method for evaluating highly anisotropic transfer cross sections not only eliminates the unrealistic oscillatory behavior typical of Legendre expansions, but, it also provides for an increase in cross section computational efficiency. Unlike Legendre expansion techniques which require computer storage of eight or more moments for Legendre reconstitution, the triangular method only requires the storage of a single value (i.e., the total group-to-group transfer cross section). Furthermore, computational time can be saved by using the triangular transfer cross section representation since Legendre reconstitution is not needed; cross section values can readily be calculated by simple linear interpolation of a triangular distribution.

Only hydrogen and oxygen cross sections were examined in this work. However, the methods employed are completely general. Because of their relatively smooth fast neutron scattering cross sections, it is expected that elements such as deuterium, boron, and lithium may also lend themselves to effective anisotropic transfer cross section evaluation by the approximate triangular technique.

The triangular approximation has been incorporated into discrete ordinate transport calculations to obtain emergent energy and angular dependent fluxes from water slabs illuminated with a normally incident neutron beam. Although minor differences are noted as the polar scattering angle approaches ± 1 , these calculations compare favorably with results obtained using exact scattering

distributions. In the forward directions, results from approximate cross sections underpredict those obtained using exact transfer cross sections. As the polar angle increases, the transmitted flux obtained by using triangular distributions tends toward the exact result. The differences between calculations using exact and approximate cross sections are wholly dependent upon the ability of triangular distributions to model exact anisotropic scattering cross sections. The fact that triangularly approximated emergent fluxes for water slightly underpredict exact results is not a general rule which can be applied to all elements. Further investigation of how good the triangular approximation is for elements other than hydrogen and oxygen must first be carried out before any general statements regarding the conservatism of this approximation can be made. The important point to note is that results obtained using triangularly approximated cross sections are in fair agreement with exact transport calculations. The average deviation between exact and approximate results in Figs. 36 and 37 is only 16%.

To insure that discrete ordinate transport results using approximate cross sections were justly compared to those calculated using exact values, particular attention was given to quadrature set selection. This work has demonstrated that discretization of the polar angle in transport calculations is not entirely arbitrary. It depends upon the degree of scattering anisotropy present for the particular problem under consideration. For a given nuclei, it is possible to predetermine the minimum order quadrature required to adequately discretize the polar angle. Such an ability is important since it can avoid costly computer errors caused by under- or over-specifying the size of a numerical quadrature.

Several possibilities exist for further study in areas related to this work. One of the most important areas which warrants further investigation

relates to the examination of the triangular approximation for elements other than hydrogen and oxygen. Two elements of particular interest might be lithium and deuterium because of their low atomic mass (which increases scattering anisotropy) and specific application in fusion reactor blanket and shield studies. Future studies might also center around the nature and ability of quadrilaterally shaped distributions to represent transfer cross sections for energy structures of unequal lethargy widths. Although this work primarily dealt with equal lethargy width energy structures, it is sometimes convenient to employ other types of energy structures. This is particularly true when studying neutron transport through a strong resonance or antiresonance region of a material. One last area which merits future development is that of quadrature set selection. The techniques necessary to establish the adequacy of a given quadrature for use in highly anisotropic scattering problems were developed in this work. Future work in this area could be directed toward the development of a computer code capable of carrying out an adequacy evaluation on numerical quadratures for neutron as well as gamma ray transport problems (energy-momentum constraints also impose restrictions on scattering angles in gamma ray transport).

In summary, the approximate triangular technique employed provides for simple and effective evaluation of angular scattering transfer cross sections. The new technique used to evaluate the adequacy of angular quadratures holds promise to eliminate much of the guess work involved in selection of numerical quadrature sets for transport calculations. It is expected that methods introduced in this work will add to the understanding of anisotropic neutron transport, and provide a basis to carry out transport calculations more efficiently and accurately.

5.0 Acknowledgements

The author cannot adequately express his gratitude to Dr. J. K. Shultis for advice and consultation frequently provided in matters technical and otherwise. The financial aid of the National Science Foundation Grant ENG73-03644 is gratefully acknowledged. The computer time and assistance provided by the Kansas State University Computing Center is also recognized.

Most sincere thanks go to Carol Adams for the time and effort spent typing this text. Lastly, the author would like to extend a special thanks to his parents and fiancée who provided continued encouragement throughout his graduate and undergraduate years of study.

6.0 References

1. D. H. Timmons, "Treatment of Hydrogen Scattering in Multigroup S Transport Calculations," Trans. Am. Nucl. Soc., 16, p 350 (1973).ⁿ
2. L. L. Carter, C. A. Forest, "Transfer Matrix Treatments for Multigroup Monte Carlo Calculations - The Elimination of Ray Effects," Nucl. Sci. Eng., 59 (1), pp 27-45, (1976).
3. J. P. Odom, "Neutron Transport with Highly Anisotropic Scattering," Ph.D. Dissertation, Kansas State University, Manhattan, Kansas, (1975).
4. "ANISN: A One-Dimensional Discrete Ordinates Transport Code," RSIC Code Package CCC-82, Oak Ridge National Laboratory, (1969).
5. B. Davison and J. B. Sykes, Neutron Transport Theory, (Oxford University Press, London, 1958).
6. G. Bell and S. Glasstone, Nuclear Reactor Theory, (Van Nostrand Reinhold Company, New York, 1970).
7. A. M. Weinberg and E. P. Wigner, The Physical Theory of Neutron Chain Reactors, (University of Chicago Press, Chicago, 1959).
8. A. D. Galanin, Thermal Reactor Theory, (Pergamon Press, New York, 1960).
9. R. V. Meghreblin and D. K. Holmes, Reactor Analysis, (McGraw Hill Book Company, New York, 1960).
10. Argonne National Laboratory, "Reactor Physics Constants," second edition, ANL-5800 (1963).
11. A. Ginsberg and M. Becker, "Models for Anisotropic Weighting Spectra," Trans. Am. Nucl. Soc., 14, p 368, (1971).
12. T. Fuse, A. Yamaji, T. Miura, "Comparison of One- and Two-Dimensional Discrete Ordinates Calculations with Experimental Results," CONF-721018, 5, pp 1459-71, (1972).
13. M. Becker, Response to "Comment on 'Influence of Deep Minima on Multigroup Cross Section Generation'", Nucl. Sci. Eng., 58, p 261, (1975).
14. R. Q. Wright, J. L. Lucius, N. M. Greens, et al., "SUPERTOG: A Program to Generate Fine Group Constants and P_N Scattering Matrices from ENDF/B," ORNL-TM-2679, (1969).
15. B. J. Toppel, A. L. Rago, and D. M. D'Shea, "MC² -- A Code to Calculate Multigroup Cross Sections," ANL-7318, (1967).
16. N. M. Greene and C. W. Craven, Jr., "XSDRN: A Discrete Ordinates Special Averaging Code," Trans. Am. Nucl. Soc., 14, p 368, (1971).

17. T. Hill, "Azimuthally Dependent Neutron Transport in Slab Geometry," Ph.D. Dissertation, Kansas State University, Manhattan, Kansas, (1972).
18. ORNL-RSIC, "DLC/2, 99 Group Neutron Cross Sections Based on ENDF/B," Oak Ridge National Laboratory (1971).
19. J. P. Odom and J. K. Shultis, "Anisotropic Neutron Transport without Legendre Expansion," Nucl. Sci. Eng., 59, p 278, March 1976.
20. D. I. Darber, et al., "Angular Distributions in Neutron-Induced Reactions: Volume I, Z Equals 1 to 20," Brookhaven National Laboratory, BNL-400 (3rd Ed.)(Vol. 1), Jan. 1970.
21. H. V. Buttler, Nuclear Physics: An Introduction, (Academic Press, New York, 1968).
22. F. A. R. Schmidt, "Attenuation Properties of Concrete for Shielding of Neutrons Less than 15 MeV," ORNL-RSIC-26, (1970).
23. K. D. Lathrop, F. W. Brinkley, "TWOTRAN-II: An Interface Exportable Version of the TWOTRAN Code for Two-Dimensional Transport," LA-4848-MS, (1973).
24. E. Inonu, P. F. Zweifel, Developments in Transport Theory, (Academic Press, New York, 1967).
25. I. N. Sneddon, Fourier Transforms, (McGraw-Hill Book Co., Inc., New York, 1951).
26. M. Abramowitz, I. A. Stegun, Handbook of Mathematical Functions, National Bureau of Standards, Applied Mathematics Series-55, (1972).
27. A. A. Abagyan, L. P. Bass, and T. A. Germogenova, "Spatial, Energy, and Angular Distributions of Radiations in Reactor Shielding," Fourth International Conference on Reactor Shielding, Paris; Eyrolles, pp 471-500.
28. S. Chandrasekhar, Radiative Transfer, (Dover Publications, Inc., New York, 1960).
29. J. L. Carlstedt and T. M. Mullikin, "Chandrasekhar's X- and Y-Functions," Astrophysics Journal, Supp. 113, 12, March (1966).
30. Communique, W. Meyer to K. Shultis, Kansas State University, Sept. 10, 1975.
31. Communique, W. Meyer to K. Shultis, Kansas State University, Oct. 9, 1975.
32. E. A. Attia and A. A. Harms, "A New Expansion for Highly Anisotropic Neutron-Neucleous Scattering," Nucl. Sci. Eng., 59, p 319, (1976).
33. S. Lindahl, Private communication, Kansas State University, 1975.

Appendix A

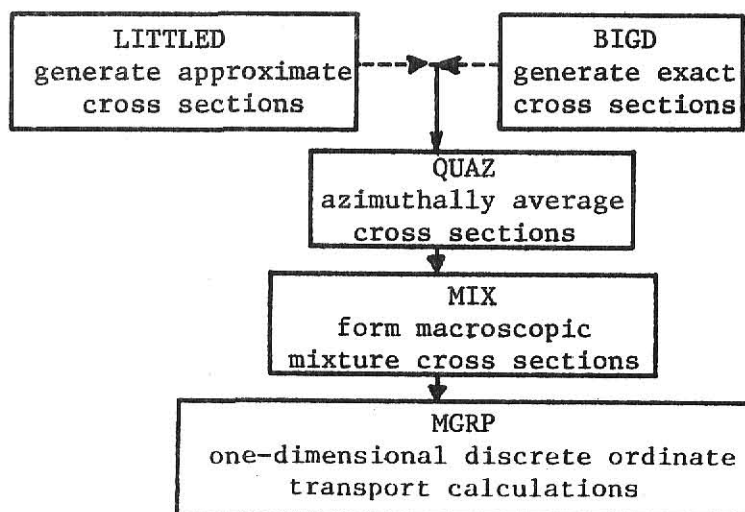
Computer Programs

The main computer codes utilized by this work are presented in this appendix. Among those shown are LITTLED, QUAZ, MIX, and MGRP. Other programs that were used include:

1. DLC/2 RETRIEVAL code, which retrieves multigroup cross sections from DLC/2 library tapes, available with ANISN package from Radiation Shielding Information Center [18],
2. MGIW, which generates numerical quadratures of any type, developed by Jeffrey Ryman, graduate student, Kansas State University, 1976,
3. X-Y FUNCTION, which performs slab transmission calculations for particles that scatter isotropically in a medium, developed by J. K. Shultis, Associate Professor of Nuclear Engineering, Kansas State University, 1976.

Of the computer programs listed in this appendix, only LITTLED was developed by the author. The purpose for including the listings of QUAZ, MIX, and MGRP is to document the code package used to carry out the transport calculations in this work. More qualitative information as to the nature of these three codes can be found in Ref. [3].

The following diagram illustrates the manner in which the four computer codes are related



In this work the transport calculations start with LITTLED. This program generates approximate group-to-group angular transfer cross sections, $\sigma_{g' \rightarrow g}(\underline{\Omega} \cdot \underline{\Omega}')$. If exact, rather than approximate, transfer cross sections are to be used in transport calculations, then the computer code BIGD should be used in place of LITTLED.

Calculated values of $\sigma_{g' \rightarrow g}(\underline{\Omega} \cdot \underline{\Omega}')$ can be fed directly into QUAZ. This program carries out azimuthal averaging of angular transfer cross sections. The result is a matrix which contains $\sigma_{g' \rightarrow g}(\mu_i \rightarrow \mu_j)$ values for all possible combinations of $g' \rightarrow g$ and $(\mu_i \rightarrow \mu_j)$. QUAZ output for two or more elements is normally fed through the computer program MIX, which forms macroscopic mixture cross sections to be used in the discrete ordinates transport code MGRP. If neutron transport through a slab composed of only one element is being considered, then MIX may be bypassed. For such a case, output from QUAZ would feed directly into MGRP.

The computer code MGRP solves the azimuthally symmetric multigroup neutron transport equation for one-dimensional slab geometry. The finite difference discrete ordinate technique employed is based upon Eq. (3.1). The output from this code is the reflected and transmitted angular densities for all groups and spatial mesh points within the slab.

All programs are written in FORTRAN IV, level G, for the Kansas State University IBM 370/158 computer. Program variables are defined within each listing through the liberal use of comment cards. Each listing is followed by a sequence of sample input data.

Appendix A (continued) - LITTLED

```

//LITTLED JOB (334462282,FJ08R3E5,1,9),*WAYNE MIKOLS*
/*TAPE9 2
// EXEC RINGWTR,PARM=9888WH
// EXEC FORTGCLG
//FORT.SYSIN CD *
      DIMENSION U(45),SGN(45,34,34),SIGSCT(34,34),E(35)
      DIMENSION SIGT(35)
      DIMENSION TITLE(20)
C*****
C *****LITTLE-D*****LITTLE-D*****LITTLE-D*****LITTLE-D*****
C
C
C
C
C NIN= INPUT UNIT FOR DLC-2 CROSS SECTION DATA
C NOUT= OUTPUT UNIT FOR DISCRETE CROSS SECTION DATA
C NGROUP=NUMBER OF GROUPS IN CROSS SECTION SET
C NUO= NUMBER OF DISCRETE ANGLES TO BE EVALUATED
C MTOP= NUMBER OF TOP MOST ENERGY DLC GROUP FROM WHICH NEUTRON SCAT
C M8OT= NUMBER OF LOWEST DLC ENERGY GROUP INTO WHICH NEUTRONS SCAT
C SIGT(J)= TOTAL GROUP CROSS SECTIONS
C SIGSCT(I,J)= SCATTERING CROSS SECTIONS FROM GROUP (I) TO (J) FOR
C              ZERO(TH) ORDER LEGENDRE MOMENT
C E(I)= ENERGY STRUCTURE OF GROUPS 1-NGROUP IN DECREASING ORDER
C A=ATOMIC MASS OF SCATTERING NUCLEUS
C DIMENSIONING OF ARRAYS: U(NUO),SGN(NUO,NGROUP,NGROUP)
C                        SIGSCT(NGROUP,NGROUP),E(NGROUP)
C                        SIGT(NGROUP),TITLE(20)
C
C
C
C
C*****
1  FORMAT(8F10.0)
2  FORMAT(16I5)
3  FORMAT(20A4)
4  FORMAT(1X,5D14.6)
5  FORMAT(6D12.5)
6  FORMAT(1X,10X,80I4.5)
7  FORMAT(1X,10X,'I1= ',I2,'      JJ= ',I2)
8  FORMAT(1X,10X,50I7.8)
9  FORMAT(1H1)
  PRINT 9
C
C  READ IN REQUIRED PROGRAM INFORMATION
C
C  READ(5,2)NIN,NOUT,NGROUP,NUO,MTOP,M8OT
C  READ(5,1)A
C  READ(NIN,4)(SIGT(J),J=1,NGROUP)
C  READ(NIN,3)(TITLE(KK),KK=1,20)
C  DO 10 I=1,NGROUP
10 READ(NIN,4)(SIGSCT(I,J),J=1,NGROUP)
   NNGRP=NGROUP+1
   READ(5,1)(E(I),I=1,NNGRP)
C
C  PRINT OUT MULTIGROUP ENERGY STRUCTURE
C
C  PRINT 58,A
C  ALPHA=((A-1.0)/(A+1.0))**2
58  FORMAT (1X,10X,'ATOMIC MASS OF SCATTERING NUCLEUS=',F7.3,/)
  PRINT 13

```

Appendix A (continued) - LITLED

```

DO 14 I=MTOP,MBOT
  II=I-MTOP+1
  IPI=I+1
14 PRINT 12, I, E(I), E(IPI), SIGT(I)
12 FORMAT(1X,10X,I3,2F10.4,7X,E11.4)
13 FDRMAT(1X,10X,'GROUP STRUCTURE',15X,'SIGT',/)
  PRINT 9
C
C   START OUTER LOOP OVER INITIAL NEUTRON ENERGY GROUPS
C
DO 30 J=MTOP,MBOT
  JJ=MTOP+MBOT-J
  JM=MBOT+1-J
C
C   START INNER LOOP OVER FINAL NEUTRON ENERGY GROUPS
C
DO 31 II=JJ,MBOT
  IM=II-MTOP+1
  IGP=JJ
  IGP1=JJ+1
  IG=II
  IG1=II+1
  IF(A.NE.1.0) GO TO 50
  GO TO 53
3
C   BEGIN CALCULATION OF TRIANGULAR CROSS SECTION FOR EACH OF THE
C   (NUO) DISCRETE DIRECTIONS FOR THE CASE WHERE (A.NE.1.0)
C
50 AA=(A+1.0)*0.5
  BB=(A-1.0)*0.5
C
C   DETERMINE ALLOWABLE UMAX AND UMIN TRANSFER RANGE
C
  UAVTOP=(E(IGP)+E(IGP1))*0.5
  UAVBOT=(E(IG)+E(IG1))*0.5
  EMIN=SQRT(E(IG1)/E(IGP))
  EMID=SQRT(UAVBOT/UAVTOP)
  EMAX=SQRT(E(IG)/E(IGP1))
  UMIN=AA*EMIN-BB/EMIN
  UMID=AA*EMID-BB/EMID
  UMAX=AA*EMAX-BB/EMAX
C
C   DETERMINE BASE LENGTH OF THE APPROXIMATING TRIANGLE
C
  IF(UMAX.GT.1.0) UMAX=1.0
  IF(UMAX.LT.-1.0) UMAX=-1.0
  IF(UMID.LT.-1.0) UMID=-1.0
  IF(UMID.GT.1.0) UMID=1.0
  IF(UMIN.GE.-1.0) ULOW=UMIN
  IF(UMIN.LT.-1.0) ULOW=-1.0
  DELU=(UMAX-ULOW)/(FLOAT(NUO-1))
  DO 57, KKK=1, NUO
    CREM=KKK-1
57  U(KKK)=ULOW+CREM*DELU
    IF(E(IG).LT.(ALPHA+E(IGP1))) GO TO 80
C
C   DETERMINE WHETHER THE ENTIRE TRIANGULAR AREA LIES WITHIN
C   THE -1.0 TO +1.0 RANGE FOR (U). IF THE TOTAL AREA DOES, GO TO 54.
C   IF THE TRIANGLE IS TRUNCATED BY THE -1.0 BOUNDARY, CALCULATE THE
C   APPROXIMATING TRIANGLE'S HEIGHT (SIGMAX) USING B1,B2, AND B3

```

Appendix A (continued) - LITTLED

```

C      IF(UMIN.GT.-1.0) GO TO 54
      B1=UMAX-UMID
      B2=UMID+1.0
      B3=-1.0-UMIN
      DENOM=B1+B2+(B2*B3/(B2+B3))
      IF(DENOM.EQ.0.0) PRINT 65,UMAX,UMID,UMIN,JJ,II
      FORMAT(1X,10X,'DENOM=0.0',3(5X,F10.5),2I7)
65
C      CALCULATE THE HEIGHT OF THE APPROXIMATING TRIANGLE IN BARNS
C
      SIGMAX=SIGSCT(JJ,II)/(3.14159265*DENOM)
      GO TO 56
71
      SIGMAX=0.0
      GO TO 56
54
      CONTINUE
      IF((UMAX-UMIN).EQ.0.0) PRINT 66,UMAX,UMIN,JJ,II
      FORMAT(1X,10X,'UMAX-UMIN=0.0',2F12.5,2I7)
66
C      CALCULATE THE HEIGHT OF THE APPROXIMATING TRIANGLE IN BARNS
C
      SIGMAX=SIGSCT(JJ,II)/(3.14159265*(UMAX-UMIN))
      CONTINUE
56
C      CALCULATE TRIANGULARLY APPROXIMATED CROSS SECTION AT EACH OF
C      THE DISCRETE (NUD) DIRECTIONS
C
      DO 51 K=1,NUD
      IF(E(IG).LT.(ALPHA*E(IGP1))) GO TO 55
      IF(U(K).LE.UMIN) GO TO 55
      IF(U(K).GE.UMAX) GO TO 55
      IF((UMID-UMIN).EQ.0.0) PRINT 67,UMID,UMIN,JJ,II
      FORMAT(1X,10X,'UMID-UMIN=0.0',2F12.5,2I7)
67
C      SGN(K,IM,JM) IS THE TRIANGULAR CROSS SECTION IN DISCRETE
C      DIRECTION K FOR NEUTRONS OF INITIAL ENERGY GROUP IM AND
C      FINAL ENERGY GROUP JM
C
      IF(U(K).LT.UMID) SGN(K,IM,JM)=SIGMAX*(U(K)-UMIN)/(UMID-UMIN)
      IF(U(K).LT.UMID) GO TO 51
      IF((UMAX-UMID).EQ.0.0) PRINT 68,UMAX,UMID,JJ,II
      FORMAT(1X,10X,'UMAX-UMID=0.0',2F12.5,2I7)
68
      SGN(K,IM,JM)=SIGMAX*(UMAX-U(K))/(UMAX-UMID)
      GO TO 51
55
      CONTINUE
      SGN(K,IM,JM)=0.0
51
      CONTINUE
      GO TO 62
C
C      BEGIN CALCULATION OF TRIANGULAR CROSS SECTION FOR THE CASE
C      WHERE A=1.0
C
53
      CONTINUE
      IF(II.NE.JJ) GO TO 40
      UMIN=SQRT(E(IG1)/E(IG))
      UMAX=1.0000
      GO TO 41
C
C      DETERMINE BASE LENGTH OF TRIANGLE
C

```

Appendix A (continued) - LITLED

```

40  UMIN=SQRT(E(IG1)/E(IGP))
    UMAX=SQRT(E(IG)/E(IGP1))
    UCRIT=SQRT(E(IG)/E(IGP))
41  CONTINUE
    DELU=(UMAX-UMIN)/(FLOAT(NUO-1))
    DO 20 KKK=1,NUO
    CREM=KKK-1
20  U(KKK)=UMIN+CREM*DELU
3
C   CALCULATE APPROXIMATING TRIANGLE'S HEIGHT
C
    SIGMAX=(SIGSCT(JJ,II)/(1.*3.14159265))/(UMAX-UMIN)
C
C   CALCULATE TRIANGULAR CROSS SECTION FOR TRANSFER FROM ENERGY
C   GROUP IM TO ENERGY GROUP JM IN DISCRETE DIRECTION K
C
    DO 32 K=1,NUO
    IF(U(K).LT.UMIN) GO TO 42
    IF(II.EQ.JJ) SGN(K,IM,JM)=((U(K)-UMIN)/(1.-UMIN))*SIGMAX
    IF(II.EQ.JJ) GO TO 32
    IF(U(K).GT.UMAX) GO TO 42
    IF(U(K).LE.OCRIT) SGN(K,IM,JM)=((U(K)-UMIN)/(OCRIT-UMIN))*SIGMAX
    IF(U(K).LE.OCRIT) GO TO 32
    SGN(K,IM,JM)=((UMAX-U(K))/(UMAX-OCRIT))*SIGMAX
    GO TO 32
42  SGN(K,IM,JM)= 0.0
32  CONTINUE
62  CONTINUE
C
C   PRINT OUT TRIANGULARLY APPROXIMATED CROSS SECTIONS ON OUTPUT
C   UNIT (INPUT) IN A FORMAT ACCEPTABLE FOR INPUT TO COMPUTER
C   PROGRAM "QUAZ"
C
    WRITE(ROUT,5) (U(K),K=1,NUO)
    WRITE(ROUT,5) (SGN(K,IM,JM),K=1,NUO)
60  CONTINUE
    WRITE(6,11)JJ,II
    FORMAT(1X,10X,I10,'          TO          ',I10)
    IF(E(IG).GT.(ALPHA*E(IGP1))) GO TO 63
    PRINT 64
64  FORMAT(1X,10X,'NO-TRANSFER')
    GO TO 31
63  CONTINUE
    NUO=NUO-4
    DO 60 IPRINT=1,NUO,5
    K1=IPRINT
    K2=IPRINT+4
60  WRITE(6,61) (U(KPRINT),SGN(KPRINT,IM,JM),KPRINT=K1,K2)
61  FORMAT(5(1X,OPF10.4,1PE14.4))
31  CONTINUE
30  CONTINUE
    STOP
    END
/*
//GO.FT01F001 DD UNIT=TAPE9,DISP=OLD,
//      DCR=(RECFM=FB,LRECL=80,BLKSIZE=3200),
//      VOL=SER=9833KS,
//      DSN=DLC2,
//      LABEL=(1,SL)
//GO.FT03F001 DD UNIT=TAPE9,DISP=NEW,

```

Appendix A (continued) - LITTLED

```

//      DCB=(RECFM=FB,LRECL=80,BLKSIZE=3200),
//      VOL=SER=98824M,
//      DSN=HYDRO,
//      LABEL=(19,SL)
//GO.SYSIN DD *
      1      3      34      41      1      2] NIN,NOUT,NGROUP,NUO,MTOP,MBOT
1.0000
14.918      13.499      12.214      11.052      10.000      9.0484      8.1873      7.4082
6.7032      6.0653      5.4881      4.9659      4.4933      4.0657      3.6788      3.3287
3.0119      2.7253      2.4667      2.2313      2.0190      1.8268      1.6530      1.4957
1.3534      1.2246      1.1080      1.0026      .90718      .82085      .74274      .67206
.60810      .55023      .49787
/*

```

A
E(I)

Appendix A (continued) - QUAZ

```

//QUAZ2      JOB (334462282,FJ08R3E5,5,9,5000),'WAYNE MIKOLS'
//TAPE9      2
//          EXEC RINGWTR,PARM=988RWM
//          EXEC FORTGCLG
//FCRT.SYSIN DD *
C ***** QUAZ ***** QUAZ ***** QUAZ ***** QUAZ *QUAZ
C* PROGRAM FINDS THE ALLOWABLE W.W' TRANSFER RANGE AND THEN GENERATES *QUAZ
C*THE VALUES OF F(U'->U) MATRIX AT U-QUAD POINTS,USER SUPPLIES SCATTER *QUAZ
C*FUNCTION IN SUM CARD *QUAZ
C*INPUT PARAMETERS..... *QUAZ
C  MG  = # OF GROUPS. *QUAZ
C  N   = ORDER OF MU-QUADRATURE (OUTGOING DATA). *QUAZ
C  NP  = ORDER OF PHI QUADRATURE. *QUAZ
C  M   = ORDER OF MU-QUADRATURE (INGOING DATA). *QUAZ
C  ACC = NUMBER OF MATERIALS. *QUAZ
C  NOUT = OUTPUT UNIT. *QUAZ
C  NIN  = INPUT UNIT. *QUAZ
C  IHS  ~ IF IHS.NE.0 HARD SPHERE ENERGY LIMITS NOT USED AND W*W' RANG *QUAZ
C        IS -1 TO +1. *QUAZ
C  E(MG+1) = ENERGY GROUP STRUCTURE. *QUAZ
C  U(N)   = MU QUADRATURE POINTS. *QUAZ
C  W(N)   = MU QUADRATURE WEIGHTS. *QUAZ
C  P(NP)  = PHI QUAD POINTS. *QUAZ
C  WW(NP) = PHI QUAD WEIGHTS. *QUAZ
C  IA     = ATOMIC MASS NUMBER OF MATERIAL. *QUAZ
C  SGN(M,MG,MG) = MULTIGROUP ANGLE DEPENDENT SCAT X-SECTION. *QUAZ
C  UO (M,MG,MG) = SCAT ANGLES AT WHICH SGN ARE GIVEN (READ FROM UNIT N) *QUAZ
C  DIMENSIONING OF OTHER ARRYS: *QUAZ
C  CP(NP), F(N), B(N,N), GL(MG,MG), GU(MG,MG), US(N,N), YOU(N,N). *QUAZ
C *QUAZ
C *QUAZ
C  DIMENSION U(32),W(32),P(32),WW(32),CP(32),GL(27,27),GU(27,27),F(32) *QUAZ
C  I),E(28),B(20,20), US(20,20),YOU(20,20), UO(20,10,10),SGN(20,10,10) *QUAZ
C *QUAZ
C *****READ INPUT PARAMETERS *QUAZ
C *QUAZ
C  READ (5,101)  MG,N,NP,M,NOC,NOUT,NIN,IHS *QUAZ
C  MGG=MG+1 *QUAZ
C  READ(5,105) (E(I),I=1,MGG) *QUAZ
C  READ(5,100) (U(I),I=1,N) *QUAZ
C  READ(5,100) (W(I),I=1,N) *QUAZ
C  READ(5,100) (P(I),I=1,NP) *QUAZ
C  READ(5,100) (WW(I),I=1,NP) *QUAZ
C 101 FORMAT (16I5) *QUAZ
C 105 FORMAT (6F10.0) *QUAZ
C 100 FORMAT(3025.15) *QUAZ
C  PRINT 98, MG,N,NP,M *QUAZ
C 98 FORMAT (1H0,'NR OF GROUPS =' ,I3,' MU-QUADRATURE =' ,I3, *QUAZ
C 2' PHI-QUAD. =' ,I3,' NR OF MU-Q PTS =' ,I3//' ENERGY GROUP LIMITS' *QUAZ
C 3) *QUAZ
C  PRINT 99, (E (I), I=1,MGG) *QUAZ
C 99 FORMAT (10F12.6) *QUAZ
C  PI=3.14159265358979300 *QUAZ
C  DO 300 I=1,N *QUAZ
C  SI=(1.00-U(I))*U(I)**0.5 *QUAZ
C  DO 300 J=1,N *QUAZ
C  SJ=(1.00-U(J))*U(J)**0.5 *QUAZ
C  US(I,J)=U(J)*U(I) *QUAZ
C 300 YOU(I,J)=SJ*SI *QUAZ
C  DO 8 K=1,NP *QUAZ

```

Appendix A (continued) - QUAZ

```

      8 CP(K)= COS(P(K))                                QUAZ
      DO 1000 ICASE=1,NGC                               QUAZ
      READ (5,101) IA                                   QUAZ
150 PRINT 115 ,IA                                       QUAZ
115 FORMAT(1H0,'W.W RANGE FOR SCATTER FROM GROUP TO GROUP. MASS OF SCATTER =',13) QUAZ
C                                                     QUAZ
C*****CALCULATE W.W' RANGE                           QUAZ
C                                                     QUAZ
      DO 5 JX=1,MG                                       QUAZ
      J=MSG-JX                                           QUAZ
      JJ=J+1                                             QUAZ
      DO 118 I=J,MG                                       QUAZ
      II=I+1                                             QUAZ
      GL(I,J)=0.5*(IA+1)*(E(II)/E(J))**0.5-(IA-1)*0.5*(E(J)/E(II))**0.5 QUAZ
      GU(I,J)=0.5*(IA+1)*(E(I)/E(JJ))**0.5-(IA-1)*0.5*(E(JJ)/E(I))**0.5 QUAZ
      IF(GU(I,J).GT.1.00) GU(I,J)=1.00                 QUAZ
      IF(GL(I,J).LT.-1.0) GL(I,J)=-1.0                 QUAZ
      PRINT 420, J,I,GL(I,J),GU(I,J)                   QUAZ
420 FORMAT(28X,13,3X,13,20Z0.6)                       QUAZ
      IF(GU(I,J).LE.-1.0) GO TO 118                     QUAZ
      READ(NIN,106)(UO(K,I,J),K=1,M)                   QUAZ
      READ(NIN,106)(SGN(K,I,J),K=1,M)                   QUAZ
106 FORMAT(60I2.5)                                     QUAZ
118 CONTINUE                                           QUAZ
      5 CONTINUE                                         QUAZ
      DO 6 IE=1,MG                                       QUAZ
      II=IE+1                                             QUAZ
      DO 7 JE=1,IE                                       QUAZ
      JJ=JE+1                                             QUAZ
      IF(GU(IE,JE).GT.-1.0) GO TO 188                   QUAZ
      DO 250 I=1,N                                       QUAZ
      DO 250 J=1,N                                       QUAZ
250 B(I,J)=0.0                                         QUAZ
      GO TO 10                                           QUAZ
188 DO 1 I=1,N                                          QUAZ
      SUM=0.00                                           QUAZ
      DO 2 J=1,N                                          QUAZ
      SUM=0.00                                           QUAZ
C                                                     QUAZ
C*****PERFORM INTEGRATION OVER THE AZIMUTHAL ANGLE PHI
C                                                     QUAZ
      DO 9 K=1,NP                                       QUAZ
      G=US(I,J)+YOU(I,J)*CP(K)                         QUAZ
      IF(G.LT.GL(IE,JE).OR.G.GT.GU(IE,JE)) GO TO 9     QUAZ
      L=1                                                 QUAZ
22 IF (UO(L,IE,JE).GE.G) GO TO 33                     QUAZ
      IF(L.GE.M)GO TO 33                                 QUAZ
      L=L+1                                              QUAZ
      GO TO 22                                           QUAZ
33 D1=UO(L,IE,JE)-UO(L-1,IE,JE)                       QUAZ
      D2=G-UO(L-1,IE,JE)                               QUAZ
      D3=UO(L,IE,JE)-G                                 QUAZ
      XX=(D2*SGN(L,IE,JE)+D3*SGN(L-1,IE,JE))/D1        QUAZ
      IF(XX.LT.0.0)XX=0.0                               QUAZ
      SUM=SUM+HW(K)*XX                                   QUAZ
      9 CONTINUE                                         QUAZ
      B(I,J)=SUM*2.0                                     QUAZ
      2 SUM=B(I,J)*W(J)+SUM                             QUAZ
      1 F(I)=SUM                                         QUAZ

```

Appendix A (continued) - QUAZ

```

PRINT 600,JE,IE,(F(I),I=1,N)
600 FORMAT (2X,214,1P12E10.2,/10X,12E10.2)
10 WRITE (NOUT,113)((B(I,J),J=1,N),I=1,N)
113 FORMAT(6E12.5)
7 CONTINUE
6 CONTINUE
1000 CONTINUE
STOP
END

```

QUAZ
QUAZ
QUAZ
QUAZ
QUAZ
QUAZ
QUAZ
QUAZ

```

/*
//GO.FT01F001 DD UNIT=TAPE9,DISP=OLD,
// DCB=(RECFM=FB,LRECL=80,BLKSIZE=3200),
// VOL=SER=9905KS,
// DSN=OXYGEN,
// LABEL=(25,SL)
//GO.FT03F001 DD UNIT=TAPE9,DISP=(NEW,KEEP),
// DCB=(RECFM=FB,LRECL=80,BLKSIZE=3200),
// VOL=SER=9888WM,
// DSN=OXYGEN,
// LABEL=(33,SL)
//GO.SYSIN DD *

```

6	14	32	20	1	8	9	0	MG,N,NP,M,NOC,NOUT,NIN,IHS	
3.0119	2.7253	2.4667	2.2313	2.0190	1.8268	1.6530	1.4957	Group Structure	
-.9745539562			-.870765928				-.7029225757		
-.5			-.2970774243				-.1292344072		
-.0254460438			.0254460438				.1292344072		DP-7 Quadrature
.2970774243			.5				.7029225757		
.870765928			.9745539562						
.0647424831			.1398526957				.1909150253		DP-7 Quadrature
.2089795918			.1909150253				.1398526957		Weights
.0647424831			.0647424831				.1398526957		
.1909150253			.2089795917				.1909150253		
.1398526957			.0647424831						
0.429791486228259D-02			0.226013801107392D-01				0.553513079721679D-01		
0.102249275541303D 00			0.162858313807309D 00				0.236612749819336D 00		
0.322824031228741D 00			0.420687256611229D 00				0.529286717683086D 00		
0.647614439389240D 00			0.774559650648890D 00				0.908439100859103D 00		
0.104949812700964D 01			0.119492436852379D 01				0.134386002063359D 01		
0.149491451196836D 01			0.164667748803164D 01				0.179773197936641D 01		
0.194666763147621D 01			0.209209187299036D 01				0.223265289914090D 01		
0.236703234935111D 01			0.249397756061076D 01				0.261230328231691D 01		
0.272090474338877D 01			0.281876796877126D 01				0.290497925018066D 01		
0.297873368619269D 01			0.303934272445870D 01				0.308624069202783D 01		
0.311899061988926D 01			0.313729408513772D 01						
0.110248045284354D-01			0.255637541457267D-01				0.398657546195275D-01		Gauss-32
0.538372467683217D-01			0.672864572697205D-01				0.801075474971032D-01		Quadrature
0.921807392997089D-01			0.103079125048217D 00				0.113640484003060D 00		
0.122826658726746D 00			0.130866037327990D 00				0.137683557082944D 00		
0.143215563959790D 00			0.147410406698531D 00				0.150228918945643D 00		
0.151644784878579D 00			0.151644784878579D 00				0.150228918945643D 00		
0.147410406698531D 00			0.143215563959790D 00				0.137683557082944D 00		
0.130866037327990D 00			0.122826658726746D 00				0.113640484003060D 00		
0.103393284248217D 00			0.921807392997089D-01				0.801075474971032D-01		
0.672864572697205D-01			0.538372467683217D-01				0.398657546195275D-01		
0.255637541457267D-01			0.110248045278071D-01						

16] Mass Number

/*

Appendix A (continued) - MIX

```

//IMIX      JOB (334462282,FJ08R3E5,,9),'WAYNE MIKOLS',TIME=(3,00)
/*TAPE9      2
/*REGION     400K
//          EXEC RINGWTR,PARM=9888WM
//          EXEC FORTGCLG
//FORT.SYSIN DD *
C ***** MIX *****
C
C      THIS PROGRAM FORMS COMPOSITE CROSS SECTIONS FOR OUTPUT DATA
C      FROM COMPUTER PROGRAM QUAZ
C
C      MG = # OF GROUPS.
C      N = ORDER OF QUADRATURE.
C      NINA= INPUT UNIT FOR MATERIAL (A)
C      NINB= INPUT UNIT FOR MATERIAL (B)
C      NUT = OUTPUT UNIT.
C      AA = # OF ATOMS OF SORT A PER MOLECULE.
C      BB = # OF ATOMS OF SORT B PER MOLECULE.
C      AC = NUMBER DENSITY OF MOLECULES.
C      SIGA, SIGB = TOTAL CROSS SECTIONS FOR A AND B.
C      ARRAYS : B(N,N),SIGA(MG),SIGB(MG), A(X,N,N), X=MG*(MG+1)/2
3
      DIMENSION A(190,18,18),B(18,18),SIGA(27),SIGB(27)
      READ(5,101)MG,N,NINA,NINB,NUT
      READ(5,210) AA,BB,AC
      READ(5,210) (SIGA(I),I=1,MG)
      READ(5,210) (SIGB(I),I=1,MG)
101 FORMAT (16I5)
210 FORMAT (8F10.0)
100 FORMAT(6E12.5)
      WRITE (6,95) MG,N,AA,BB,AC
95 FORMAT (1H0,'MG=',I3,' N=',I3,' NR OF ATOMS A PER MOLEC. =',
2F4.0,' NR OF ATOMS B =',F4.0,' NUMBER DENSITY OF MOLEC. =',F10.6)
3)
      WRITE (6,96) (SIGA(I), I=1,MG)
96 FORMAT (1H0,'TOT X-SECTIONS FOR A =',(10F12.6))
      WRITE (6,97) (SIGB(I), I=1,MG)
97 FORMAT (1H0,'TOT X-SECTIONS FOR B =',(10F12.6))
      AD=AA*AC
      BD=BB*AC
      MGG=(MG*(MG+1))/2
      DO 10 IG=1,MGG
10 READ(NINA,100) ((A(IG,I,J), J=1,N), I=1,N)
C
      DO 3 IG=1,MGG
      READ(NINB,100) ((B(I,J),J=1,N),I=1,N)
      DO 3 I=1,N
      DO 3 J=1,N
3 A(IG,I,J)=AD*A(IG,I,J) + BD*B(I,J)
      REWIND 2
C      TOTAL CROSS SECTIONS.
      DO 5 I=1,MG
5 SIGA(I)=AD*SIGA(I)+BD*SIGB(I)
      WRITE (6,99)
99 FORMAT (1H0,' TOTAL CROSS SECTIONS FOR MIXTURE. ')
      WRITE(6,100) (SIGA(I),I=1,MG)
      DO 20 IG=1,MGG
20 WRITE (NUT,100) ((A(IG,I,J), J=1,N), I=1,N)
      STOP
      END

```

Appendix A (continued) - MIX

```

/*
//GO.FT01F001 DD UNIT=TAPE9,DISP=OLD,
//      DCB=(RECFM=FB,LRECL=80,BLKSIZE=3200),
//      VOL=SER=9905KS,
//      DSN=HYDRO,
//      LABEL=(26,SL)
//FT02F001 DD UNIT=TAPE9,DISP=OLD,
//      DCB=(RECFM=FB,LRECL=80,BLKSIZE=3200),
//      VOL=SER=9888WM,
//      DSN=OXYGEN,
//      LABEL=(33,SL,,IN)
//FT03F001 DD UNIT=TAPE9,DISP=(NEW,KEEP),
//      DCB=(RECFM=FB,LRECL=80,BLKSIZE=3200),
//      VOL=REF=*.FT02F001,
//      DSN=M2CAPP,
//      LABEL=(34,SL,,OUT)
//GO.SYSIN DD *
      8   14   1   2   3]MG,N,NINA,NINB,NUT
2.0      1.0      0.03343]AA,BB,AC
0.68421  0.75181  0.82398  0.90082  0.98240  1.0688  1.1600  1.2561 ]SIGA(I)
0.64808  0.79340  0.87754  0.65065  0.67241  0.77823  0.79260  0.94894 ]SIGB(I)
/*

```

Appendix A (continued) - MGRP

```

//MGRP      JOB (334462282,FJ06R3E5,,9),'WAYNE MIKOLS',TIME=(8,00)
/*TAPE9
/*REGION      512K
//          EXEC FORTGCLG
//FORT.SYSIN DD *
C ***** MGRP ***** MGRP ***** MGRP ***** MGRP
C
C *SOLVES 1-D AZIMUTHALLY SYMMETRIC MULTIGROUP CASE WITH ARBITRARILY *MGRP
C *HIGH ORDER OF ANISOTROPY. INPUT PARAMETERS ARE..... MGRP
C   MG = # OF GROUPS. MGRP
C   N  = ORDER OF QUADRATURE. MGRP
C   M  = # OF MESH POINTS. MGRP
C   KP = SET = 1 IF REGIONAL INTEGRATION USED. MGRP
C   NL = INTEGRATION U-RANGE FOR REGIONAL INTEGRATION. MGRP
C   KF = IF = 0 THE SOURCE IN TOP GROUP, IF NOT MULTIGROUP SOURCE MGRP
C         MUST BE SUPPLIED. MGRP
C   IS = SOURCE ANGLE ( IN QUADRATURE SET). MGRP
C   NLM = WITHIN GROUP ITERATION LIMIT. MGRP
C   NIN = INPUT UNIT. MGRP
C   IPRINT = IF .NE. 0 PRINT ANGULAR FLUX VECTOR. MGRP
C   MTOP = HIGHEST ENERGY GROUP IN WHICH THERE LIES A SOURCE MGRP
C   DEL = MESH SIZE. MGRP
C   T  = CONVERGENCE ACCURACY. MGRP
C   ST = ACCELERATION PARAMETER. MGRP
C   SIGT(MG) = TOTAL CROSS SECTIONS. MGRP
C   U(N) = QUADRATURE POINTS. MGRP
C   W(N) = QUADRATURE WEIGHTS. MGRP
C   A(N,N) = SCATTERING CROSS SECTIONS. MGRP
C   F(M,N,MG) = EXTERNAL SOURCE (IF KF.NE.0). ALSO NEUTRON DENSITY. MGRP
C DIMENSIONING OF OTHER ARRAYS: MGRP
C   G(M,N,MG) = NEUTRON DENSITY AT SPATIAL MIDPOINT. MGRP
C   Q(M,N) = WITHIN GROUP SCATTERING. MGRP
C   SNN(M,N) = DOWN SCATTERING. MGRP
C   JLN(N), JU(N) = LOWER AND UPPER REGIONAL INTEGRATION LIMITS. MGRP
C
C   REAL*4 SIGT(35),U(16),W(16),JL(16),JU(16),A(16,16),
C   IQ(136,16),SNN(136,16), F(136,16,19),G(136,18,19)
C   READ (5,100) MG,N,M,KP,NL,KF,IS,NLM,NIN,IPRINT,MTOP
C   READ (5,220) DEL,T,ST
C   READ (5,220) (SIGT(I), I=1,MG)
C   READ(5,109) (U(J),J=1,N)
C   READ(5,109) (W(J),J=1,N)
100  FORMAT (16I5)
220  FORMAT (8F10.0)
109  FORMAT (3D25.15)
180  FORMAT(6D12.5)
C   MGG=MG+1
C   N2=N/2
C   NP=N2+1
C   STO=ST
C
C   PRINT 120, MG,N,M,KP,NL,KF,IS,NLM,DEL,T,ST,U(15)
120  FORMAT (1H1, 'NR OF GROUPS      =',I3,
C   2' QUADRATURE      =',I3/' MESH POINTS      =',I3,
C   3' REGIONAL INT.  =',I3/' REG INT PARAM.    =',I3,
C   4' SOURCE TYPE    =',I3/' SOURCE DIRECTION =',I3,
C   5' MAX NR OF ITER =',I3/' MESH SIZE      =',F10.6,
C   6' ACCURACY       =',F10.6/' ACC PARAM.    =',F10.6,
C   7' SOURCE ANGLE   =',F10.6/' TOTAL CROSS SECTIONS')
C   PRINT 123, (SIGT(I), I=1,MG)

```


Appendix A (continued) - MGRP

```

DO 500 J=JJ, JJU
500 SNN(K, I)=SNN(K, I) + G(K, J, JE)*A(I, J)*W(J)
130 CONTINUE

C*****CALCULATE DIFFUSE TRANSMISSION IN SOURCE DIRECTION
KEG=MG
IF (KF.EQ.0) KEG=1
MS=2
IF (IPRINT.EQ.0) MS=M
DO 6667 KE=1, KEG
DO 6667 K=MS, M
6667 F(K, IS, KE)=F(K, IS, KE)~ EXP(-DEL*(K-1)*SIGT(KE)/U(IS))*F(1, IS, KE)
IF (IPRINT.EQ.0) GO TO 3002
PRINT 2004
2004 FORMAT('1', 'ANGULAR DENSITY BY MESH PT, ANGLE, AND GROUP')
DO 2000 KE=1, MG
DO 2000 K=1, M
PRINT 2005, KE, K
2005 FORMAT(1H0, 'GROUP', I4, 2X, 'MESH PT', I4)
2000 PRINT 2006, (F(K, I, KE), I=1, N)
2006 FORMAT(1X, 5D20.10)
3002 CONTINUE
DO 2003 KE=1, MG
KRE=KE+MTOP-1
PRINT 2224, KRE
2224 FORMAT(1///, 'GROUP', I3, ' MU', 8X, 'TRANSMISSION MU', 8X,
2'REFLECTION')
DO 2003 I=1, N2
J=N2+I
2003 WRITE (6, 2250) U(I), F(I, J, KE), U(I), F(1, I, KE)
2250 FORMAT (10X, F10.6, 1PE14.5, 0PF12.6, 1PE14.5)
C*****CALCULATE ALBEDO, TRANSMITTANCE AND SCALAR FLUX
PRINT 800
800 FORMAT(1///, ' SCALAR FLUX BY GROUP REFLECTED FACE TRANSMITTED
1FACE')
RR=0.0
TT=0.0
DO 5000 KE=1, MG
KRE=KE+MTOP-1
FLUXR=0.0
FLUXT=0.0
DO 5001 J=1, N2
JJ=N2+J
FLUXR=FLUXR+W(J)*F(1, J, KE)
FLUXT=FLUXT+W(JJ)*F(M, JJ, KE)
RR=RR-F(1, J, KE)*W(J)*U(J)
5001 TT=TT+F(M, JJ, KE)*W(JJ)*U(JJ)
5000 PRINT 801, KRE, FLUXR, FLUXT
801 FORMAT(18X, I2, D14.5, 5X, D14.5)
PRINT 5002, TT, RR
5002 FORMAT(1/, ' TRANSMITTANCE=', D20.10, 2X, 'ALBEDO=', D20.10)
5004 STOP
END

/*
//GO, FTOIFOCI DD UNIT=TAPE9, DISP=OLD,
// DCB=(RECFM=FB, LRECL=80, BLKSIZE=3200),
// VOL=SER=9888WM,
// DSN=H2QAPP,
// LABEL=(34, SL)
//GO, SYSIN DD *

```

Appendix A (continued) - MGRP

19	18	136	0	0	1	18	10	1	0	1	MG, N, M, KP, NL, KF, IS, NLM, NIN, IPRINT, MTOP	DEL, T, ST SIGT(I)
C.150000	0.00001	0.150										
C.095024	0.099855	0.10792			0.10237		0.10427		0.11149	0.11418	0.12222	
C.12134	0.14246	0.14678			0.15374		0.18104		0.21527	0.23879	0.21729	
C.19426	0.20120	0.19912										
-1.000000000		-0.980955155							-0.959976549			
-0.867865601		-0.728792425							-0.707106781			
-0.550201326		-0.342012327							-0.115954330			
C.115954330		0.342012327							0.550201326			
0.707106781		0.728792425							0.867865601			
C.959976549		0.980955155							1.000000000			
C.010975014		0.000000000							0.066783999			
0.116620315		0.160285186							0.000000000			
0.195235062		0.219156322							0.230944098			
C.230944098		0.219156322							0.195235062			
C.000000000		0.160285186							0.116620315			
C.066783999		0.000000000							0.010975014			
C.2302	0.2447						0.1777		0.8085			
1.730	2.602						3.728		5.385			
6.150	6.084						6.015		7.109			
8.111	8.577						8.448		9.978			
11.196	17.751						23.033					

THE TRIANGULAR APPROXIMATION FOR HIGHLY ANISOTROPIC
GROUP-TO-GROUP TRANSFER CROSS SECTIONS

by

WAYNE JOHN MIKOLS

B.S. Kansas State University, 1974

AN ABSTRACT OF A MASTER'S THESIS

submitted in partial fulfillment of the
requirements for the degree

MASTER OF SCIENCE

Department of Nuclear Engineering

Kansas State University

Manhattan, Kansas

1976

Abstract

This study represents an investigation of approximate numerical techniques which can be used to evaluate highly anisotropic scattering transfer cross sections. Anisotropic scattering occurs in many important particle transport problems. The present work evaluates the utility of approximate elastic scattering cross sections for the study of fast neutron transport through water slabs.

Empirical and theoretical considerations suggest that highly anisotropic angular transfer cross sections for multigroup equal lethargy width energy structures may be accurately modeled by triangular functions. The use of triangular representations greatly simplifies cross section evaluations. The only actual cross section information required by this triangular method is the total group-to-group elastic transfer cross sections for all group transfers being considered. This is in sharp contrast to customary Legendre expansion techniques which generally require nine angular moments or expansion coefficients for evaluation of each group-to-group transfer cross section considered.

The usefulness of approximated cross sections depend upon their ability to reproduce transport calculations based upon exact cross section information. A discrete ordinates transport code is used to compare calculations of transmitted angular densities based upon exact and approximate cross sections. Results for an 8 inch water slab show no significant differences. To insure that discrete ordinate transport results calculated from approximate cross sections are justly compared to those calculated using exact values, particular attention is given to quadrature set selection. A simple mathematical criterion is developed which enables evaluation of the ability of a quadrature set to describe angular particle transfer.